FRAGMENTABLE BICYCLO[3.3.1]NONANE CATIONIC MATERIALS AND THEIR APPLICATIONS TO NUCLEIC ACID DELIVERY AND ANTIMICROBIAL FUNCTION

A Dissertation
Presented to
The Academic Faculty

by

Zhishuai Geng

In Partial Fulfillment
of the Requirements for the Degree
Doctor of Philosophy in the
School of Chemistry and Biochemistry

Georgia Institute of Technology
August 2018

FRAGMENTABLE BICYCLO[3.3.1]NONANE CATIONIC MATERIALS AND THEIR APPLICATIONS TO NUCLEIC ACID DELIVERY AND ANTIMICROBIAL FUNCTION

Approved by:

Dr. M. G. Finn, Advisor
School of Chemistry and Biochemistry
Georgia Institute of Technology

Dr. Stefan France
School of Chemistry and Biochemistry
Georgia Institute of Technology

Dr. Seth Marder, Co-advisor
School of Chemistry and Biochemistry
Georgia Institute of Technology

Dr. Jennifer Curtis
School of Physics
Georgia Institute of Technology

Dr. John Reynolds
School of Chemistry and Biochemistry
Georgia Institute of Technology

Date Approved: May 10, 2018

ACKNOWLEDGEMENTS

I am very grateful for all the guidance and support from advisors, mentors and friends through the last six years. It's so fortunate for me to meet all these people and have the chance to take and finish this thesis project.

First, I would like to thank my advisor Professor M. G. Finn for not only providing directions on science but also setting an example for a decent person. When he taught me the experimental design to confirm hypothesis, it also shaped my thinking style. I also benefitted from the freedom he provided to chase after research interests me most. Without his encouragement, inspiration and emotional support, I wouldn't be able to overcome obstacles one after one even at my most difficult time. His diligence, patience, curiosity and enthusiasm towards science have deeply affected me and set the model of both a good scientific researcher and teacher.

I am also thankful to my co-divisor Professor Seth Marder for teaching me critical thinking and scientific communication. I am also grateful for the opportunity to be involved in a project on surface modification and his support on that. That exposed me to a new field and also affected dramatically my later research.

I am grateful for the insightful discussion and suggestions on polymer chemistry, organic synthesis and biophysics from my thesis committee members, Dr. Reynolds, Dr. France and Dr. Curtis. I really appreciate your time and input.

I could never thank enough the fantastic lab members encountered in my graduate life. I had several great mentors who are open and kind. I would thank Dr. Cody Higginson

for his patience to train me on many organic, polymer fundamental and instrumental operation; his enthusiasm to inspire me keep trying new ideas; the insightful discussion between him and I at countless late night and for just being a good companion and friend I learnt so much (again, not limited to science) from. I would thank Ms. Jenny Cheng for her help on every aspect a biology to accelerate my progress and strengthen my confidence; Dr. Sergio Paniagua, Dr. Anthony Giordano and Dr Siyuan Zhang for their training on surface chemistry and showing me the entry of this field; Thank Dr. Mei kwan Yau and Dr. Allison Geoghan for their assistance on improving my English writing and presentation skills and the encouragement and care between good friends; Thank Robert Hincapie for always coaching me on biological fundamentals and technique support with more details than I need to know.

I also feel fortunate to be able to work with or overlap with a number of great students and scientists in Finn lab and Marder lab. In Finn lab I would acknowledge Dr. Craig McKay, Dr. Srinivas Tekkam, Dr. Nick Bruno, Dr. Christian Scheibe, Dr. Carlos Chavez, Dr. Tamara Vilches and Dr. Jiri Schimer for synthetic technique supports; Thank Dr. Liangjun Zhao, Stephen Crooke, Jefferey Noble and Asheley Chapman for their generous offer of biomaterials and suggestions on biology assay design; Thank Breanne Hamlett, Kirstie Thompson, Lucrezia De Pascalis and Jennifer Beveridge for being nice to keep my safety in check. In Marder lab I would thank Dr. Tim Parker for helping me start in lab and helpful directions to organic synthesis. Thanks to Sue Winters, Michele Yager, Denise Bale and Walaa Compton for keeping the group business organized so I can focus on research.

I am also grateful for the help from both inside and outside chemistry department. Wenbin Wei in Curtis Lab from physics department on confocal fluorescent microscope; Caroline Hansen in Lam Lab from Biomedical Engineering department for providing blood cells; Jiaying Liu in Roy Lab from Biomedical Engineering department for useful discussion on transfection; Bo Song in Wong Lab from Material Science and Engineering department for support on conductivity test. Jiajia Xue for providing PDA-PCL. Yuehui Zhao for suggestions on plasmid transformation and DNA sequencing.

I also feel fortunate to become a mentor to Mr. Mark Garren. His persistence and strong motivation have pushed the projects far. The teaching experience also inspires me to think about teaching methods and leadership. In that way, we witnessed the growth of each other.

Finally, I would like to thank my parents, who always believe in me even we are so far apart and even they don't understand what I am doing. This love will be remembered forever and take me far to my future.

Thanks to all the friends and colleagues I met in Gatech. It's you who help me become what I am and achieve what I did.

TABLE OF CONTENTS

LIST OF TABLES

LIST OF FIGURES

LIST OF SYMBOLS AND ABBREVIATIONS

AMP	antimicrobial peptide
ATRP	atom-transfer radical-polymerization
BCN	bicyclo[3.3.1]nonane
$CDCl_3$	deuterated chloroform
CFU	clony forming unit
CHO	Chinese hamster ovary cells
CMC	critical micelle concentration
COD	cyclooctadiene
CPC	cetylpyridinium chloride
CTAB	cetyl trimethylammonium bromide
CuAAC	copper-catalyzed azide-alkyne cycloaddition
Cys	cysteine
D_2O	deuterated water
DABCO	1,4-diazabicyclo[2.2.2]octane
DCM	dichloromethane
DLS	dynamic light scattering
DMAP	4-dimethylaminopyridine
DMSO	dimethylsulfoxide
DSC	differential scanning calorimetry
E. coli	*Escherichia coli*
EDC	1-Ethyl-3-(3-dimethylaminopropyl)carbodiimide
EWG	electron-withdrawing group

GFP	green fluorescent protein
GPC	gel permeation chromatography
HC	hemolytic concentration
HeLa	Henrietta Lacks human cervical cancer cells
LB	lysogeny broth
MeCN	acetonitrile
MHB	Mueller-Hinton Broth
MIC	minimum inhibition concentration
MRSA	Methicillin-resistant *Staphylococcus aureus*
MTT	(3-(4, 5-dimethylthiazolyl-2)-2, 5-diphenyltetrazolium bromide)
N/P	nitrogen to phosphorous ratio
OD	optical density
PAA	poly(amido amine)
PAE	poly(β-amino esters)
PBS	phosphate buffered saline
PCL	polycaprolactone
PCR	polymerase chain reaction
PDA	polydopamine
PDMAEMA	poly dimethylamino ethyl methacrylate
PEG	polyethylene glycol
PEI	polyethylenimine
PLL	polylysine
QAC	quaternary ammonium compound
RBC	red blood cell
ROMP	ring opening metathesis polymerization

SEM	scanning electron microscopy
siRNA	small interfering RNA
TEA, Et3N	triethylamine
TEM	transmission electron microscopy
TGA	thermogravimetric analysis
THF	tetrahydrofuran
THPTA	tris-hydroxypropyltriazolylmethylamine
TLC	thin layer chromatography
Tris	tris(hydroxymethyl)aminomethane
XPS	X-ray photoelectron spectroscopy

SUMMARY

The goal of the research reported in this thesis is to investigate reversible bond formation in bicyclo[3.3.1] system through anchimeric assistance and use that as building blocks to assemble functional cationic materials, with both low and high molecular weights, linear and hyperbranched architecture. The degradability/fragmentability of the resulting materials could be easily tuned based on physical organic fundamental principles. The application of them in gene delivery demonstrated comparable efficiency to commercial available standards. The materials also demonstrated desired broad spectrum antimicrobial activity with less likelihood of resistance development and potential to be used as antimicrobial coating. With more optimization, this new type of cationic material is promising to achieve goals traditional polycation could not.

CHAPTER 1. INTRODUCTION

(Part of chapter 1 is adapted with permission from Geng, Z., Degradable Cationic Polymer: A Class of Material to Address Bacteria Resistance. *Med & Analy Chem Int J* **2018**, 2(1): 108-112.)

1.1 Anchimeric-assisted substitution of bicyclo[3.3.1]nonane system.

1.1.1 *General introduction of anchimeric assistance*

While nucleophilic substitution of halide is a common reaction in organic synthesis, it is often slow and can proceed in low yield from competing elimination reactions. To overcome this problem, intramolecular activation by proximal substituent groups assisting the departure of leaving group was employed long ago[1] (example in Figure 1). The term neighboring group participation and anchimeric assistance was established as follows[2].

"When a substituent stabilizes a transition state or an intermediate by forming a bond to the reaction center, this effect is called neighboring group participation. If such participation leads to an enhanced reaction rate, the neighboring group is said to provide anchimeric assistance." Nowadays these two terms are used almost interchangeably in literature and throughout this document.

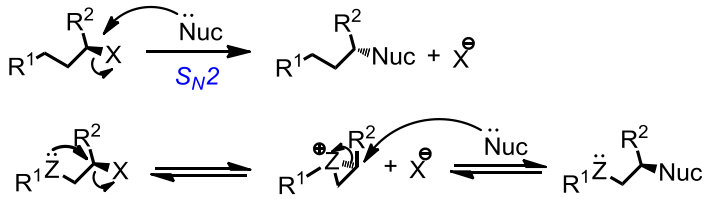

Figure 1 A comparison between anchimeric assisted substitution and normal S_N2 substitution.

Pre-requisites for anchimeric assistance to take place includes:

1. The neighboring group must possess electron density that allows a bond formation with the electrophilic center of the molecule.

2. Effective overlap between the orbitals of the incipient carbocation and those of the neighboring group in the transition state.

3. Any competing reaction must be slower than the process involving neighboring group participation.

The electron density in the neighboring group can be localized through lone pairs, π-orbitals, or σ-orbitals (coming together with hyperconjugation usually)[3-4]. Employment of lone pairs, known as n-participation, is most common and produces the largest effects among these three types of anchimeric assistance[3]. Sulfur, nitrogen and oxygen are the internal nucleophiles heavily involved in n-participation anchimeric assistance (example in Figure 2 from Morita's work in 1969). The electronegativity of these atoms causes inductive destabilization when the carbocation intermediate is formed. However, this destabilization is less essential for the more electron-rich S than for O or N and the strength of it decreases rapidly with distance. For instance it is strongly affected by a leaving group in β-position rather than δ or γ^5 (which also exist, shown in Figure 3 adapted from Grob's work in 1973). Combined with entropy calculation, it is summarized that sulfur usually forms three membered episulfonium ion, while smaller and harder nitrogen and oxygen favor intermediates with five or six membered rings[6-7].

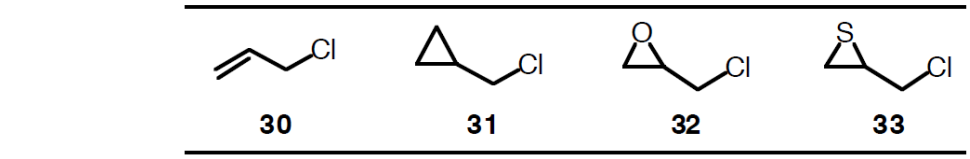

	30	31	32	33
Relative rate	1	30	100	3000
		σ	*n*	*n*

Figure 2 Examples of anchimeric assistance involved with σ and n participation.

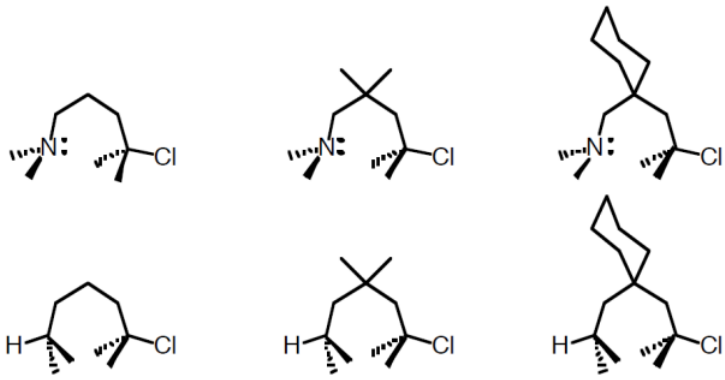

k_N/k_C	0.89	7.2	70

Figure 3 Examples of anchimeric assistance at δ position.

Due to the stabilization of the carbocation intermediate, reaction rates are often enhanced greatly in n-participation anchimeric assistance. Furthermore, the presence of an internal nucleophile can make the covalent bond formation reversible. Therefore, the anchimeric assistance mechanism will allow for better control of diversified bond formation and cleavage by varying either the internal activation groups or substituting nucleophiles/leaving groups.

1.1.2 *Bicyclo[3.3.1]nonane electrophiles*

Sulfur mustards (known as mustard gas) are among the best examples to illustrate anchimeric assisted substitution. It is recognized as a super toxic reagent because the cyclic intermediate facilely formed through anchimeric assistance is so reactive that it tends to alkylate guanine nucleotide in DNA permanently, which prevented cellular division and generally lead to programmed cell death or the development of cancer[8].

The discovery of bicyclo[3.3.1]nonane (abbreviated as BCN) derivatives and their reactivity on anchimeric assisted substitution (shown in Figure 4) were first reported by Weil[9], Corey[10], and Lautenschlaeger[11]. The BCN electrophile is usually cis, cis-1, 5-cyclooctadiene (1, 5-COD) derived species bearing a donor atom in the 9-position and leaving groups β to the donor. Sharing similar structural characteristic with volatile mustard gas, BCN molecule, however, is much easier to handle since it is a solid with low vapor pressure. And since it is a conformationally restricted system, the anchimeric assistance effect of anchimer to β atom can be even more striking. 2,6-Dichloro-9-thiabicyclo[3.3.1]nonane, with chlorine as X and sulfur as Z, is one of the most common example which is also the main focus of my research.

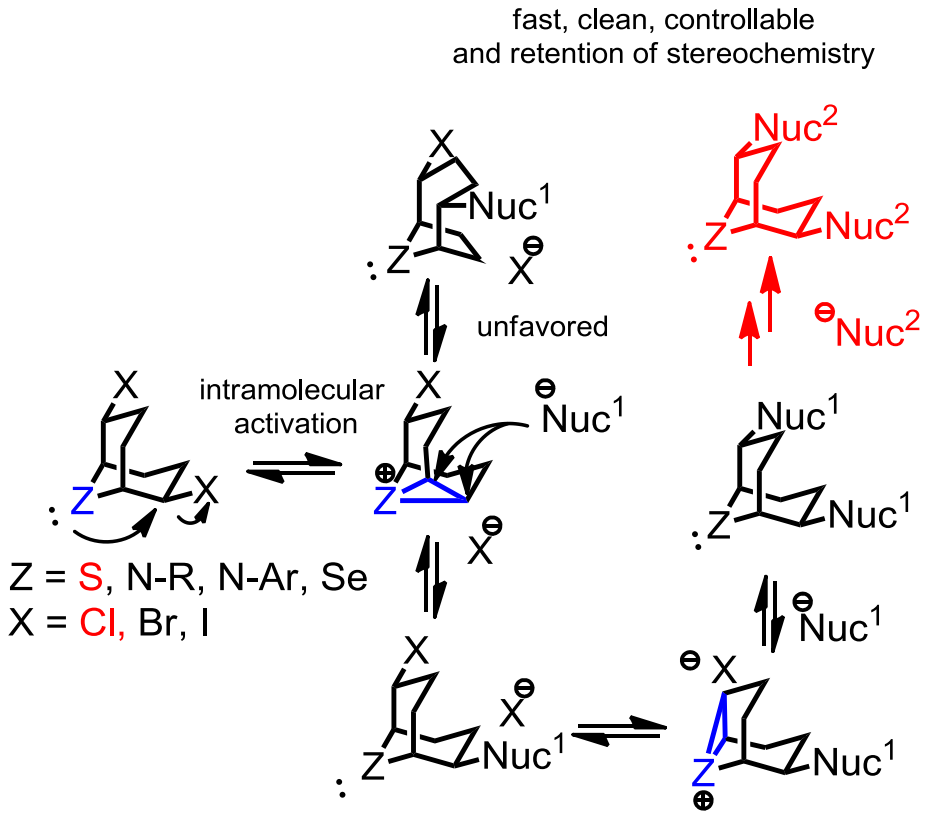

Figure 4 Mechanism of nucleophilic substitution based on anchimeric assisted substitution.

1.1.2.1 Synthesis of bicyclo[3.3.1]nonane electrophiles

Finn group revisited this old reaction and broadened the scope of nucleophiles to react with BCN dielectrophile in 2001[12]. Before that, although some literature reported the reactivity and stereochemistry retention of BCN compounds[13], there is no systematic work demonstrating the substitution reaction could be employed as a tool to assemble functional material modularly.

The optimized synthesis of thia-BCN has been previously developed[12]. The *anti*-dichlorosulfide is commonly synthesized through electrophilic addition of SCl_2 (or S_2Cl_2,

then SO_2Cl_2) to 1, 5-COD. The dual-chair structure of the bicyclo [3.3.1] skeleton prevented sulfenium ion from crosslinking double bonds to give polymerized side product. As a result, this type of compound is economically available and a convenient bivalent scaffold for anchimeric assisted condensation. With our advanced preparation method (Figure 5), this 2, 6-Dichloro-9-thiabicyclo[3.3.1]nonane can be made in 2 steps without purification of starting material-1, 5-COD-and recrystallized in 100 g scale at a cost of only approximately $30 per mole. 2, 6-Dichloro-9-selenabicyclo[3.3.1]nonane was synthesized in a similar way with $SeCl_2$, generated from elemental selenium and sulfuryl chloride in chloroform.

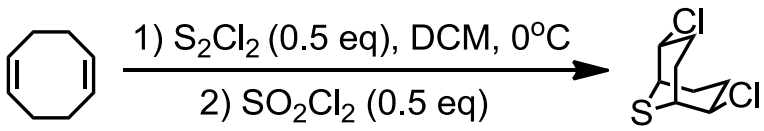

Figure 5 Improved synthesis of 2, 6-Dichloro-9-thiabicyclo [3.3.1] nonane.

2, 6-Dichloro-9-azabicyclo[3.3.1]nonane, a more interesting dielectrophile with an additional attachment point at nitrogen, was made via a different synthetic route. Early routes focused on the aminohalogenation of 1,5-COD, but the reactions were poorly reproducible. In contrast, ring-opening of the *cis*-diepoxide made from 1,5-COD was a better option. Mixtures of azabicyclo[3.3.1]-and [4.2.1]nonane diols were formed after ring-opening, and upon treatment with thionyl chloride yielded the thermodynamically more stable [3.3.1] product, as shown in Figure 6. The high yielding conversion of 1,5-COD to the starting *syn*-diepoxide catalyzed by methylrheniumtrixoide (MTO) makes this a practical route to synthesize large quantities (at least 1 gram) of aza-based BCN

electrophiles. A number of analogues having aromatic and aliphatic amines, in addition to the parent ammonia (NH) species, were synthesized as hydrochloride salts and were isolated as pure solids.

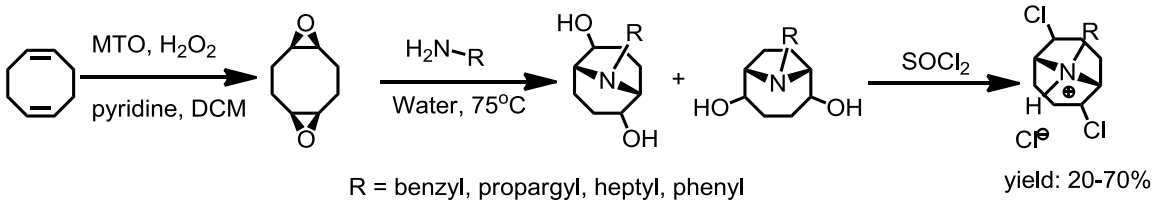

Figure 6 Synthesis of 2, 6-Dichloro-9-azabicyclo [3.3.1] nonane.

1.1.2.2 Substrate scope and reaction rates for substitution

A variety of heteroatom nucleophiles have been tested for this reaction including secondary amines, tertiary amines, N-containing heterocycles, halides, azides, alkoxides[12] and even Grignard reagents[14]. Majority of the substitution reactions worked very well in polar solvents including water, except for some bulky heterocyclic nucleophiles and tertiary amines.

Besides, the substitution reactions towards different types of BCN electrophiles have also been investigated. It was observed in previous study conducted in 2011 that the substitution rate increased by 1000 times when the internal nucleophile was changed from phenyl amine to selenium[15] (shown in Figure 7 adapted from Accurso's work in 2011). However, different external nucleophile towards the same BCN electrophile did not exert profound effects. Furthermore, the solvent was also proved to affect the rate dramatically.

Given other results generated from previous study, the formation of cyclic intermediate was confirmed to be the rate-determining step for this BCN-based anchimeric assistance.

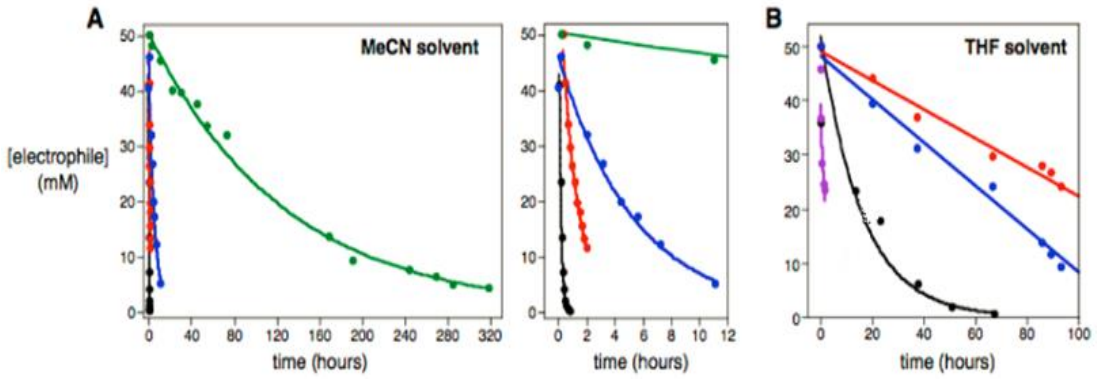

Figure 7 Substitution rate curves for different BCN electrophiles: Phenyl (green), propargyl (blue), sulfur (red), heptyl (black) and Se (purple). Each color represents an electrophile reacted with different internal nucleophile.

1.1.2.3 Reversibility of the reaction.

The biggest advantage of using BCN scaffold to generate privileged materials is the feature of reversible bond formation. This has also been examined previously by our group[12]. The thiocyanate and isothiocyanate substituted BCN adducts can be interconverted by heating, involving the elimination and re-addition of the SCN^- group. When performing the reactions in acetonitrile, substitution of DABCO immediately precipitated the resulting dications as the kinetic products, as shown in Figure 8. However, in methanol, everything stayed in solution, leading to the exclusive formation of the thermodynamically favored pyridine adduct in the presence of DABCO (Figure 9). Both of these phenomena showed that the bond between BCN electrophile and hetero-atom nucleophiles are reversible under specific conditions.

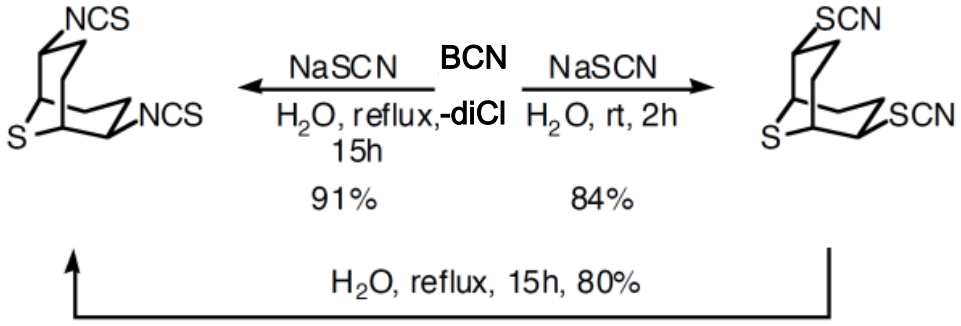

Figure 8 Reversible reaction of dichloro-BCN with thiocyanate.

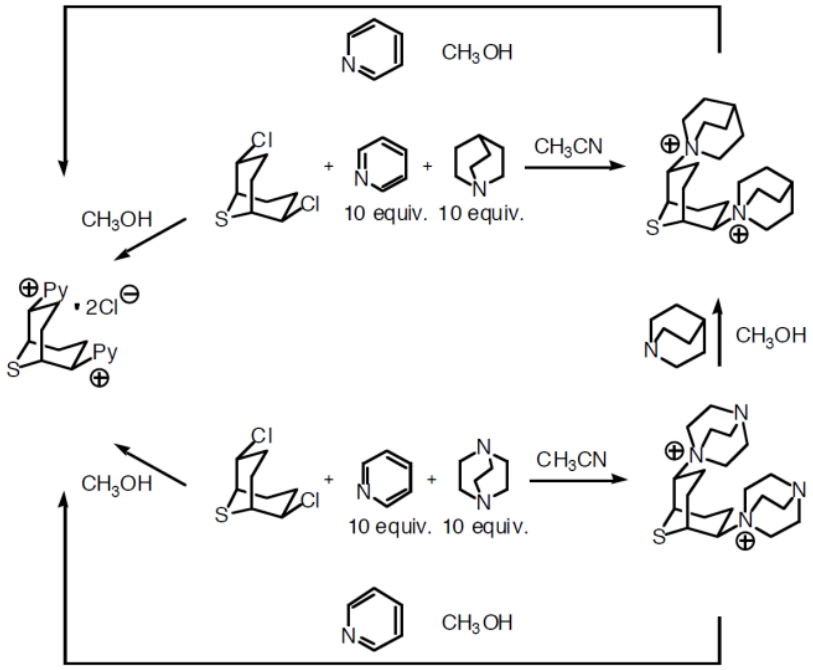

Figure 9 Competitions between pyridine and tertiary amine in acetonitrile *vs.* methanol.

The reversibility originated from the favorable placement of the internal nucleophile, balanced by the ring strain of the sulfonium intermediate. So a strong nucleophile is not required to capture the reactive intermediate at the first step of substitution, which at the

same time is also likely to be a not bad leaving group as well. The reversibility will be shut down when the inner nuleophile was deactivated, such as oxidation of sulfur (shown in Figure 10) or protonation of nitrogen in the electrophilic core.

Thus, it is promising to develop well controlled dynamic material for diverse applications as soon as the detailed fundamental fragmentation study is well established. Since a nontrivial number of nulceophilic substituted product examined for this reaction is charged species, it is of benefit to take advantage of the transformation from positive charged to neutral (by changing substituent) and build up materials based on that.

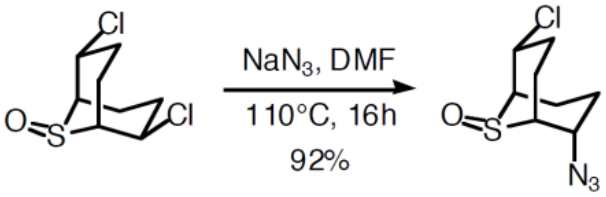

Figure 10 Mono-substituted product was obtained exclusively from substitution of oxidized BCN-dichloride at high temperature and with extended reaction time, indicating shut down of anchimeric assistance.

1.1.3 *Anchimeric assistance employed in polymer preparation and modification*

To bring this privileged BCN double substitution to full fruition, developing new method of employing it to build up polymers is necessary. However, according to the careful review of previous examples, employing anchimeric assistance in polymer synthesis was uncommon in contrast with the use of small molecule through this special mechanism. Some related examples are reviewed here.

Neighboring ester group, a non-privileged anchimer, was observed to assist the cationic ring-opening polymerization in some cases[16] (Figure 11).

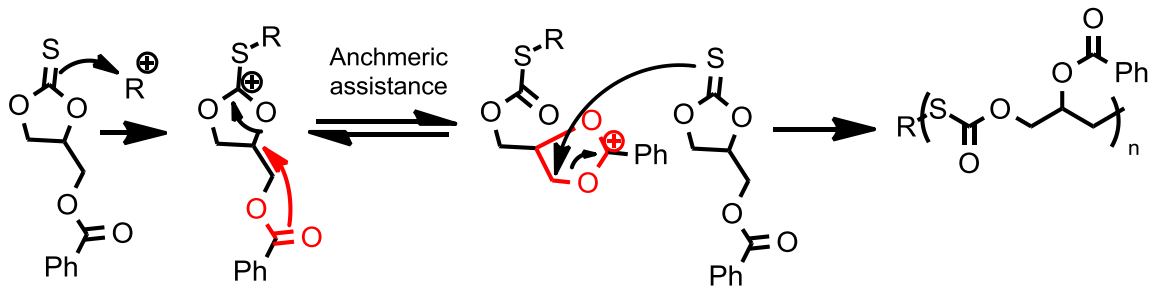

Figure 11 Cationic ring-opening polymerization of cyclic monothiocarbonates by neighboring group (labeled in red) participation (adapted from Nemoto's work in 2001) [16].

Dendrimers capped by 2-carbamoylbenzoates were built up and went through hydrolysis with assistance of neighboring carbamoyl moiety under basic condition (Figure 12). It showed the anchimeric assistance employable in fragmentable materials, even though the major component of dendrimer was not made from it[17].

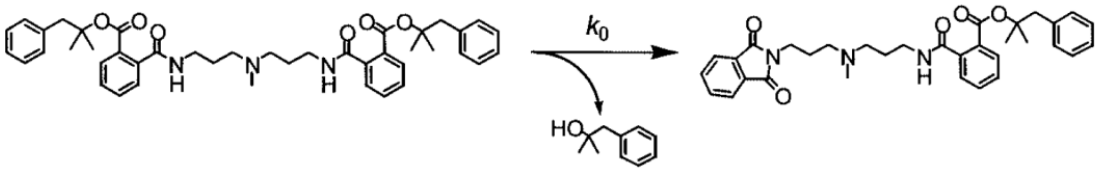

Figure 12 Schematic representation of the first step in the neighboring group assisted release of alcohol from dendrimer precursors (copied from Trachsel's work in 2009) [17].

The only related example of n-participation anchimeric assistance in polymer backbone construction was reported by Tirrell group in 1981. [18] Poly[(chloromethyl)thiirane] with mustard gas motif in main chain were synthesized and

reported to keep the potential to transform to another type of polymer after facile anchimeric assisted substitution. Still the chain propagation step was not related to anchimeric assistance (Figure 13).

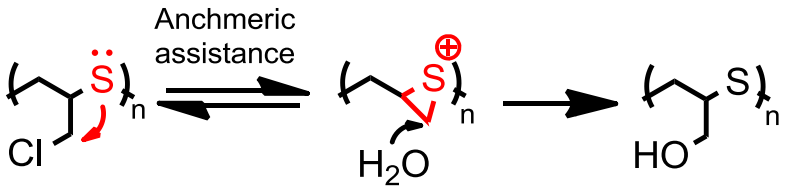

Figure 13 Anchimeric assistance by sulfur atom in the backbone of poly [(chloromethyl)thiirane] (adapted from Zussman's work in 1981). [18]

The limited study of polymer development associated with anchimeric assistance was due to the lack of superior reaction. According to the context provided in previous sections, the substitution based on BCN molecules is promising to give diversified material connected by dynamic covalent bond, easier to be controlled and more reliable. Thus, detailed fundamental study on adapting this reaction to condensation polymerization requirement and controlling the property of the resulted material are necessary.

1.2 Cationic polymers and their applications in chemical biology.

1.2.1 *Polycationic material for transfection*

1.2.1.1 General introduction of vectors for transfection

Transfection ("transformation" plus "infection") refers to the delivery of nucleic acids into eukaryotic cells for expression of desired (DNA) or silencing undesired (siRNA or RNAi) proteins. Efficient transfection will allow the treatment of disease from gene level.

However, cellular uptake of free nucleic acids is hindered by their charge, size, and instability in presence of enzymes[19]. Research over the last decades has focused on the development of novel carriers and strategies to improve the efficacy and safety of this process.

Transfection reagents are subdivided into viral and non-viral vector. While viruses are currently the most efficient transfection vectors, they suffer from a number of innate disadvantages (antigenicity, potential mutagenesis, limited size of cargo, etc) that jeopardizes their use as potential therapeutic agents[20].

As for non-viral reagents, it usually requires condensation of gene with positively charged cationic lipid or polymer based systems to enable binding of those condensation complexes to plasma membrane through electrostatic attraction and further be internalized by the cells[19].

1.2.1.2 Cationic polymers for transfection

Cationic polymers have gained significantly more attention because of the flexibility in polymer chemistries that allowed improvements to design, formulation, and precise control of structure and surface modifications enabling use in a plethora of biomedical applications[21]. Besides, larger nucleic acid loading capacity and ease of large-scale production are also the advantages compared with cationic lipid[22]. Various cationic polymers, both natural and synthetic, have been evaluated for transfection purposes[21].

Natural cationic polymers (including chitosan, gelatin, dextran, cellulose and cyclodextrin) have been extensively investigated due to being derived from renewable resources and low toxicity[23]. However, these materials showed batch to batch variation and have comparatively low efficiency due to the lack of positive charged centers, which can be overcome by synthetic polymers. For example, the block structures with degradable linkages and bioactive groups could be incorporated by various organic reactions and make it easy to catch up with other synthetic polycations due to high biocompatibility and biodegradability[24].

Several types of the most extensively studied synthetic cationic polymers are briefly summarized here in Table 1 (Adapted from Samal's review in 2012).

Table 1 Summary of cationic polymer developed for transfection.

Name	Nature	Structure
PEI	LPEIs (linear PEI) contain only secondary amines	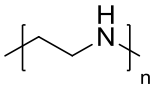
	BPEIs (Branched PEI) contain primary, secondary and tertiary amines	
PLL	Homopolymer of the L-lysine.	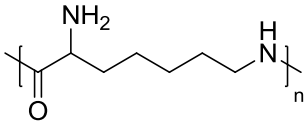
PAA	Synthetic cationic polymer containing tertiary amino groups.	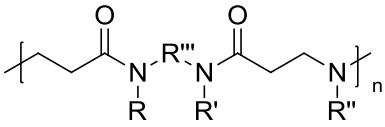
PAE	Amine containing polyesters	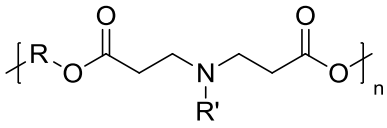
PDMAEMA	Synthetic cationic polymer containing tertiary amino groups.	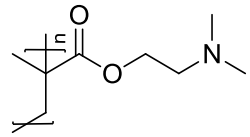

The motif that all of these synthetic cationic polymers share is amino groups, which readily turned into protonated charged form in intracellular condition. Linear, branched and dendritic examples have been developed for each type of polymer which usually possesses a combination of primary, secondary and tertiary amine[25-26]. In addition to amino groups, PAE and PDMAEMA also contain ester groups that are hydrolysable linkage at lower pH[27-28]. Though not degradable by themselves, PEI, PLL and PAA can still be turned into biodegradable materials with incorporation of pH, light or reduction sensitive linkages connecting the repeating units. Thus, they still constituted the majority of polycations developed for transfection[29].

1.2.1.3 Obstacles in transfection and requirement for new generation of polycationic material

Though synthetic polymers show great potential, their low gene transfection efficiency greatly limits their clinical applications. For instance, polyethylenimine (PEI), one of the few most effective and versatile polymeric core vectors, remains around 10^5 times less efficient than its viral counterpart[30]. A recent review attributed that to the potential "slits" the complexes made of polymeric vectors and DNA therapeutics have to pass, including endocytosis, escape from endolysosomal entrapment, eventual release of DNA from the polyplexes and so on (the whole detailed mechanism of transfection was proposed in 2002 in Figure 14 here). A lot of them are affected by the strength of interaction between the nucleic acid and the carrier[31].

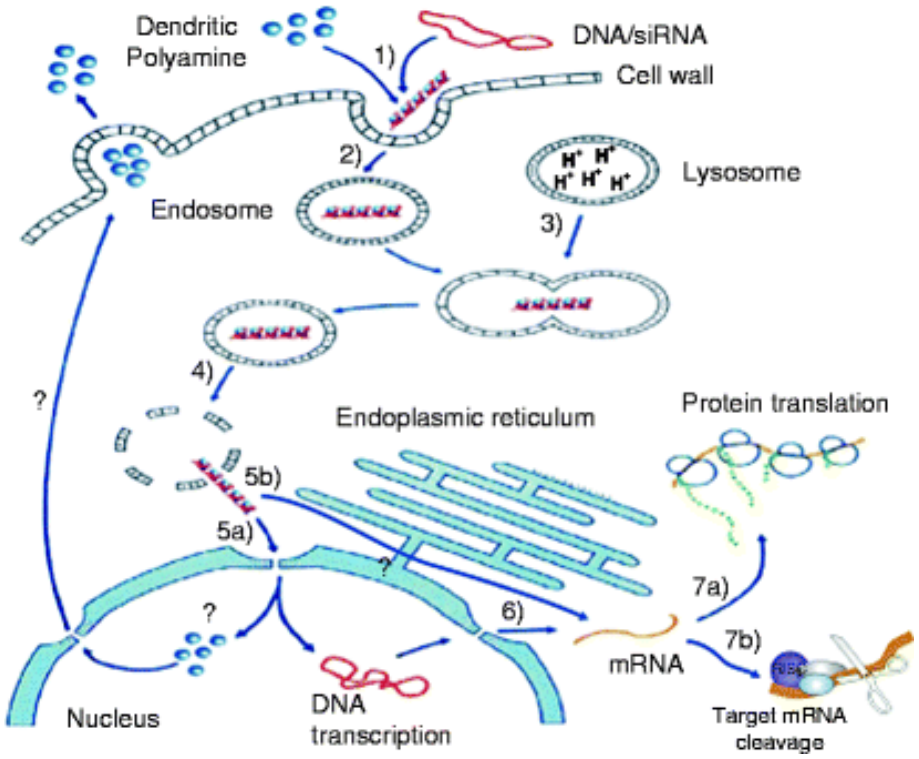

Figure 14 Mechanism of gene transfection in general. (1) formation of the complex (polyplex), (2) endocytosis of the polyplex, (3) fusion of endosome and lysosome, (4) release of the polyplex into the cytosol, (5a) incorporation of the polyplex into the nucleus, (5b) release of the siRNA into the cytosol, (6) transcription of the DNA into mRNA followed by release of the polyamine back into the cytosol, (7a) translation of mRNA, and (7b) mRNA degradation. Copied from Haag's review in 2010[31].

The first step of transfection is to condense nucleic acid into small polyplexes which is easier to be taken up through endocytosis by cells. The predominant process of polyplex uptake is receptor mediated or dependent. As for smaller polyplexes (< 200 nm), they are generally taken up through the clathrin pathway[32].

The molecular weight and chain length of a polymer have a significant effect on its cellular uptake[33]. The longest PEI chains commonly used in transfection reached 25 kDa. High-molecular-weight (HM_w) polymers showed better DNA binding (reducing the size of

polyplex and bringing more effective positive charges to backbone), compared with same weight concentration of Low-molecular-weight (LM_w) polymer, and thus leading to more effective cellular uptake. Several research groups have reported that at least six to eight charges per single polymer chain are required for effective nucleic acid condensation[34]. However, this may not apply to other types of polymer and also longer polymers are not always facilitate overall nucleic acid delivery. For example, Wu et al. reported higher transfection efficiency in LM_w (7 kDa) disulfide-PEI transfected cells compared with HM_w (400 kDa) disulfide-PEI[35]. These could be attributed to both lower cytotoxicity (which is believed to originate from membrane disruption caused by hydrophobic moieties on the polymer) and better DNA unpackaging ability, which will be mentioned again in later discussion.

Charge density and rigidity of polymer chain are also affecting the transfection efficiency[36]. It is intuitive that having more protonated N centers per mass will facilitate the assembly of polyplex, and thus tertiary amine will be more efficient than primary amine due to higher basicity. Studies that both support and contradict this trend have been reported[37]. When the rigidity of main chain is increased, such as addition of a rigid ring in monomer, colloidal stability of the polyplex will be diminished, leading to weak binding between polymer and nucleic acid. Besides, cellular uptake can be further enhanced by grafting targeting ligands onto polymers for targeted delivery of cargo[38].

Once taken up into the cells, polyplexes have to escape through the endosomal pathway to release the siRNA or DNA into the cytoplasm[32]. The endosomal pathway starts with the early endosomes, which become progressively acidic as they mature into

late endosomes (pH 5-6) and ends with the fusion with the lysosomes (pH 4-5) and the content is then degraded by enzymes[39].

The majority of cationic polymers that successfully mediate efficient nucleic acid delivery benefits from their strong buffering capacity in the pH range from 5 to 7[33, 35, 39-40]. It is hypothesized that polyamines prevent acidification of the endosomes by acting as "proton sponges" (Figure 15). This leads to an increase in proton influx followed by an enhanced accumulation of counterion and osmotic swelling[41].

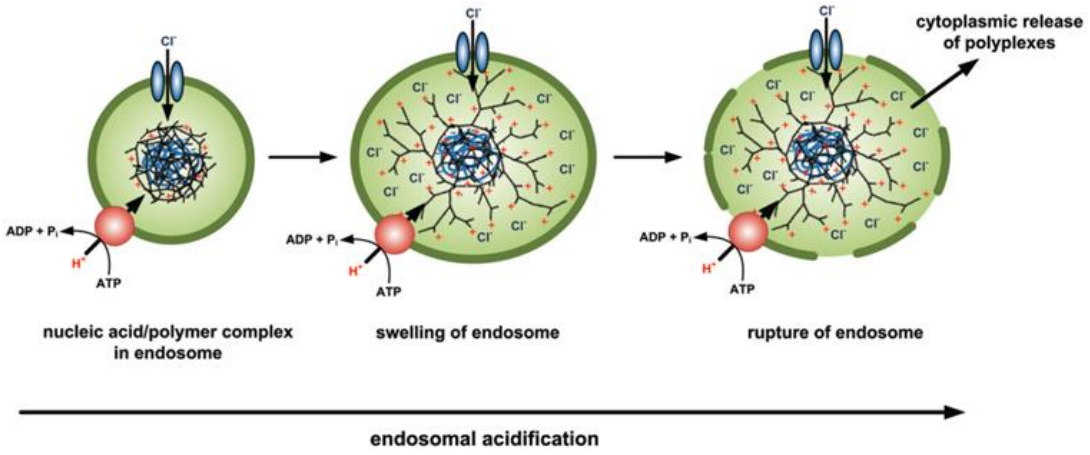

Figure 15 Endosomal rupture mediated by polymers with a buffer capacity in the endosomal pH range which can trigger (a) the proton-sponge effect and (b) polymer swelling according to the umbrella hypothesis. It is copied from Sonawane's review in 2003.[41]

An extension of the proton-sponge effect was introduced with the umbrella hypothesis, which describes the ability of polymers to expand volumetrically when protonated at lower pH. The polymer will unfold from a collapsed state into an extended conformation after protonation of amino groups due to the electrostatic repulsion of the neighboring charged amino groups. Tang et al. have shown that this increase in volume

caused by polymer swelling contributes to endosomal escape of the polyplexes[42]. This effect also accounts for higher transfection efficiency of dendritic polymers and highly hyper-branched polymers in some cases.

Polyplexes are required not only to have high stability to ensure the cargo is protected from serum enzymes, but also be able to disassemble at the right time and location enabling the release. This has been identified as a long-time overlooked barrier for efficient gene delivery[34, 43]. As mentioned before, shorter polycations have a higher probability of dissociating from nucleic acid, enabling higher gene expression over a short period of time. The compromise is higher polymer to DNA ratio to maintain stability of polyplex[44]. One goal of current carrier design should be to strike an optimal balance between protection and release in order to maximize transfection.

Though a bunch of acid-cleavable linkers and cytosolic reductive linkers, such as ester[29], acetals/ketals[45], imines[46] and disulfide bond[47] (these reversible reactions are shown in Figure 16), have been smartly employed in connecting branched PEI into stimuli responsive transfection material, the challenges still exist. It still remains unclear that where polyplexes should be disassembled to achieve efficient gene silencing or expression[22, 36, 42, 44-52]. For DNA delivery, this question will be expanded to nuclear internalization, which is another barrier after endosome escape[53]. But even for siRNA, which directly function at RNA-induced silencing complex (RISC) in cytoplasm, protection after endosome escape could be still desirable due to the fragility of siRNA, especially under acidic condition of endosome[54]. With the acidic sensitive linker, it is possible that the polymer will fragment into small pieces and dissociate from nucleic acid

in endosome, thus the premature protection loss will be harmful for efficient delivery. Furthermore, the fragmentation will not be able to degrade polycations into monomeric constituent units in experimental time scale, which means toxicity is hard to be dramatically lowered[52, 55].

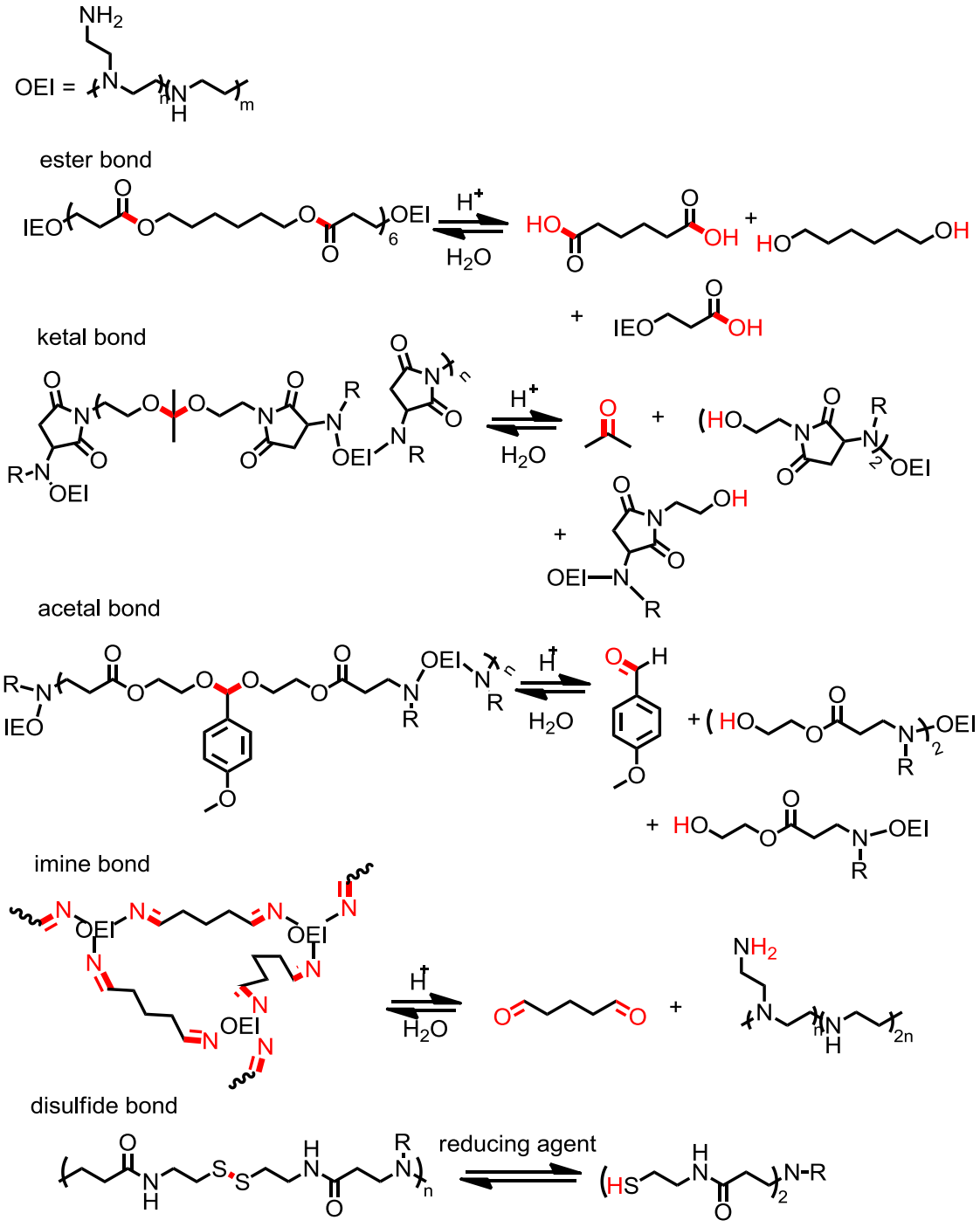

Figure 16 Reversible bond formation used in transfection vector synthesis. Reversible bonds are highlighted in red.

1.2.2 *Polycations for antimicrobial*

1.2.2.1 Resistance development against traditional antimicrobial

Microbial infection is one of the major challenges to human health worldwide. Millions of deaths are caused by infectious diseases and defective medical device or equipment resulted from the bacteria growth.[56] A variety of drugs have been developed to combat bacterial infection. However, due to the injudicious usage of these drugs, some bacteria have acquired resistance to most of them over the years. Nowadays researchers aim to develop novel antimicrobial drugs that can wipe out pathogenic bacteria before the emergence of resistance.[57] Thus, in order to treat infections, it is essential to reduce bacteria resistance towards antimicrobial compounds.

There are several classes of most commonly used antimicrobial compounds: quaternary ammonium compounds (QACs), silver nanoparticles (AgNPs) and antimicrobial peptides (AMPs) in addition to traditionally used small-molecule antibiotics, such as penicillin.

Traditional small-molecule antibiotics based on the inhibition of key enzymes are susceptible to the development and rapid dissemination of mutations in the target that already confer resistance in the past decades and call for substitutions[58]. AgNPs is usually classified as more environmental unfriendly compounds due to their transformation product's long half-life, general accumulation and toxicity towards live organism[59].

QACs has also been used widely as broad spectrum antimicrobials since they target bacteria membrane which requires more genetic mutations.[60] Thus those small QACs have been touted as being difficult to generate resistance against, but this is proving to be

incorrect by recent reports.[61] Commercial antimicrobial QACs have high stability and therefore show inevitable accumulation in the environment. Long exposure of sublethal doses of QACs will drive the evolution and finally the selected strains will be immune to similar structures.[62] However, this mechanism has not gathered enough attention towards current development of new antimicrobials.

AMPs, primarily also cationic in nature, are a class of larger molecules often used by microorganisms for defensive purposes. While it has been stated or supposed that resistance to these agents is harder to develop, their natural origin ensures that a variety of resistance mechanisms are known to exist or can be evolved.[63] Still, the ability of natural antimicrobial peptides to disrupt bacterial membrane integrity has inspired the development of many different types of charged synthetic oligomers or short polymers.[64-66] Since a great number of these molecules have been reported to successfully resist the natural defence mechanisms, they represent a promising approach towards antimicrobial applications.

The slow resistance development to charged oligomers/polymers may be attributed to its multivalent display of charged center. It has been reported that even for the small QACs, increasing the number of charge centers from one to two will significantly reduce the probability of emergence of resistance. A variety of polycations have been tested as potential antimicrobials and the resistance development is also taken into consideration, including polyionenes[67-68] and polymers acquired from controlled polymerization with charged groups installed onto side chain (shown in Figure 17).

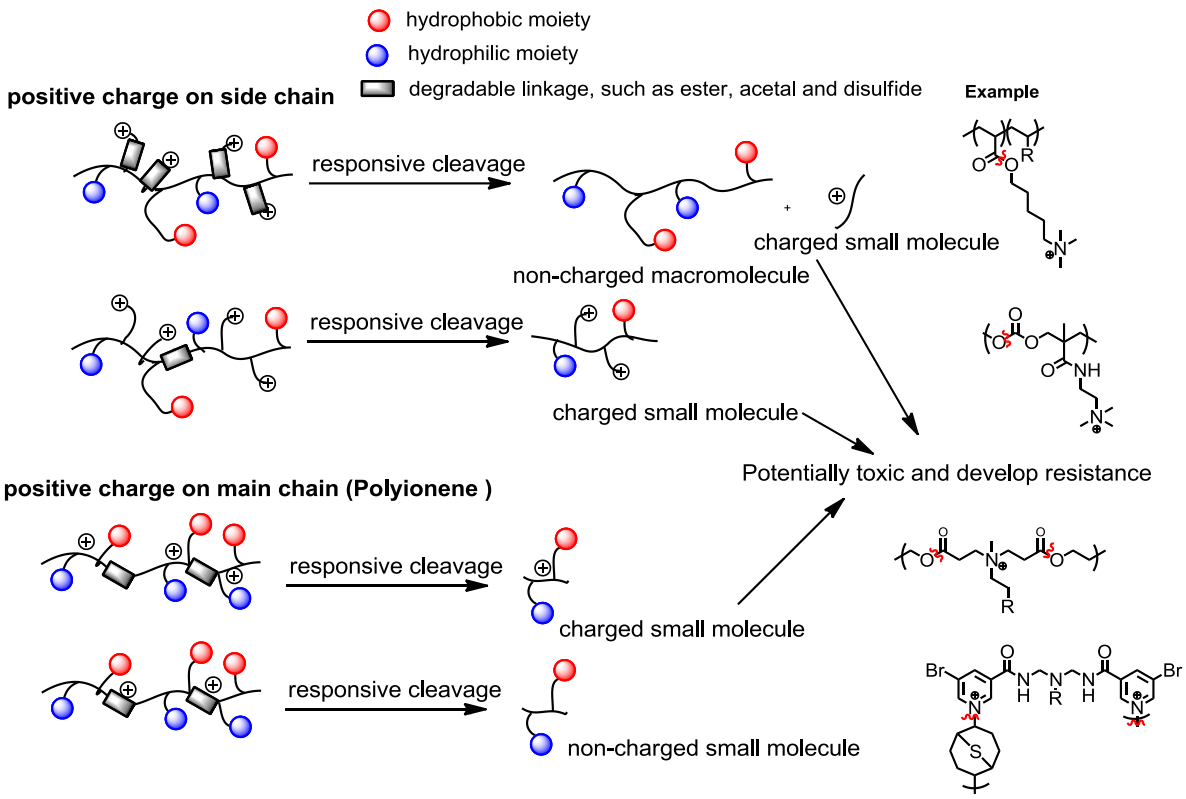

Figure 17 Classes of degradable polycations and their potential towards resistance development.

1.2.2.2 Biodegradable polycations and their potentials as antimicrobial materials

Currently the antimicrobial resistance has been characterized mainly through two dimensions. The most common way is to monitor the changes in MIC (minimum inhibition concentration) after repeated use of drugs at sub-lethal doses. This assay usually requires certain concentration of healthy bacteria cells at logarithmic growth phase to be treated with a series of drug solution with varying concentration over a number of weeks, which is not trivial to perform.

Another way to confirm the potential of anti-resistance-development from material/molecule is to examine its activity towards clinically isolated drug-resistant bacterial strains, the most common example of which is MRSA (methicillin resistant *Staphylococcus aureus*). A variety of cationic compounds, both small molecules and macromolecules, have been confirmed to be effective towards superbugs, which were resisted to most common traditional antibiotics[69]. However, the strains resisting QACs have not been widely tested in new antimicrobial cationic materials yet. Combining with the long-term monitoring MIC, the test against strains with already developed resistance will assist in the design and development of new generations of antimicrobial cationic polymers.

Conventional antibiotics, such as ciprofloxacin, have become the most popular benchmark to be compared with novel cationic polymer in this method.[67] It has been clearly proved that cationic polymer has great potential in reducing the rate of resistance development, however, the comparison between different types of cationic polymers is still lacking. In some recent reviews, degradable QAC has been introduced as the newest interesting leading design. Thus, novel degradable polycations, multivalent version of QAC, might lead to a solution to slow down the resistance development.

Not only benefiting from slow resistance-development, biodegradable cationic polymers are also facilely employed as building blocks for various biomaterials. Wound dressing materials were usually required to break down in a certain time window while maintaining antimicrobial function. Both natural and synthetic polymer based hydrogel could incorporate degradable cationic motif.[70] After the materials were broken down, the

degraded product in low molecular weight was expected to be less toxic and easy to be metabolized.

Another application is to coat degradable polycations on the surface of bulk material or device. Each layer of coating is decorated (covalently attached) or packed (via supramolecular interaction) with cationic antimicrobial components.[68, 71] After one layer is exhausted or fouled, the environmental stimulated degradation will regenerate an active antimicrobial surface to kill bacteria. This mechanism allows slow release of antimicrobials from the surface to the outer environment, which could help reducing the bacteria resistance.

CHAPTER 2. THIABICYCLONONANE-BASED FRAGMENTABLE CATIONIC ADDUCTS AND POLYCATIONS

（Chapter 2 is adapted with permission from
Geng, Z.; Finn, M. G., Fragmentable Polycationic Materials Based on Anchimeric Assistance. *Chemistry of Materials* **2016,** *28* (1), 146-152.
Geng, Z.; Finn, M. G., Thiabicyclononane-Based Antimicrobial Polycations. *Journal of the American Chemical Society* **2017,** *139* (43), 15401-15406.）

A new family of modular, fragmentable cationic adducts, oligo- and polycations has been developed based on the reactions of 9-thiabicyclo[3.3.1]dichloride and related compounds with substituted dipyridyl nucleophiles by an anchimeric assistance mechanism. Each bond-forming event in this condensation polymerization process generated a positive charge in the main chain. Product lengths were found to be dependent on the reactivity of the electrophile, which was tunable by changing the nature of the leaving group β to sulfur. Both monomers were easily synthesized. The polycations decomposed by hydrolysis at rates dependent on the leaving-group ability of the pyridyl unit, which correlated roughly with the pK_a of its conjugate acid. Polymer decomposition occurs simultaneously throughout the length of the chains, rather than from the ends.

2.1 Novel active thiabicyclo[3.3.1]nonane electrophile

While the substitution chemistry of BCN compound **1a** (Figure 18, X = Cl) is quite clean, its reaction rate at room temperature (rate constant ≈ 2.4×10^{-4} $M^{-1}s^{-1}$) and thermodynamic driving force were thought to be incompatible with the generation of long polymers by the simple condensation route outlined in Figure 18.

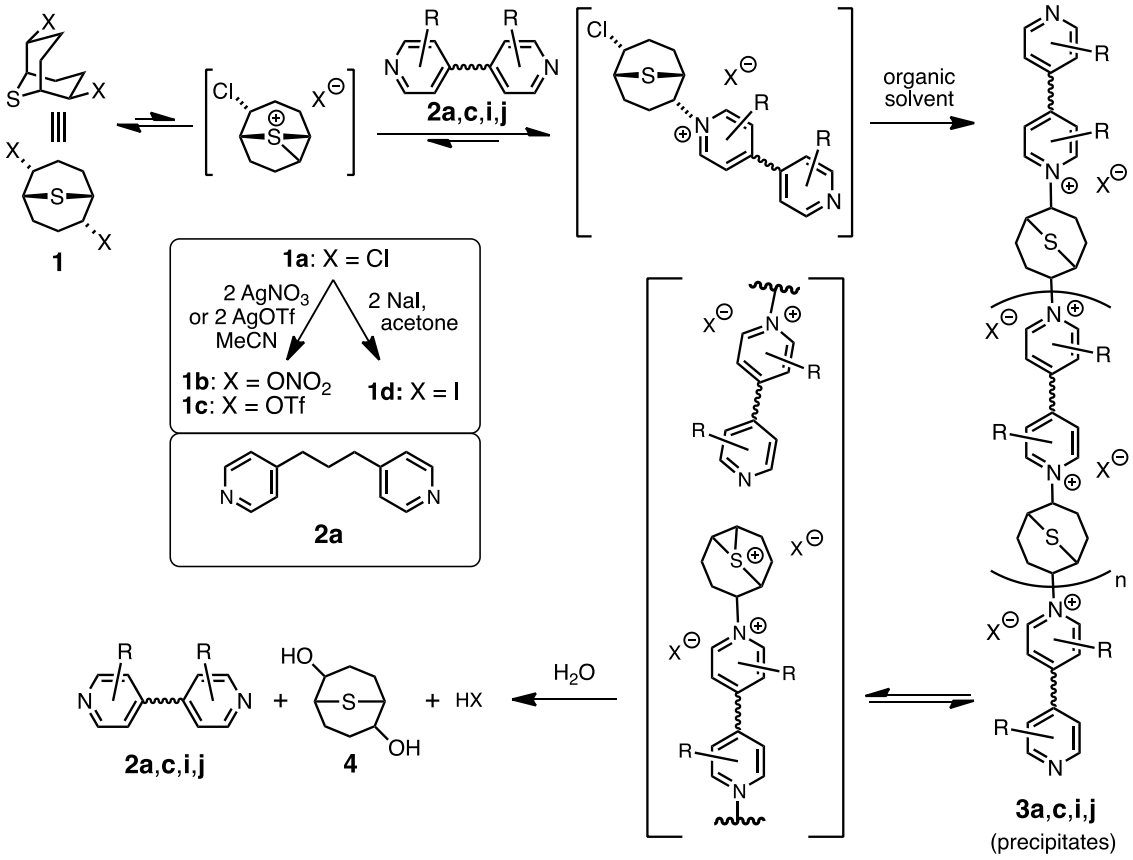

Figure 18 Schematic representation of BCN-based condensation polymerization and depolymerization, both processes taking place via anchimeric assistance.

Different halophilic transition metals were tested for their ability to speed the substitution reactions of **1** by interaction with the leaving group, accelerating the rate-limiting formation of the strained episulfonium intermediate. Representative Al, Sn, and Pd species showed no effect (Table 2). Silver salts were quite effective, prompting the isolation of the resulting intermediates as described below.

Table 2 Survey of halophilic metal complexes for the acceleration of reactions of 1 with $PhCH_2NH_2$ (10 equiv) in acetonitrile at room temperature.

Entry	Halophilic metal complex	Reaction time
1	None	16 h
2	AgOTf	2 h
3	$AgNO_3$	4 h
4	$AlCl_3$	>16 h
5	$SnCl_2$	14 h
6	$PdCl_2$	12 h
7	$Pd(OAc)_2$	14 h
8	$Zr(Cp)_2Cl_2$	>16 h
9	$Pd(PPh_3)_2Cl_2$	>16 h

Treatment of **1a** with silver nitrate or silver triflate in acetonitrile afforded **1b** or **1c** in high yield after filtration of AgCl. The triflate **1c** proved to be the most reactive, but was not useful under practical conditions because of its high sensitivity to hydrolysis with atmospheric moisture or trace water in the solvent. The nitrate derivative **1b**, in contrast, was stable enough to be separated and characterized by ^{1}H NMR. The apparent Finkelstein reaction of **1a** with sodium iodide in acetone gave **1d** in high yield, which was similarly stable to isolation by filtration and characterization. The NMR spectra revealed significant differences in the chemical shift of the equivalent H atoms on C1 and C5, suggesting that the order of reactivity would be iodide (**1d**) ≥ nitrate (**1b**) > chloride (**1a**), correcting for the upfield shift characteristic of C-H bonds next to iodine due to factors unrelated to the electron density of the C-halogen bond[72].

A preliminary assessment of substitution reactivity was obtained by competition reactions in which an equimolar mixture of two electrophiles was treated with half an equivalent of benzylamine (Figure 19). These pairwise comparisons, as well as reaction of all three electrophiles together confirmed the above order of reactivity, with nitrate approximately 10 times more reactive than chloride, and iodide at least 5 times more reactive than nitrate. These differences are expected to be general since the reaction rate is only weakly dependent on the nature of the capturing nucleophile.

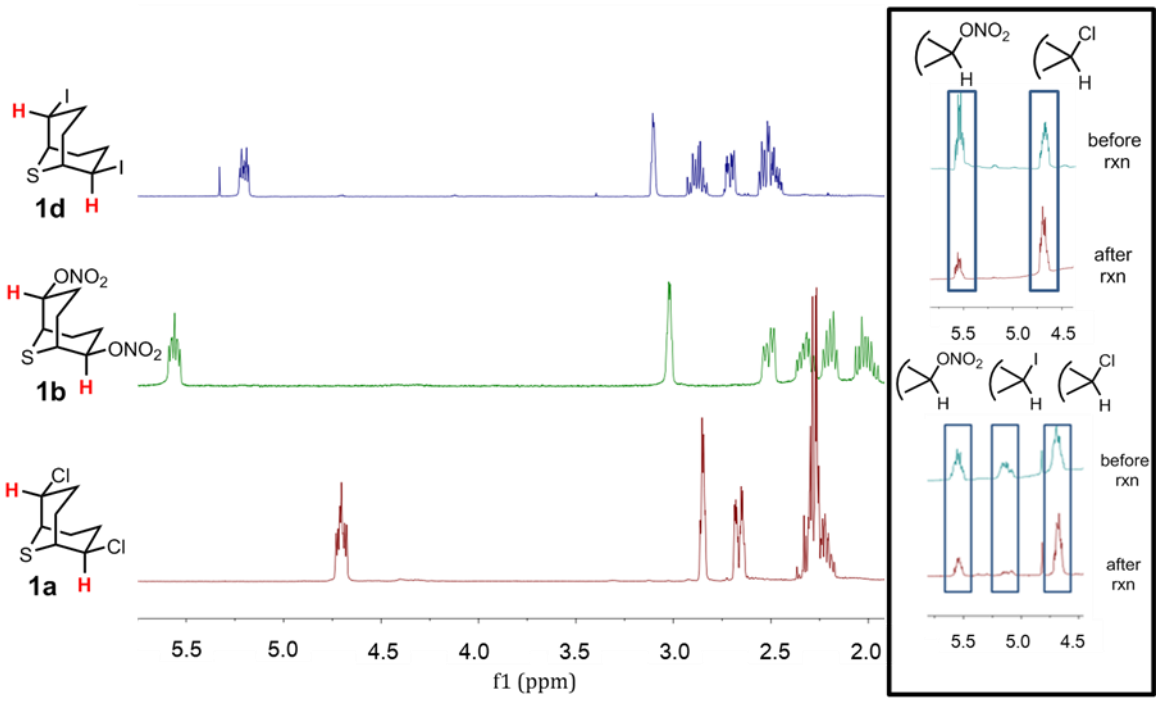

Figure 19 (Left) 1H NMR spectra of BCN electrophiles. (Inset) C1/5-H 1H NMR resonances of equimolar mixtures of pairs of electrophiles after reaction with 0.5 equiv. of benzylamine, confirming the reactivity order iodide > nitrate > chloride.

2.2 Synthesis and fragmentation of cationic adduct

The previously-reported[73] parent pyridine derivative **5a** was highly stable toward fragmentation in water (less than 5% hydrolysis observed after 1 week at 50 °C), so pyridine nucleophiles were chosen to include primarily electron-withdrawing groups to enhance this rate. Such pyridine derivatives are necessarily poorer nucleophiles for the forward step, so the enhanced reactivity of **1b** was essential to the efficient synthesis of the corresponding substituted pyridine dicationic adducts, as shown in Table 3. Each adduct dinitrate was isolated, characterized, and heated at 50 °C in deuterated buffer; following the disappearance of the adduct by NMR, first-order rate constants of fragmentation were

obtained. The NMR spectra also confirmed the clean nature of the reaction, giving diol **4** and the released pyridines.

Table 3 Comparison of pseudo first order fragmentation of pyridine adducts at 50 °C; pK_a refers to the conjugate acid of the pyridine calculated using Advanced Chemistry Development (ACD/Labs) Software V11.02 (© 1994-2015 ACD/Labs).

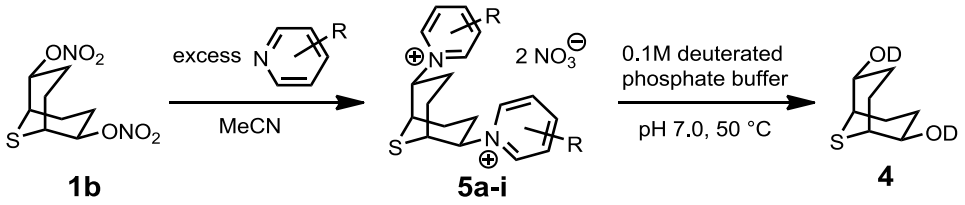

1b **5a-i** **4**

Cpd	R	pK_a	k_{frag} (h^{-1})	k_{rel}	half life (h)
5a	H	5.23	< 1 x 10^{-4}	-	-
5b	3-CO_2Me	3.19	(3.03 ± 0.38) ×10^{-2}	1.86	23.2 ± 3.1
5c	4-CO_2Me	3.16	(3.66 ± 0.33) ×10^{-2}	2.25	19.1 ± 1.8
5d	3-CO_2NH_2	3.54	(3.18 ± 0.32) ×10^{-2}	1.95	21.7 ± 1.8
5e	4-CO_2NH_2	3.39	(1.62 ± 0.10) ×10^{-2}	1.00	42.7 ± 2.7
5f	3-Br	2.87	(6.59 ± 0.58) ×10^{-2}	4.05	9.9 ± 1.1
5g	3-CN	1.78	(74.8 ± 5.4) ×10^{-2}	46.2	0.9 ± 0.1
5h	3-CF_3	2.8	(10.8 ± 0.98) ×10^{-2}	6.68	6.4 ± 0.8
5i	3-Br, 5-OMe	2.26	(7.51 ± 0.53) ×10^{-2}	4.64	9.2 ± 0.8

Table 4 Comparison of pseudo first order fragmentation of pyridine adducts at 37 °C.

Cpd	R	pK_a	k_{frag} (h^{-1})	k_{rel}	half life (h)
5c	4-CO_2Me	3.16	(0.16 ± 0.01) ×10^{-2}	0.3	422±41
5g	3-CN	1.78	(5.87 ± 0.71) ×10^{-2}	11	11.8±1.9
5h	3-CF_3	2.8	(1.14 ± 0.16) ×10^{-2}	2.1	61±8
5i	3-Br, 5-OMe	2.26	(0.55 ± 0.04) ×10^{-2}	1	127±10
5j	3-Br, 5-CO_2NH_2	1.22	(9.34 ± 0.87) ×10^{-2}	17	7.4±0.5
5k	3-Br, 5-CO_2Me	0.84	(11.9 ± 1.13) ×10^{-2}	22	0.24±0.01
5l	3-CO_2Me, 5-CO_2Me	1.16	(10.9 ± 1.81) ×10^{-2}	20	0.27±0.01

The stability of pyridine adducts to fragmentation in water was found to roughly correlate with pyridine basicity (Figure 20). This is consistent with the idea that more

nucleophilic pyridine groups are more difficult to eject from the pyridinium adduct structure, and that Brønsted basicity is indicative of nucleophilicity. In practice, half-lives were shown to vary over a 40-fold range (Table 3). Decomposition rates at 37 °C, tested for potential applications *in vivo*, were found to be much slower than at 50 °C, as expected for a fragmentation reaction. (For example, **5c** underwent hydrolysis approximately 23 times faster at 50 °C than at 37 °C.) To tune these potential release rates to a reasonably fast range, two electron-withdrawing groups were used, taking care to leave the *ortho* positions free to avoid steric problems in adduct formation (Table 4). Some additional limits were imposed on the process by the observation that pyridines having too many (or too potent) electron-withdrawing substituents were unable to react cleanly with **1b** or **1d**. For example, the strongly electron-deficient 3-bromo-5-amidopyridine (calculated pK_a = 1.22) did not form a clean adduct unless reacted with the most reactive ditriflate electrophile, **1c**. The resulting compound **5j** underwent relatively fast fragmentation (half life less than a day), as expected. EWGs such as this, having a carboxylate-based substituent, should allow us to link such pyridines together to make higher-valent monomers for the synthesis of fragmentable polymers and crosslinked materials.

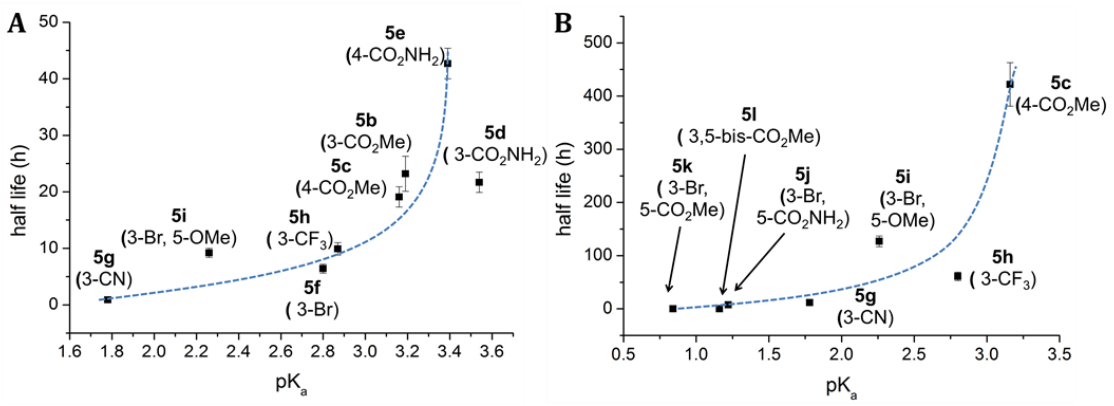

Figure 20 (A) Adduct half life at 50 °C *vs.* pyridine basicity, Table 3. (B) Adduct half life at 37 °C *vs.* pyridine basicity, Table 4. In each case, pyridine basicity is indicated by the calculated pK$_a$ of the conjugate acid. Dotted lines are meant simply to highlight the approximate trends, and are not mathematical fits.

2.3 Synthesis, characterization and fragmentation of polycations

The condensation polymerization of a dipyridine nucleophile and BCN electrophile was explored using the parent compound **2a** (Figure 18, Table 5). Reaction of **1a** and **2a** in MeCN solvent at 50 °C, conditions that produce good yields of adducts with pyridine itself, give only small oligomers (average n = 3). In contrast, dinitrate **1b**, generated in situ from **1a** and $AgNO_3$, gave copious quantities of precipitate within two minutes of mixing with an equimolar amount of **2a**, all in MeCN. Filtration and washing provided the corresponding species **3a**•$(NO_3)_{2n}$.

Characterization of this material was aided by its high solubility in water and by the fact that the second substitution event on each BCN core is usually faster than the first, so that chains are capped by the pyridine nucleophile. ^{1}H NMR in D_2O therefore showed distinct residues for non-alkylated pyridines at each end, enabling an estimate of average

chain length of approximately n=10 for **3a** prepared under these conditions (molecular weight approximately 4000, an example shown in Figure 21). Gel permeation chromatography (GPC) analysis also showed minor fractions with longer retention time, consistent with shorter chains or cyclic oligomers.

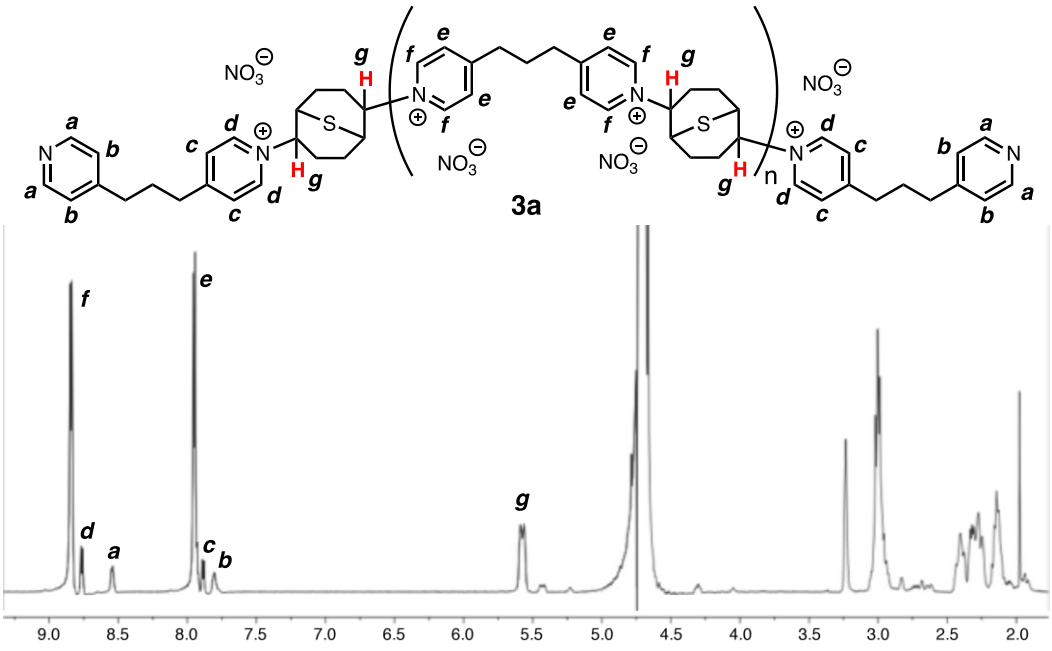

Figure 21 ^{1}H NMR spectrum of oligomer made from 1b and 2a (Table 5, entry 3).

Somewhat higher molecular weights were obtained with heating to 50 °C (n ≈ 13), or with the use solvents better able to support the developing polycation and therefore to delay precipitation until longer chain lengths are achieved. In a brief survey of activating silver salts and solvents, the use of $AgPF_6$ in DMSO was found to give the largest average molecular weights as determined by NMR end-group analysis (Table 5); dispersity could not be assessed because of the lack of suitable GPC standards (values obtained against dextran standards in water were wildly divergent from estimates made by NMR) and

because m/z values for molecules of different chain lengths are close enough to make deconvolution of the mass spectra of these mixtures impossible. Values of hydrodynamic radii determined by dynamic light scattering were comparable with those of ammonium ionenes with similar degrees of polymerization.[74] Analysis by TGA showed representative oligomers to have the anticipated stability (decomposition initiation at approximately 200 °C), and DSC revealed discrete glass transitions to be rare, both consistent with materials that are potentially dynamic at higher temperatures.

Table 5 Condensation polymerization of 1a + 2a.

entry	[**1a**] = [**2a**] (M)	additive (2 equiv)	solvent	temp.	M_n (kDa)	n[a]
1	0.1	None	MeCN	50 °C	1.5	3
2	0.1	None	THF/H_2O	RT	--	--
3	0.1	$AgNO_3$	MeCN	RT	4-5	8-10
4	0.1	$AgNO_3$	MeCN	50 °C	6	13
5	0.1	$AgNO_3$	THF/H_2O	RT	--	--
6	0.1	$AgBF_4$	DMF	RT	5.3	10
7	0.2	$AgNO_3$	DMSO	RT	9	18
8	0.2	AgOTf	DMSO	RT	11.5	23
9	0.4	$AgPF_6$	DMSO	RT	22.2	35
10	0.2	$AgBF_4$	DMSO	RT	11.4	22

a) n = average degree of polymerization

Using the conditions of Table 5, three additional oligocations were prepared from the bis(pyridine) linkers as shown in Table 6. The synthetic procedure proved to be modular, giving oligomers of similar size ($n \approx 10$) with the same methods of isolation and analysis. The stabilities of these compounds toward fragmentation under aqueous conditions were assessed by NMR in deuterated buffer, following the disappearance of the thiabicyclononane C-H resonance adjacent to the pyridine group (position *g* in Figure 21)

and the appearance of the corresponding resonance (4.3 ppm) for the diol product **4** (Figure 22).

Table 6 Representative oligocations and half lives of fragmentation in aqueous buffer (pH 7).

nucleophile monomer	polymer	n	synth.[a]	temp (°C) [b]	half life ($t_{1/2}$)	$t_{1/2}$ of small-molecule analogue
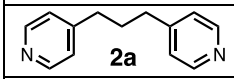 **2a**	**3a**•$(ONO_2)_n$	10	entry 3	37	no decomp.	n/a
			entry 3	50	no decomp.	n/a
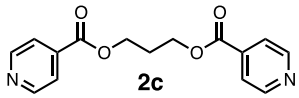 **2c**	**3c**•$(ONO_2)_n$	10	entry 3	37	624 h	422 h at 37°C (**5c**)
			entry 3	50	36 h	19 h at 50 °C (**5c**)
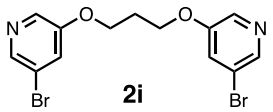 **2i**	**3i**•$(ONO_2)_n$	6	entry 3	37	70 h	127 h at 37 °C (**5i**) 9.2 h at 50 °C (**5i**)
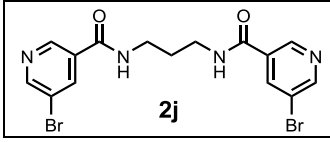 **2j**	**3j**•$(OTf)_n$	6	entry 8	37	9.2 h	5.8 h at 37 °C (**5j**)

(a) Synthetic method used to prepare the polymer, as described in the indicated entry in Table 3. (b) Temperature at which polymer decomposition was measured in aqueous buffer.

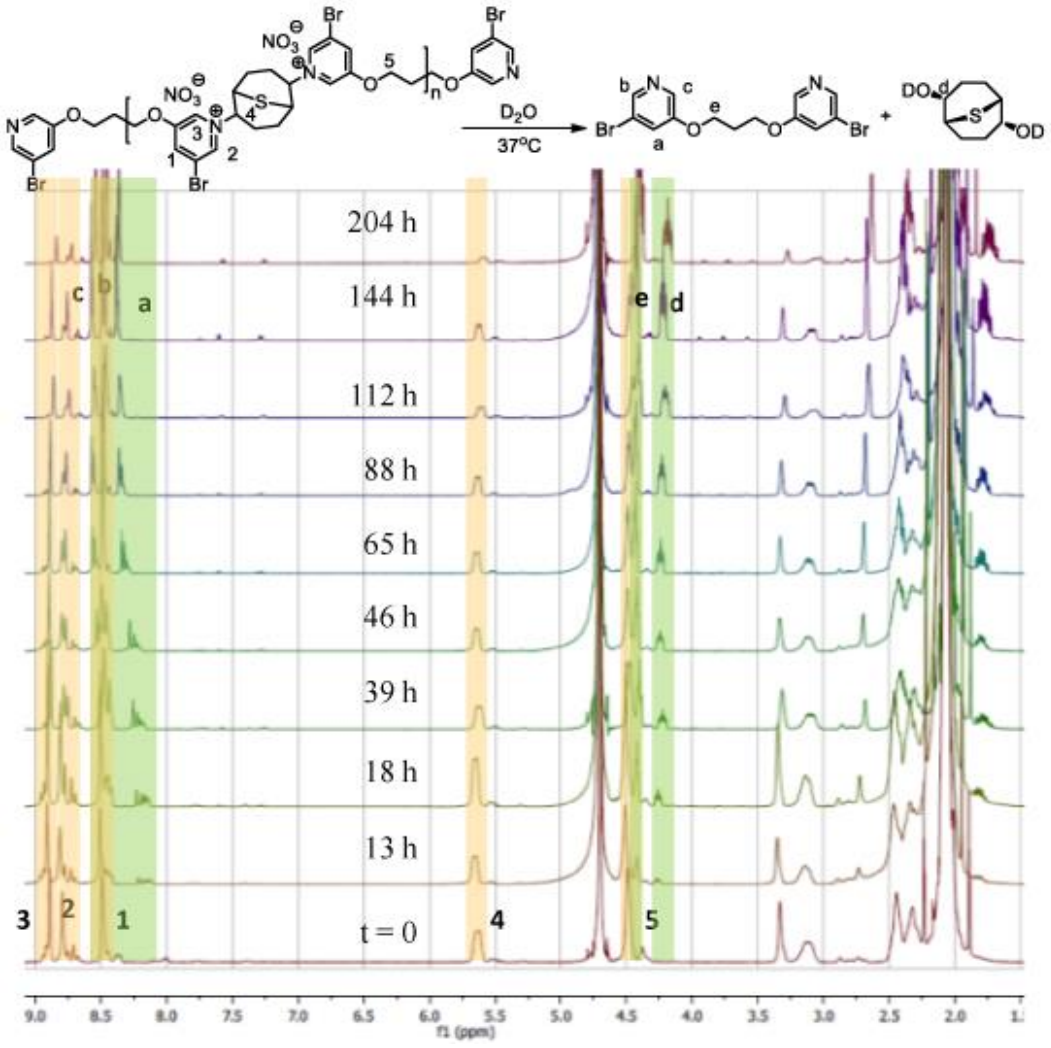

Figure 22 Monitoring fragmentation of polymer 3i in D_2O at 37 °C by ^1H NMR

The observed half-lives of the BCN-pyridine bonds in these oligomers corresponded reasonably well (within a factor of 2) with the corresponding small-molecule bis(pyridine) adducts described above, ranging from several hours to a month at physiological temperature and pH. Note of course that the oligomer structures decompose much faster than this, since the rupture of only a fraction of the bonds (occurring at approximately the same first-order rate at each position of the chain) would be necessary

to chop the linear structure into shorter pieces. Indeed, these materials are also very likely to be dynamic in nature, since breakage of a C-N(pyridyl) bond is probably followed by re-formation of that same bond more often than by irreversible capture of the intermediate episulfonium ion with water.

To further expand the scope of this class of compounds, dipyridines **2bb**-**2ii** (Table 7) were prepared by reductive amination of pyridine-4-carboxaldehyde with various amine linkers containing additional functional groups (alkyne, azide, lipophilic, and other connectors). After condensation with an equimolar amount of racemic BCN dinitrate **1b** under standard conditions (monomer concentration = 0.2 M, dry dimethyl sulfoxide solvent, room temperature, 18 hours), the precipitated polycations were isolated by filtration, washed, and characterized by a variety of techniques.

Table 7 Expanded scope of BCN polycations.

nucleophile monomer	polymer	n [a]	M_n (Da)	R_h[b] (nm)	nucleophile monomer	polymer	n [a]	M_n (Da)	R_h[b] (nm)
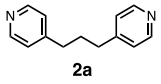 2a	3aa	20	9200	101	 2ff	3ff	8	6100	-
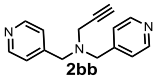 2bb	3bb	12	6200	77	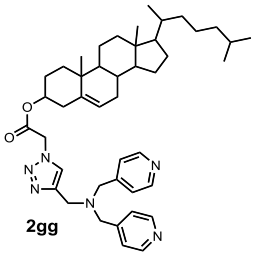 2gg	3gg	8	11600	14
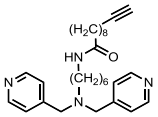 2cc	3cc	8	5800	-	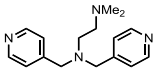 2hh	3hh	3	1600	87
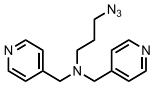 2dd	3dd	10	5500	35	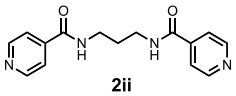 2ii	3ii	18	8800	151
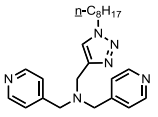 2ee	3ee	8	5300	-	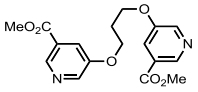 2jj	3jj	18	11000	82
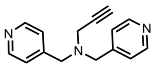 2bb (9 equiv) 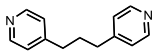 2a (1 equiv)	3kk	18	8400	-	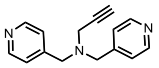 2bb (4 equiv) 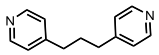 2a (6 equiv)	3ll	18	8600	-

a) n = average degree of polymerization determined by ^{1}H NMR. b) determined by dynamic light scattering in 54/23/23 (v/v/v %) water/methanol/acetic acid containing 0.5 M NaOAc.

Average chain lengths were still determined by end-group analysis using ^{1}H NMR. Gel permeation chromatography (GPC) analysis in a high-ionic strength ternary composition aqueous-based mobile phase was also performed to provide a rough estimation of relative sizes, but was less trustworthy for absolute molecular weight

determination due to the likelihood of interactions between the hydrophobic polycations and the stationary phase, a well-known phenomenon for polyelectrolytes.[74] These results, summarized in Table 7, were consistent with the formation of moderate chain lengths as expected for such step-growth condensation polymerization reactions.

The longer components **3ii** and **3jj** gave similar results, but most of the other reactions afforded oligomeric products (8-12 repeat units) that were still of functional interest. Two random copolymers were also prepared with different mixtures of **2a** and **2bb**. The composition of the polycation products in each case matched the feed ratio of monomers and were of the same average chain length, demonstrating approximately equal reaction rate for each substitution step and highlighting the modularity of the synthetic approach. Polymer **3jj** was made to allow for control of the overall charge of the material, since complete hydrolysis of the ester groups would provide a carboxylate anion for each pyridinium cationic center at neutral or basic pH.[75-76]

Two representative polymer examples, **3aa** and **3ff**, showed no evidence of micelle formation by a standard conductivity vs. concentration measurement from 0.01-1 mg/mL (Figure 23). The hydrodynamic radius of each polymer in aqueous solution was estimated by dynamic light scattering at 1 mg/mL, and is consistent with minimal aggregation. We expect these structures to be fairly rigid rods with relatively modest variations in detailed structure depending on the relative chirality of each thiabicyclononane fragment. Minimized structures of two tetrameric analogues of **3aa** are shown in Figure 24, which are approximately 17 Å long per repeat unit. Molecular mechanics calculations were performed with Spartan16 without consideration of counterion or solvent contributions.

We expect the synthesized polymers to contain random sequences in terms of diastereomeric composition of diad, triad, or larger substructures.

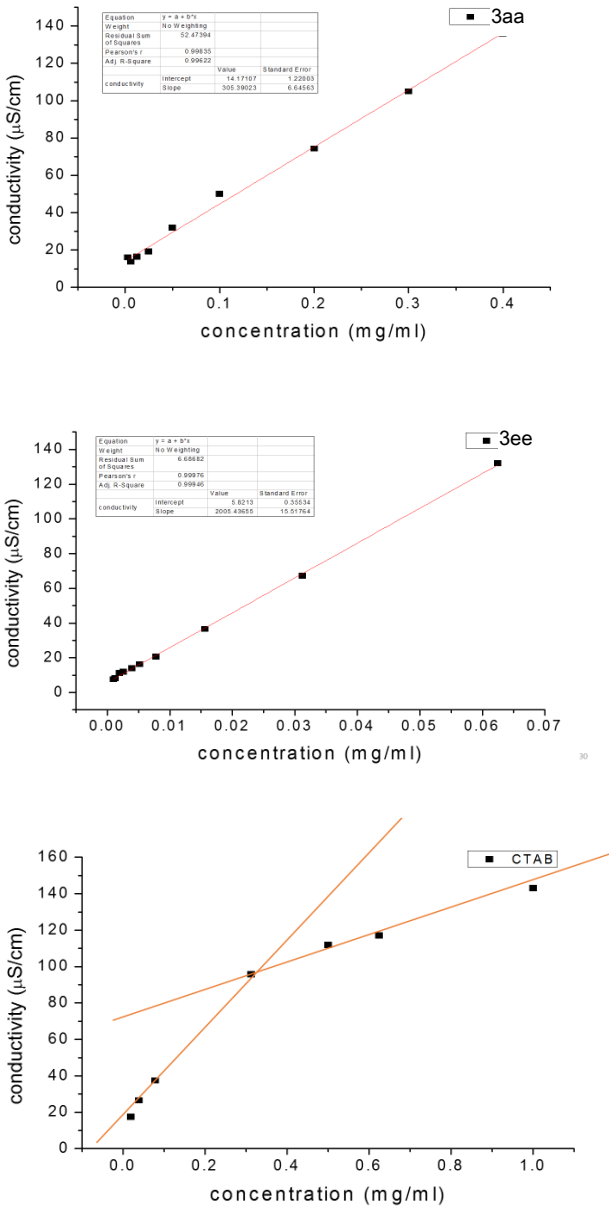

Figure 23 CMC determined by conductivity-concentration plots for 3aa, 3ee and CTAB.

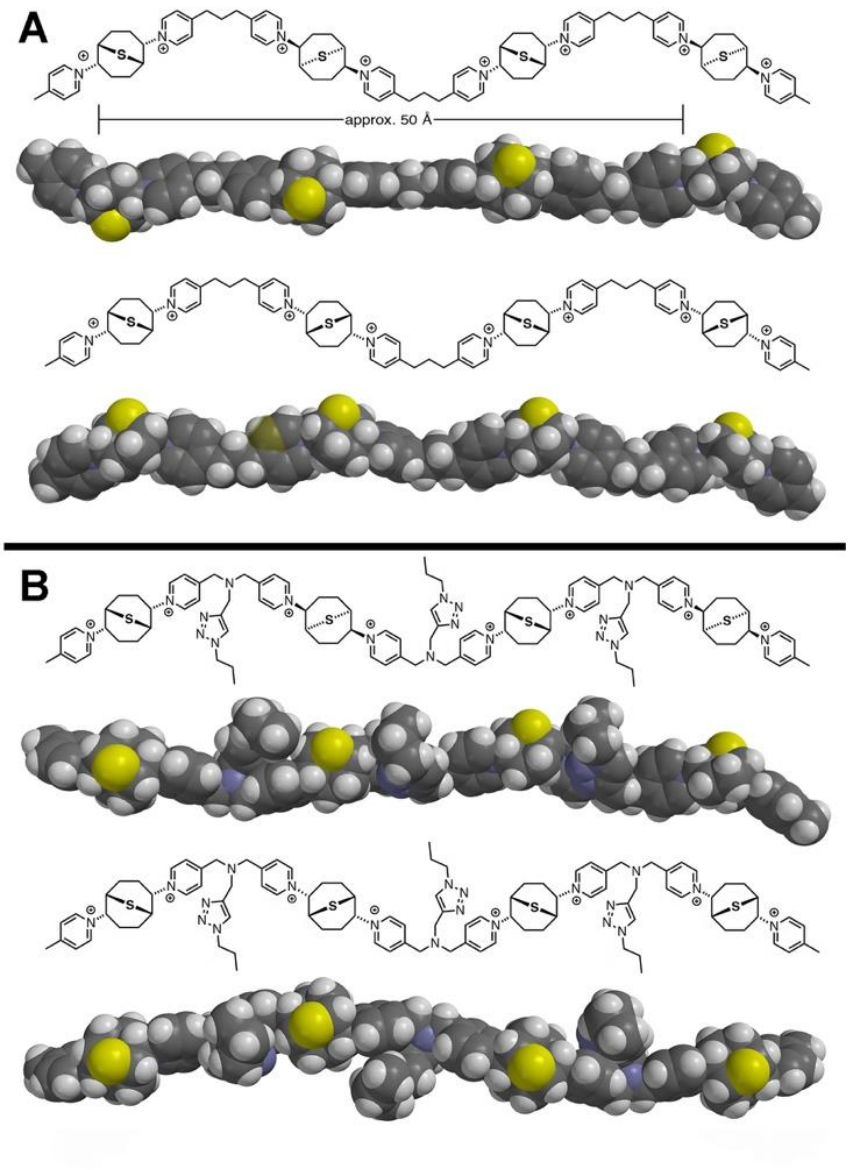

Figure 24 Energy-minimized model structures of oligomeric analogues of (A) 3aa and (B) 3ee, the latter with a propyl group on each triazole rather than an octyl group to simplify the calculation. For each set, structures having bicyclononane units of the same (top) and alternating (bottom) chirality are shown.

2.4 Conclusion

A new type of fragmentable oligocation has been developed through facile nucleophilic substitution of BCN scaffolds by divalent pyridines. The efficiency of this process depends on the leaving group ability of the group being substituted, consistent with rate-limiting activation of the electrophile by formation of a highly reactive episulfonium ion. Degrees of polymerization from approximately 3 to 30 were observed for these condensation polymerization processes. A range of polymer stabilities could be engineered by tuning the nucleophilicity and leaving group ability of the pyridine units, with pyridine basicity serving as a reasonably good guide to these properties.

It is also shown here that the bicyclo[3.3.1]nonane dinitrate core is nicely balanced in its reactivity, allowing it to be conveniently handled on the benchtop, yet reactive enough with pyridine nucleophiles to form interesting oligomeric and polymeric structures under mild conditions, in which each bond-forming event creates a positive charge. The easy incorporation and post-polymerization addressing of alkyne groups by CuAAC ligation with azide and the ability to control the average number of such "clickable" handles incorporated by the composition of the feedstock mixture both make these new examples of this subclass of polyionenes available for wide usage, some of which will be included in next two chapters.

2.5 Experimental

2.5.1 *Synthesis and characterization of new compounds*

2.5.1.1 Syntheses of BCN electrophiles and intermediates.

2,6-Dichloro-9-thiabicyclo[3.3.1]nonane (**1a**) synthesized as previously described[77]. ^{1}H NMR (400 MHz, $CDCl_3$) δ 4.71 (d, *J* = 3.3 Hz, 2H), 2.85 (dd, *J* = 6.8, 3.6 Hz, 2H), 2.72 – 2.61 (m, 2H), 2.36 – 2.18 (m, 6H). ^{13}C NMR (126 MHz, $CDCl_3$) δ 62.34, 37.10, 32.40, 28.12. Unless noted otherwise, all ^{13}C spectra are recorded with broadband proton decoupling.

2,6-Dinitro-9-thiabicyclo[3.3.1]nonane (**1b**). **1a** (21 mg, 0.1 mmol, 1 equiv) and silver nitrate (34 mg, 0.2 mmol, 2 equiv) were mixed in 0.5 mL MeCN and stirred overnight at room temperature. The resulting AgCl was removed by centrifugation and the solvent was evaporated to give **1b** as a colorless oil (22 mg, 86% yield). ^{1}H NMR (400 MHz, $CDCl_3$) δ 5.66 – 5.50 (m, 2H), 3.02 (d, *J* = 3.1 Hz, 2H), 2.51 (dd, *J* = 14.5, 6.7 Hz, 2H), 2.32 (dd, *J* = 9.8, 3.0 Hz, 2H), 2.20 (dt, *J* = 13.5, 6.7 Hz, 2H), 2.11 – 1.92 (m, 2H). ^{13}C NMR (101 MHz, $CDCl_3$) δ 82.24, 32.72, 26.92, 24.84.

2,6-Diiodo-9-thiabicyclo[3.3.1]nonane (**1d**). Compound **1a** (252 mg, 1.2 mmol, 1 equiv) and sodium iodide (540 mg, 3.6 mmol, 3 equiv) were mixed in 6 mL acetone and stirred overnight at room temperature. NaCl was filtered off and the solution was evaporated. The resulting solid was dissolved in CH_2Cl_2, leaving behind excess sodium iodide. Evaporation of this solution gave **1d** as a yellow powder (270 mg, 58% yield). ^{1}H NMR (500 MHz, $CDCl_3$) δ 5.26 – 5.12 (m, 2H), 3.11 (t, *J* = 3.4 Hz, 2H), 2.95 – 2.81 (m, 2H), 2.71 (ddd, *J* = 11.6, 6.1, 4.0 Hz, 2H), 2.58 – 2.42 (m, 2H). ^{13}C NMR (126 MHz, $CDCl_3$) δ 38.50, 36.11, 35.75, 32.35.

2.5.1.2 Syntheses of BCN cationic adducts.

Representative procedure for the synthesis of pyridine adducts of both small molecules and oligomers (Table 3, Table 4, Figure 18). Compound **1a** (21 mg, 0.1 mmol, 1 equiv), silver nitrate (34 mg, 0.2 mmol, 2 equiv) and the pyridine of interest (0.2 mmol, 2 equiv) were mixed in 0.5 mL MeCN and stirred overnight at room temperature under inert atmosphere. The precipitate was collected and washed with MeCN. The charged adduct was dissolved in water and any remaining solids were removed by centrifugation, repeating the centrifugation step until the solution was not cloudy. The resulting solution was frozen and lyophilized to obtain the product as a colorless solid.

2,6-di-3-methoxycarbonylpyridinium-9-thiabicyclo[3.3.1]nonane dinitrate (**5b**): ^{1}H NMR (400 MHz, D_2O) δ 9.58 (s, 2H), 9.35 (d, *J* = 4.9 Hz, 2H), 9.23 – 9.08 (m, 2H), 8.47 – 8.27 (m, 2H), 5.85 (dd, *J* = 8.3, 4.0 Hz, 2H), 3.41 (s, 2H), 3.25 (q, *J* = 13.0 Hz, 2H), 2.49 (t, *J* = 14.5 Hz, 4H), 2.36 (d, *J* = 14.9 Hz, 2H). ^{13}C NMR (126 MHz, D_2O) δ 163.09, 146.47, 146.01, 144.54, 131.16, 129.01, 74.35, 53.86, 35.67, 26.25, 24.27.

2,6-di-4-methoxycarbonylpyridinium-9-thiabicyclo[3.3.1]nonane dinitrate (**5c**): ^{1}H NMR (400 MHz, D_2O) δ 9.31 (d, *J* = 6.7 Hz, 4H), 8.65 (d, *J* = 6.6 Hz, 4H), 5.92 – 5.77 (m, 2H), 3.40 (s, 2H), 3.19 (dd, *J* = 12.9, 5.5 Hz, 2H), 2.60 – 2.43 (m, 4H), 2.43 – 2.31 (m, 2H). ^{13}C NMR (126 MHz, D_2O) δ 163.50, 145.43, 144.84, 128.20, 74.39, 54.22, 35.92, 26.52, 24.68.

2,6-di-3-carbamylpyridinium-9-thiabicyclo[3.3.1]nonane dinitrate (**5d**): ^{1}H NMR (400 MHz, D_2O) δ 9.47 (s, 2H), 9.28 (d, *J* = 6.0 Hz, 2H), 8.98 (dd, *J* = 16.1, 7.3 Hz, 2H), 8.48 – 8.28 (m, 2H), 5.94 – 5.74 (m, 2H), 3.41 (s, 2H), 3.36 – 3.13 (m, 2H), 2.66 – 2.40 (m, 4H),

2.36 (d, *J* = 15.7 Hz, 2H). ^{13}C NMR (101 MHz, D_2O) δ 165.66, 145.33, 144.82, 143.44, 134.42, 128.93, 74.42, 35.82, 26.42, 24.44.

2,6-di-4-carbamylpyridinium-9-thiabicyclo[3.3.1]nonane dinitrate (**5e**): ^{1}H NMR (400 MHz, D_2O) δ 9.36 (d, *J* = 6.8 Hz, 4H), 8.53 (d, *J* = 6.7 Hz, 4H), 5.87 (dd, *J* = 10.5, 6.7 Hz, 2H), 3.45 (d, *J* = 2.7 Hz, 2H), 3.36 – 3.17 (m, 2H), 2.62 – 2.46 (m, 4H), 2.40 (dd, *J* = 9.4, 6.4 Hz, 2H). ^{13}C NMR (126 MHz, D_2O) δ 166.24, 149.13, 144.47, 126.79, 74.08, 35.78, 26.41, 24.59,

2,6-di-3-bromopyridinium-9-thiabicyclo[3.3.1]nonane dinitrate (**5f**): ^{1}H NMR (400 MHz, D_2O) δ 9.33 (d, *J* = 0.9 Hz, 2H), 9.10 (d, *J* = 5.2 Hz, 2H), 8.93 – 8.72 (m, 2H), 8.11 (dd, *J* = 8.3, 6.2 Hz, 2H), 5.90 – 5.61 (m, 2H), 3.34 (s, 2H), 3.13 (dd, *J* = 13.0, 5.7 Hz, 2H), 2.58 – 2.25 (m, 6H). ^{13}C NMR (126 MHz, D_2O) δ 149.30, 144.72, 141.88, 129.23, 123.63, 74.22, 35.83, 26.38, 24.27.

2,6-di-3-trifluoromethylpyridinium-9-thiabicyclo[3.3.1]nonane dinitrate (**5g**): ^{1}H NMR (500 MHz, D_2O) δ 9.86 (s, 2H), 9.53 (d, *J* = 6.4 Hz, 2H), 9.13 (d, *J* = 8.1 Hz, 2H), 8.53 – 8.48 (m, 2H), 6.01 – 5.89 (m, 2H), 3.52 (d, *J* = 2.4 Hz, 2H), 3.32 (dd, *J* = 12.9, 6.2 Hz, 2H), 2.66 – 2.48 (m, 4H), 2.42 (dd, *J* = 15.2, 4.3 Hz, 2H). ^{13}C NMR (101 MHz, D_2O) δ 149.76, 147.21, 147.17, 129.58, 114.67, 113.24, 75.11, 35.64, 26.23, 24.36.

2,6-di-3-cyanopyridinium-9-thiabicyclo[3.3.1]nonane dinitrate (**5h**): ^{1}H NMR (500 MHz, D_2O) δ 9.69 (s, 2H), 9.54 (d, *J* = 6.3 Hz, 2H), 9.07 (d, *J* = 8.2 Hz, 2H), 8.61 – 8.44 (m, 2H), 5.94 (dd, *J* = 8.3, 3.7 Hz, 2H), 3.50 (d, *J* = 3.0 Hz, 2H), 3.37 (dd, *J* = 12.9, 6.4 Hz, 2H), 2.66 – 2.45 (m, 4H), 2.45 – 2.33 (m, 2H). ^{13}C NMR (101 MHz, D_2O) δ 146.26 (s), 144.09

(d, *J* = 3.0 Hz), 142.46 (d, *J* = 4.0 Hz), 131.43 (q, *J* = 36.5 Hz), 121.26 (q, *J* = 273.2 Hz), 75.01 (s), 35.82 (s), 26.42 (s), 24.34 (s).

2,6-di-3-bromo-5-methoxylpyridinium-9-thiabicyclo[3.3.1]nonane dinitrate (**5i**): ^{1}H NMR (400 MHz, D_2O) δ 9.00 (s, 2H), 8.87 (s, 2H), 8.49 (s, 2H), 5.79 – 5.63 (m, 2H), 4.11 (s, 6H), 3.41 (d, *J* = 2.6 Hz, 2H), 3.27 (dd, *J* = 13.0, 6.1 Hz, 2H), 2.49 (td, *J* = 11.3, 6.4 Hz, 2H), 2.45 – 2.31 (m, 4H). ^{13}C NMR (126 MHz, D_2O) δ 159.03, 135.88, 133.04, 131.50, 123.55, 74.47, 57.72, 35.92, 26.48, 24.03.

2,6-di-3-bromo-5-carbamylpyridinium-9-thiabicyclo[3.3.1]nonane ditriflate (**5j**): ^{1}H NMR (500 MHz, D_2O) δ 9.47 (s, 2H), 9.41 (s, 2H), 9.17 (s, 2H), 5.77 (dd, *J* = 8.4, 4.0 Hz, 2H), 3.37 (s, 2H), 3.19 (dd, *J* = 13.1, 6.1 Hz, 2H), 2.46 (t, *J* = 11.3 Hz, 2H), 2.38 (dd, *J* = 13.2, 6.1 Hz, 2H), 2.34 – 2.25 (m, 2H). ^{13}C NMR (126 MHz, D_2O) δ 164.26, 147.54, 146.69, 141.73, 134.73, 123.69, 74.79, 35.62, 26.07, 23.87.

2,6-di-3,5-dimethoxycarbonylpyridinium-9-thiabicyclo[3.3.1]nonane ditriflate (**5k**): ^{1}H NMR (400 MHz, D_2O) δ 9.70 (s, 4H), 9.50 (s, 2H), 5.89 (d, *J* = 12.5 Hz, 2H), 3.37 (s, 2H), 3.30 (dd, *J* = 12.7, 5.2 Hz, 2H), 2.53 – 2.21 (m, 6H).

2,6-di-3-bromo-5-methoxycarbonylpyridinium-9-thiabicyclo[3.3.1]nonane ditriflate (**5l**): ^{1}H NMR (400 MHz, D_2O) δ 9.51 (s, 2H), 9.48 (s, 2H), 9.28 (s, 2H), 5.75 (d, *J* = 12.1 Hz, 2H), 3.32 (s, 2H), 3.17 (ddd, *J* = 25.6, 13.2, 6.3 Hz, 2H), 2.51 – 2.18 (m, 6H).

2.5.1.3 Synthesis of bispyridine linker.

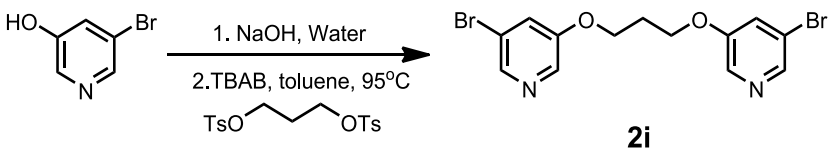

2i

5-Bromopyridin-3-ol (570 mg, 3.3 mmol, 4 equiv) was dissolved in 5 mL of 1 M NaOH with vigorous stirring for 1 h. Propane-1,3-diyl bis(4-methylbenzenesulfonate) (320 mg, 0.83 mmol, 1 equiv) and tetra-*n*-butylammonium bromide (367 mg 1.14 mmol, 1.3 equiv) in 10 mL toluene were added. The solution was heated to 95 °C overnight. The mixture was cooled, the solvent removed by rotary evaporation, and the product was purified by column chromatography (2:1 hexanes/EtOAc) elution. The desired product, 1,3-bis((5-bromopyridin-3-yl)oxy)propane (**2i**), was obtained as a white powder (216 mg, 67% yield). ^{1}H NMR (400 MHz, $CDCl_3$) δ 8.32 (d, *J* = 1.6 Hz, 1H), 8.27 (d, *J* = 2.5 Hz, 1H), 7.41 (s, 1H), 4.23 (t, *J* = 5.9 Hz, 2H), 2.39 – 2.29 (m, 1H). ^{13}C NMR (126 MHz, $CDCl_3$) δ 154.99, 143.04, 136.22, 123.70, 120.26, 64.48, 28.71.

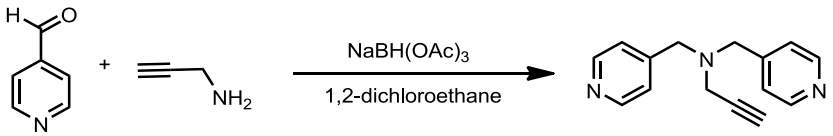

4-pyridinecarboxaldehyde (1.71g, 16 mmol) and propargylamine (330 mg, 6 mmol) (or respective amine for other bispyridine linkers) were mixed in 1,2-dichloroethane (60 mL) and then treated with sodium triacetoxyborohydride (4.24 g, 20 mmol). The mixture was stirred at room tenmperature under N_2 atmosphere for overnight. The reaction mixture was quenched by adding aqueous saturated $NaHCO_3$, and the product was extracted with dichloromethane, dried ($MgSO_4$) and purified by column chromatography (1:1%:0.5%

dichloromethane/methanol/triethylamine) elution. The desired product **2bb** was obtained as a pale yellow liquid (978 mg, 70% yield).^{1}H NMR (500 MHz, $CDCl_3$) δ 8.58 (d, *J* = 5.9 Hz, 4H), 7.35 (d, *J* = 5.9 Hz, 4H), 3.71 (s, 4H), 3.29 (d, *J* = 2.3 Hz, 1H), 2.33 (t, *J* = 2.3 Hz, 1H). ^{13}C NMR (126 MHz, $CDCl_3$) δ 149.73, 147.34, 123.56, 77.10, 74.08, 56.34, 41.61.

2cc, yellow liquid (70% yield). ^{1}H NMR (500 MHz, $CDCl_3$) δ 8.58 (s, 4H), 7.32 (s, 4H), 5.59 (s, 1H), 3.54 (s, 4H), 3.20 (dd, *J* = 13.4, 6.9 Hz, 2H), 2.44 – 2.36 (m, 2H), 2.20 – 2.10 (m, 4H), 1.94 (t, *J* = 2.6 Hz, 1H), 1.67 – 1.56 (m, 2H), 1.56 – 1.41 (m, 6H), 1.41 – 1.33 (m, 2H), 1.33 – 1.19 (m, 10H). ^{13}C NMR (126 MHz, $CDCl_3$) δ 173.16, 149.85, 148.82, 123.85, 84.81, 77.41, 77.16, 76.91, 68.21, 57.67, 54.05, 39.46, 36.92, 29.77, 29.32, 29.28, 29.01, 28.74, 28.50, 27.11, 26.92, 26.82, 25.85, 18.45.

2dd, yellow liquid (70% yield).^{1}H NMR (500 MHz, $CDCl_3$) δ 8.48 (d, *J* = 5.6 Hz, 4H), 7.22 (d, *J* = 5.6 Hz, 4H), 3.50 (s, 4H), 3.24 (t, *J* = 6.7 Hz, 2H), 2.45 (t, *J* = 6.9 Hz, 2H), 1.84 – 1.58 (m, 2H). ^{13}C NMR (126 MHz, $CDCl_3$) δ 149.64, 147.93, 123.29, 57.33, 50.86, 48.96, 26.25.

2ee, 2ff and **2gg** were made from **2bb** and respective azide under the catalysis of 5 mol% of copper sulfate pentahydrate and 10 mol% of sodium ascorbate in 4:1 of H_2O/*t*-BuOH mixture overnight and then purified by column chromatography (elution with CH_2Cl_2 containing 1% MeOH and 0.5% Et_3N).

2ee, yellow liquid (70% yield). ^{1}H NMR (400 MHz, $CDCl_3$) δ 8.58 (s, 4H), 7.40 (s, 1H), 7.35 (s, 4H), 4.33 (t, *J* = 7.3 Hz, 2H), 3.75 (s, 2H), 3.63 (s, 4H), 1.98 – 1.71 (m, 2H), 1.42 – 1.12 (m, 10H), 0.85 (t, *J* = 6.8 Hz, 1H). ^{13}C NMR (126 MHz, $CDCl_3$) δ 149.76, 147.93,

143.78, 123.40, 122.12, 56.65, 50.22, 48.09, 31.50, 30.14, 28.88, 28.75, 26.33, 22.41, 17.61, 13.88.

2ff, yellow liquid (70% yield). ^{1}H NMR (500 MHz, $CDCl_3$) δ 8.56 (s, 4H), 7.39 (s, 1H), 7.34 (s, 4H), 4.34 (dd, *J* = 9.6, 4.8 Hz, 2H), 3.76 (s, 2H), 3.65 (s, 4H), 1.89 (s, 2H), 1.27 (d, *J* = 32.7 Hz, 26H), 0.87 (t, *J* = 7.8, 5.6 Hz, 3H). ^{13}C NMR (101 MHz, $CDCl_3$) δ 149.94, 148.05, 143.91, 123.55, 122.31, 56.82, 50.37, 48.24, 31.90, 30.30, 29.66, 29.63, 29.58, 29.49, 29.39, 29.34, 28.97, 26.50, 22.67, 14.11.

2gg, white powder (70% yield). ^{1}H NMR (500 MHz, $CDCl_3$) δ 8.59 (d, *J* = 3.1 Hz, 4H), 7.59 (s, 1H), 7.37 (d, *J* = 5.3 Hz, 4H), 5.40 (d, *J* = 3.7 Hz, 1H), 5.17 (s, 2H), 4.73 (tdd, *J* = 34.9, 19.9, 15.4 Hz, 2H), 3.82 (s, 2H), 3.68 (s, 4H), 2.36 (d, *J* = 7.8 Hz, 2H), 2.01 (ddd, *J* = 22.0, 9.7, 4.2 Hz, 2H), 1.93 – 1.86 (m, 2H), 1.86 – 1.80 (m, 1H), 1.68 – 1.59 (m, 6H), 1.57 – 1.44 (m, 4H), 1.36 (dd, *J* = 11.4, 6.1 Hz, 2H), 1.28 (d, *J* = 7.8 Hz, 2H), 1.23 – 1.06 (m, 6H), 1.01 (d, *J* = 8.2 Hz, 3H), 0.93 (d, *J* = 6.5 Hz, 3H), 0.90 – 0.85 (m, 6H), 0.70 (s, 3H). ^{13}C NMR (126 MHz, $CDCl_3$) δ 165.49, 149.82, 147.79, 144.19, 138.66, 123.86, 123.42, 123.25, 56.56, 56.47, 55.93, 50.87, 49.77, 47.87, 42.12, 39.49, 39.33, 37.75, 36.62, 36.34, 35.99, 35.60, 31.69, 31.62, 28.03, 27.84, 27.48, 24.09, 23.64, 22.64, 22.38, 20.84, 19.07, 18.53, 11.67.

2hh, brown liquid (70% yield). ^{1}H NMR (400 MHz, $CDCl_3$) δ 8.57 (d, *J* = 6.0 Hz, 4H), 7.33 (d, *J* = 6.0 Hz, 4H), 3.66 (s, 4H), 2.62 (dd, *J* = 8.3, 5.9 Hz, 2H), 2.49 (dd, *J* = 8.1, 5.8 Hz, 2H), 2.21 (s, 6H).^{13}C NMR (101 MHz, $CDCl_3$) δ 149.78, 148.54, 123.49, 57.92, 57.66, 52.07, 45.79.

2jj, ^{1}H NMR (400 MHz, $CDCl_3$) δ 8.83 (d, *J* = 1.5 Hz, 2H), 8.49 (d, *J* = 2.9 Hz, 2H), 7.79 (dd, *J* = 2.9, 1.7 Hz, 2H), 4.28 (t, *J* = 6.0 Hz, 4H), 3.95 (s, 6H), 2.36 (dt, *J* = 12.1, 6.1 Hz, 2H).

2.5.1.4 Synthesis of BCN polycation.

Representative procedure for the synthesis of polymers.

Compound **1a** (21 mg, 0.1 mmol, 1 equiv), silver salt (0.2 mmol, 2 equiv) and the bispyridine of interest (0.1 mmol, 1 equiv) were mixed in 0.5 ml MeCN and stirred overnight at room temperature under inert atmosphere. For aqueous soluble polymers (entries 3, 4, 5, and 7 in Table 5; entries 1-3 in Table 6), the precipitate was collected and washed with MeCN. The charged adduct was dissolved in water and any remaining solids were removed by centrifugation, repeating the centrifugation step until the solution was not cloudy. The resulting solution was frozen and lyophilized to obtain the product as a colorless solid. For organic soluble polymers (entries 6, 8, 9, and 10 in Table 5; entry 4 in Table 6; Table 7), any solid material was filtered out and the resulting solution was added to 10ml CH_2Cl_2 or toluene (for very hydrophobic polycations such as **3ff** and **3gg**) to precipitate the desired product. The material was isolated by filtration and dried to give an off-white solid or a yellow sticky solid.

2.5.2 *Characterization of BCN polymers*

2.5.2.1 Gel permeation chromatography.

Three BCN based polymers were dissolved at 0.8 mg/mL concentration in a 54/23/23 (v/v/v %) mixture of water/methanol/acetic acid, containing 0.5M NaOAc solution (conditions used in published reports[67, 74]). The major peaks between 17 and 30 mins were assigned to polymers. Calculation of molecular weight parameters by comparison to PEI standards proved to be nonsensical, so M_n, M_w, and dispersity were evaluated by comparison to PEG (for the low molecular weight range) and PEI (high molecular weight range) standards. NMR end group analysis was still regarded as the most accurate method available.

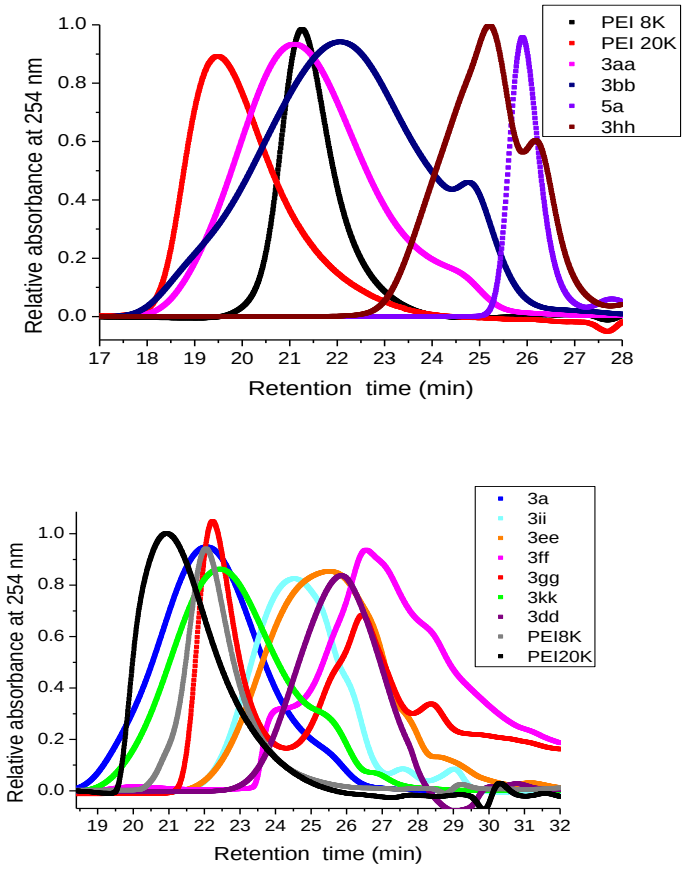

Figure 25 GPC curves of BCN polycations and PEI standards in 54/23/23 (v/v/v %) water/methanol/acetic acid, 0.5M NaOAc.

2.5.2.2 GPC analysis of BCN polymer before and after fragmentation.

Three BCN based polymers were dissolved in highly pure water at 1 mg/mL concentration solution and characterized by aqueous gel permeation chromatography (GPC, black curves in Figure 26). Separate identical solutions were heated at 37 °C for 36 hours and analyzed again by aqueous GPC (red curves in Figure 26). The major peaks between 8 and 10 mins were assigned to polymers; after heating, small molecule components were evident as peaks at longer retention times. Calculation of molecular weight parameters was performed by comparison to dextran standards.

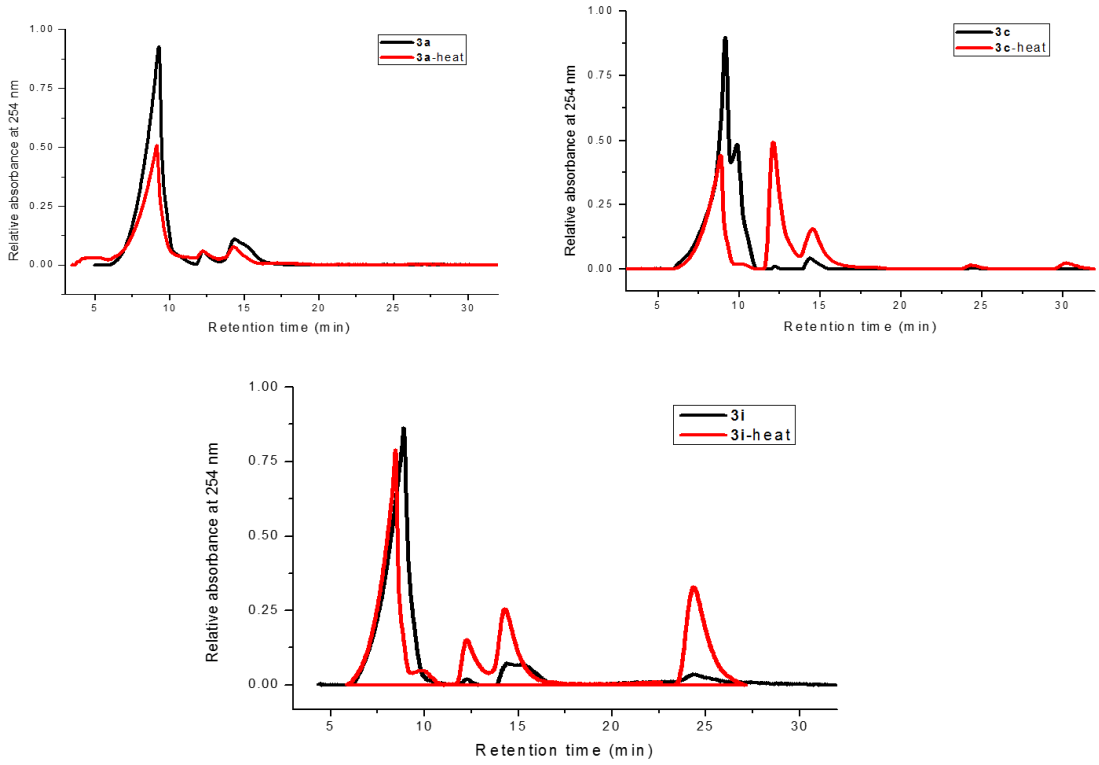

Figure 26 GPC curves of polymer 3a, 3c and 3i before (black) and after (red) fragmentation in water at 37 ºC.

2.5.2.3 Comparison of molecular weight acquired by GPC and NMR.

Table 8 Characterization of polycations by ^{1}H NMR, GPC, and DLS.

polymer	M_n (Da) [a]	M_n (Da) [b]	Đ [b]	R_h (nm) [c]	dispersity (%) [c]
3aa	9200	11000	1.36	101 ± 10	19.6
3bb	6200	n/d	n/d	77 ± 4	14.7
3dd	5500	1250	1.5	35 ± 5	45.2
3ee	5300	1400	2.04	n/d	n/d
3ff	6100	4000	1.03	n/o	n/o
3gg	11600	9000	1.07	14 ± 1	10.2
3hh	1600	n/d	n/d	87 ± 6	13.8
3ii	8800	3000	1.4	151 ± 12	10.8
3jj	11000	n/d	n/d	82 ± 5	15.9
3kk	8400	n/d	n/d	111 ± 11	12.3
PEI	8000	n/d	n/d	5 ± 1	26.8

(a) by ^{1}H NMR. (b) by GPC. (c) Hydrodynamic radius and dispersity measured by DLS in the same solvent as GPC. “n/o” denotes a sample for which no signal for an aggregate was observed. “n/d” = not determined

2.5.3 *Comparison of reactivities between different BCN intermediates*

Compound **1a** (10.5 mg, 0.05 mmol, 1 equiv) and **1b** (0.2 mL of 0.25 M MeCN solution, 0.05 mmol, 1 equiv) were combined in 1 mL MeCN. The solvent was then evaporated and the residue analyzed by ^{1}H NMR in $CDCl_3$ (Figure 27-A). In parallel, a separate identical [**1a** + **1b**] mixture in MeCN was treated with benzylamine (8.1 µL, 0.1 mmol, 1 equiv) and triethylamine (69.6 µL, 0.5 mmol, 5 equiv, previously shown to be unreactive towards BCN compounds and used to soak up any HCl produced). After 24 hours, the mixture was evaporated, redissolved in $CDCl_3$, and analyzed by ^{1}H NMR (Figure 27-B). The data show almost complete reaction of the amine with the nitrate electrophile rather than the chloride.

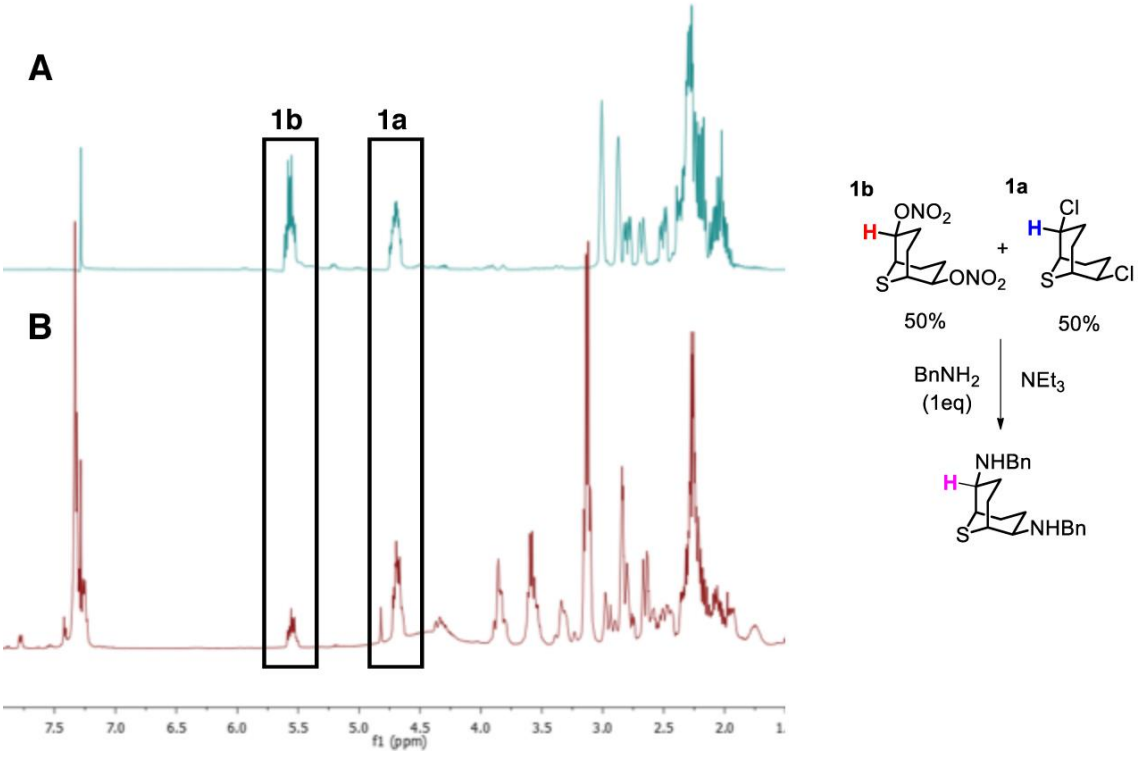

Figure 27 ^{1}H NMR analysis of competition experiment between BCN nitrate and chloride electrophiles for benzylamine.

An internal competition between all three easy-to-handle electrophiles (chloride, nitrate, iodide; **1a**, **1b**, and **1d**) was performed in a similar manner, in which 0.05 mmol of each was combined in acetonitrile and treated with slightly less than one equivalent of $BnNH_2$ (0.125 mmol) and 5 equiv. (5 mmol) of Et_3N (total volume 1 mL). NMR spectra recorded immediately and after 24 h (in each case, an aliquot was removed, evaporated, and redissolved in $CDCl_3$) are shown in Figure 28. Integration of the α-protons for each electrophile showed nearly equimolar ratios at the start, and a highly skewed distribution after reaction. The relative reactivities thus revealed are iodide > nitrate > chloride.

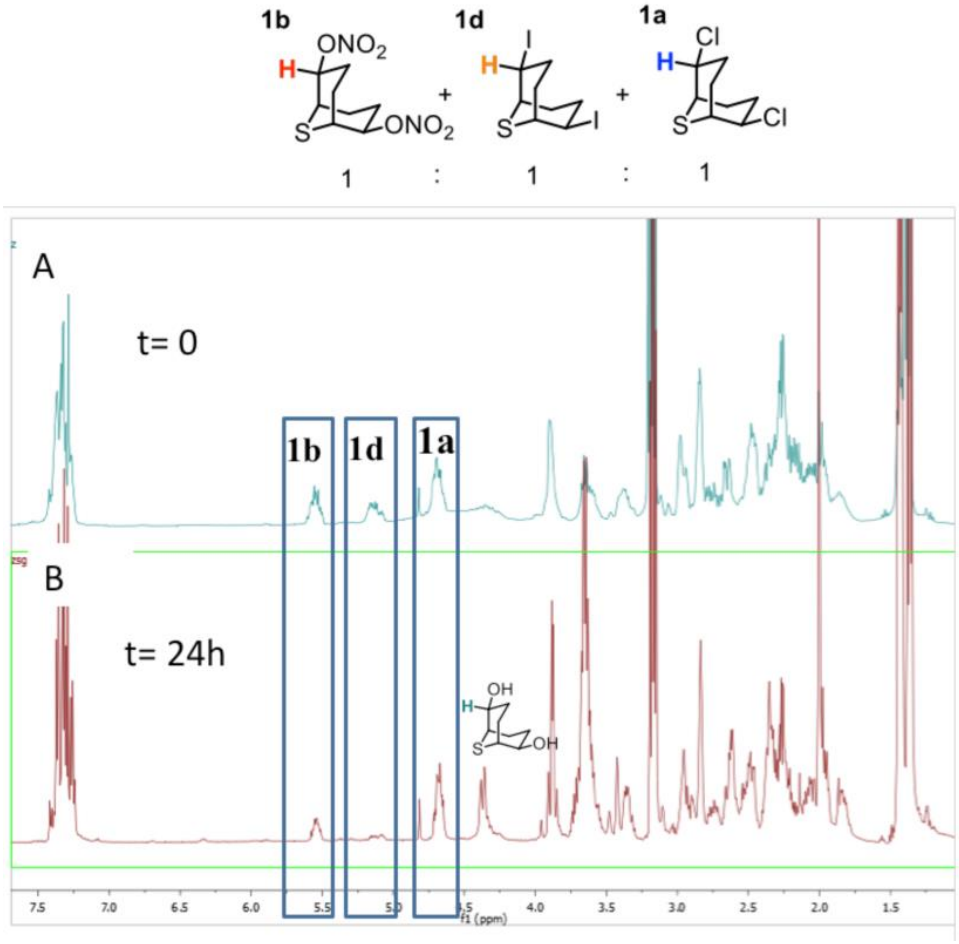

Figure 28 ^{1}H NMR analysis of competition experiment between BCN chloride, nitrate and iodide electrophiles for benzylamine.

2.5.4 *Monitoring fragmentation of representative BCN-substituted adducts by ^{1}H NMR*

Figure 29 shows representative data for compound **5d**, with the relative concentration of each species established by integration of unique resonances, labeled in the figure. The first-order kinetic treatment is shown in Figure 30.

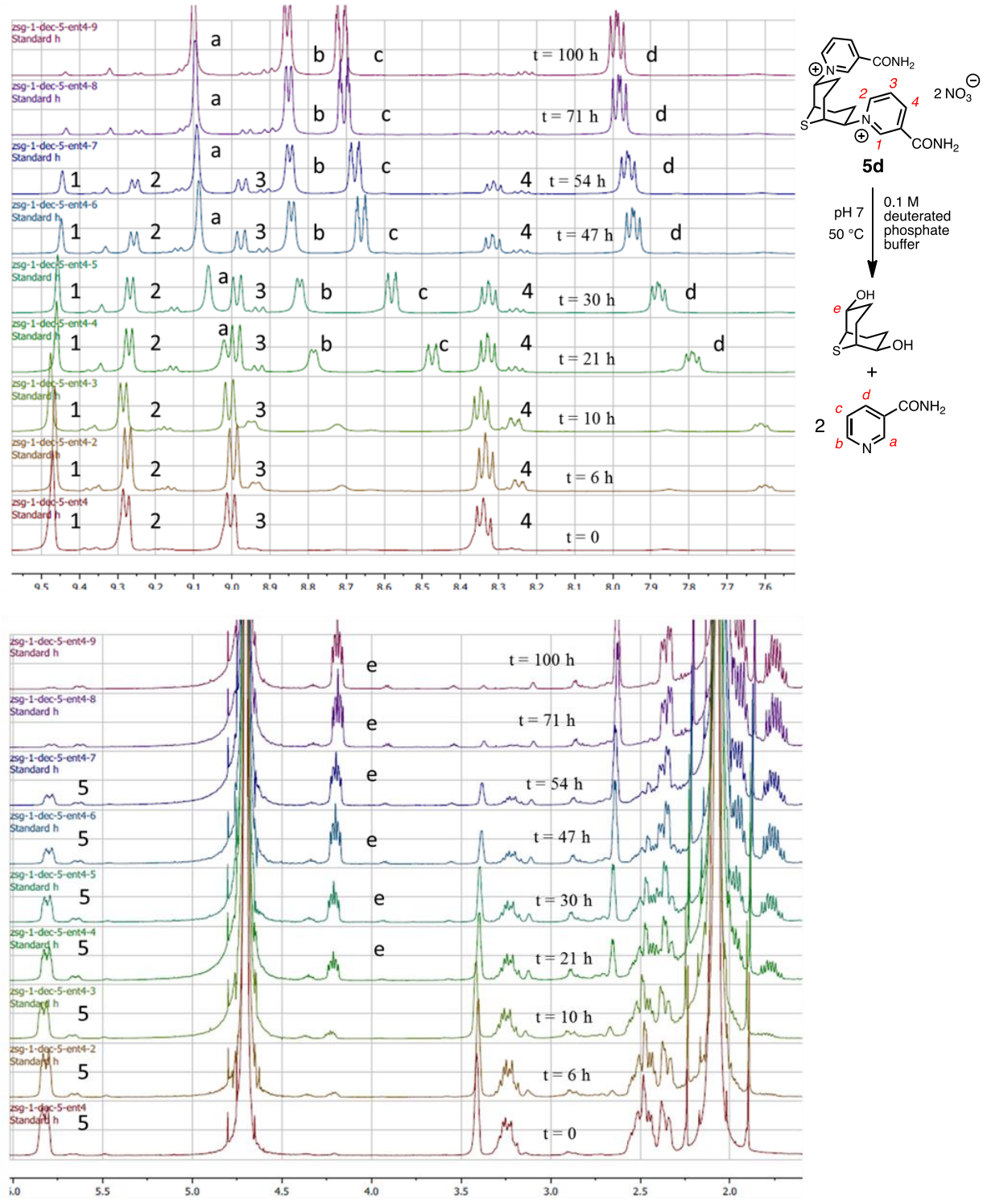

Figure 29 ^{1}H NMR spectra of 5d in deuterated aqueous phosphate buffer (pH 7) at 50 °C: (*top*) downfield region; (*bottom*) upfield region.

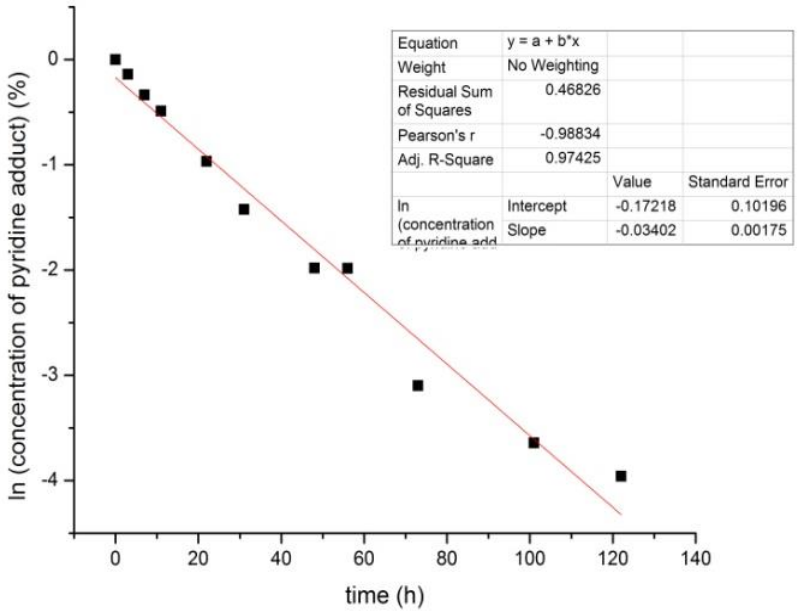

Figure 30 Pseudo-first order plot for fragmentation of 5d in deuterated buffer at 50 °C.

2.5.5 *Handy guide for prediction of fragmentation rate*

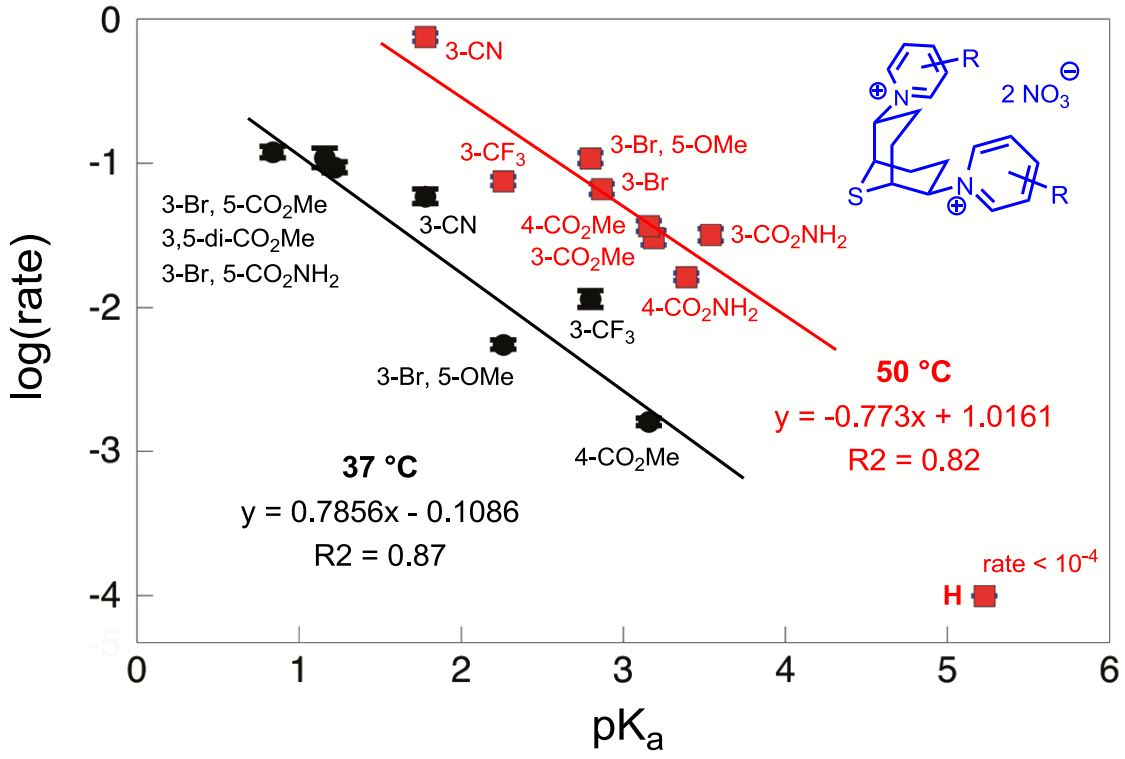

Figure 31 Basic guide of fragmentation rate of BCN adduct at 37 °C and 50 °C affected by pyridine basicity.

2.5.6 *Other dinucleophiles employed to assemble BCN polycations*

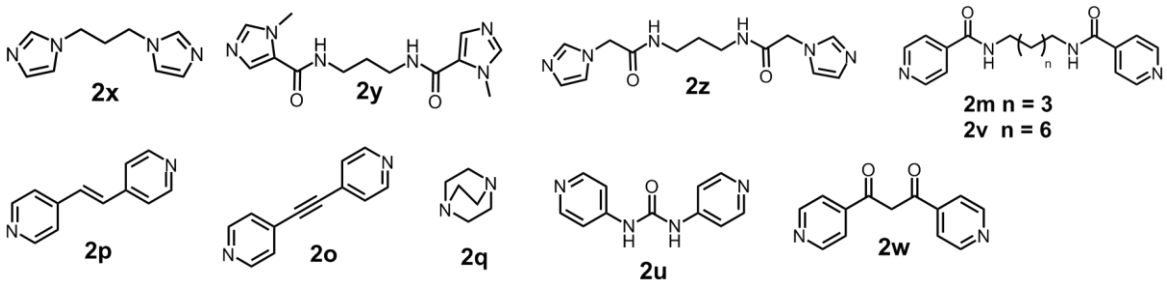

Figure 32 Structure of dinucleophiles successfully employed to assemble BCN oligocations (polymerization greater than 3).

2.5.7 *Thermal analysis of represented BCN polymers*

The thermal decomposition temperature of BCN polymers were measured on a Perkin-Elmer Pyris 1 thermogravimetric analyzer (TGA) in a nitrogen atmosphere (25 mL/min) with a heating rate of 10 °C/min. Thermal transitions of BCN polymer **3a** were measured with a TA Q200 Differential Scanning Calorimeter (DSC) in a nitrogen atmosphere (50 mL/min) with a heating/cooling rate of 10 °C/min. Each sample was scanned for three cycles and the 2nd cycle is presented here.

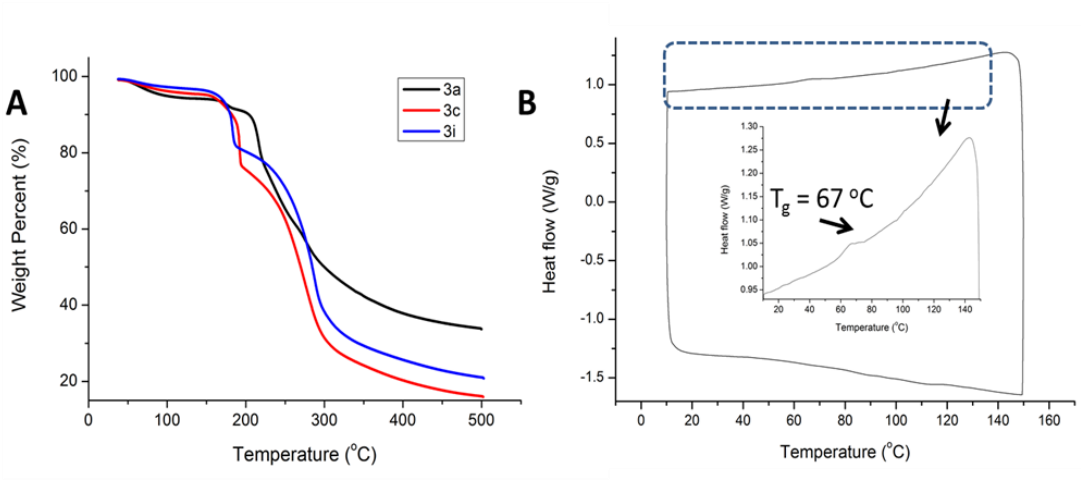

Figure 33 (A) TGA curve of polymer 3a,3c and 3i. (B) DSC curve of polymer 3a.

Polymer **3a** decomposed at around 220 °C while **3c** and **3i** decomposed below 200 °C with two obvious stage of mass loss. The glass transition of **3a** was observed at 67 °C which is comparable with the T_g of polyionenes reported before.

CHAPTER 3. APPLYING THIABICYCLONONANE-BASED POLYCATION AS TRANSFECTION AGENT

（part of Chapter 3 is adapted with permission from
Geng, Z.; Finn, M. G., Fragmentable Polycationic Materials Based on Anchimeric Assistance. *Chemistry of Materials* **2016,** *28* (1), 146-152.）

3.1 Introduction.

Cationic polymers have gained significantly more attentions over the years because of the flexibility in improvements of design and precise control of structure-property relationship to enable a plethora of biomedical applications, especially gene delivery area[78-81]. The majority of such materials nowadays employ primary, secondary, and tertiary amines that require protonation to carry the desired charges. Polyethylenimine (PEI), synthesized by the ring opening polymerization of aziridine, is one of the most popular example. Recently, a series of acid-cleavable linkers and cytosolic reductive linkers, such as ester[19], acetals/ketals[45], imines[46] and disulfide bond[47], have been smartly employed in connecting branched PEI into transfection material with better biodegradability, however with the sacrifice of charge density.

Meanwhile, permanently charged species such as quaternary ammonium or alkylated pyridinium ions are only rarely employed as linkages in the backbone of polycationic chains, although they have been used to modify polymer branches[82-83] and are the predominant positively-charged constituents of cationic lipid head groups used as small-molecule transfection reagents.[84] One typical main chain quaternary nitrogen-containing

polymers, polyionenes, usually has to be synthesized through Menschutkin reaction at comparatively high solvent-refluxing temperature via S_N2 mechanism[85-86]. So the materials provided via that pathway are usually thermally and chemically stable at physiological temperature[87], thus non-biodegradable.

Here we studied the bio-related property of BCN, such as cytotoxicity and DNA transfection efficiency and proved them to be suitable for gene delivery vehicles, which polyionenes are usually good for[88-89].

3.2 Polyplex assembly

Binding of DNA and oligocation was examined by agarose gel shift assay; a representative example is shown in Figure 34, Figure 35. Polyplex formation at a level sufficient to completely inhibit the electrophoretic migration of a 6.2-kb double-stranded plasmid was observed with polymer **3a** at a low N/P ratio of approximately 1.0. A similar result was observed for **3i**, but polymer **3c** was less efficient, showing significant but incomplete retardation of electrophoresis at N/P = 50.

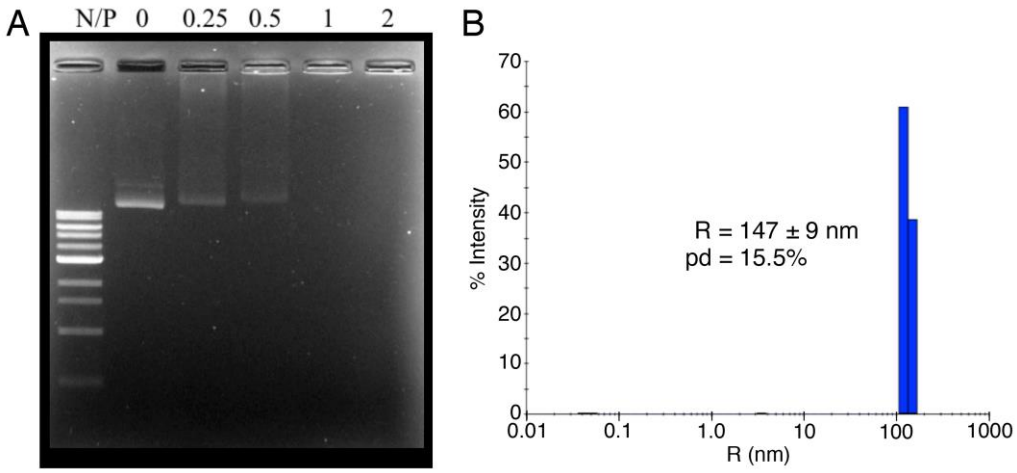

Figure 34 (A) Agarose gel electrophoresis of plasmid DNA mixed with increasing amounts of polycation 3a. (B) Dynamic light scattering of a PBS buffer solution containing these materials at N/P ratio of 2/1.

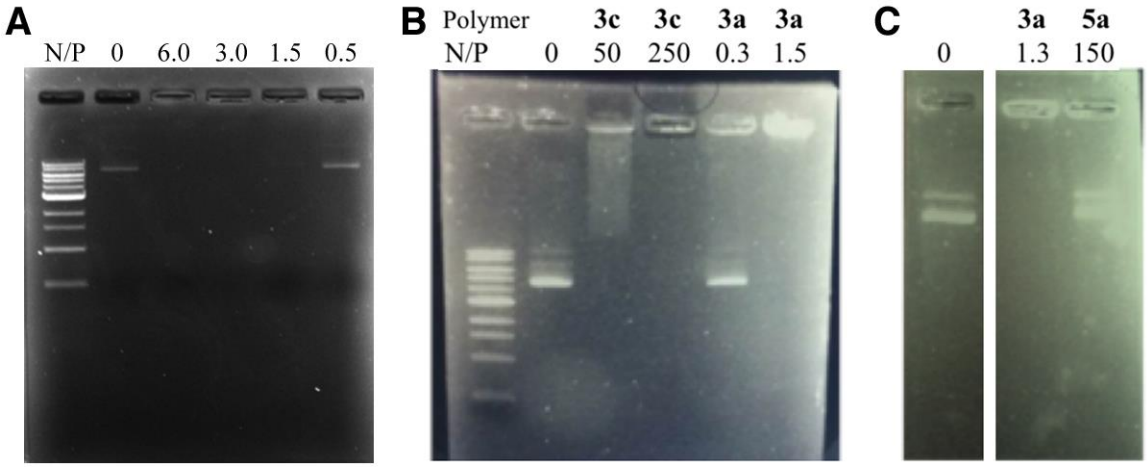

Figure 35 Polyplex formation assessed by agarose gel electrophoresis with plasmid at different N/P ratios. (A) Polymer 3i. (B) Polymer 3a *vs.* 3c. (C) Polymer 3a *vs.* small molecule analogue 5a.

Dynamic light scattering analysis and transmission electron microscopy image showed the resulting polyplexes to be of reasonable size and narrow size distribution (Table 9), with larger structures formed in PBS buffer *vs.* water. The presence of small-molecule

adduct **5a** in large excess had no effect on the electrophoresis of DNA nor was an observable polyplex formed. The polyplex formed with **3a** resisted heating at 37 °C for 48 hours, whereas particles formed with **3i** were decomposed after 24 hours of such treatment (Table 9, entries 2,5), corresponding to the fragmentation stabilities observed for the polycations alone (Table 6).

Table 9 Characterization of polymer/polyplexes formed from the indicated polycations (1 mg/ml in PBS) or polycations and double-stranded plasmid DNA (pcDNA3-EGFP, 6.2 kb, 20 ng/µL) at respect N/P. "Radius" is the hydrodynamic radius obtained by dynamic light scattering. A value of "n/o" indicates that no aggregates were observed.

Entry	cationic oligomer	N/P	conditions	radius (nm)	dispersity (%)
1	**3a**•$(NO_3)_n$	2	H_2O, RT, freshly prepared	82 ± 2	19.7
2	**3a**•$(NO_3)_n$	2	Entry 1, heated at 37 °C for 48 h	80 ± 3	16.5
3	**3a**•$(NO_3)_n$	2	PBS buffer, RT, freshly prepared	147 ± 9	15.5
4	**3i**•$(NO_3)_n$	2	H_2O, RT, freshly prepared	116 ± 6	30.5
5	**3i**•$(NO_3)_n$	2	Entry 4, heated at 37 °C for 48 h	n/o	n/o
6	**3i**•$(NO_3)_n$	2	PBS buffer, RT, freshly prepared	210 ± 18	37.8
7	**5a**•$(NO_3)_2$	150	H_2O or PBS	n/o	n/o
8	none	--	Plasmid DNA alone	n/o	n/o
9	**3a**•$(NO_3)_n$	--	PBS buffer, RT, no DNA	31 ± 2	17.6
10	**3c**•$(NO_3)_n$	--	PBS buffer, RT, no DNA	56± 4	21.4
11	**3i**•$(NO_3)_n$	--	PBS buffer, RT, no DNA	49± 3	12.4
12	**3i**•$(NO_3)_n$	--	Entry 11,heated at 50 °C for 4 h	n/o	n/o

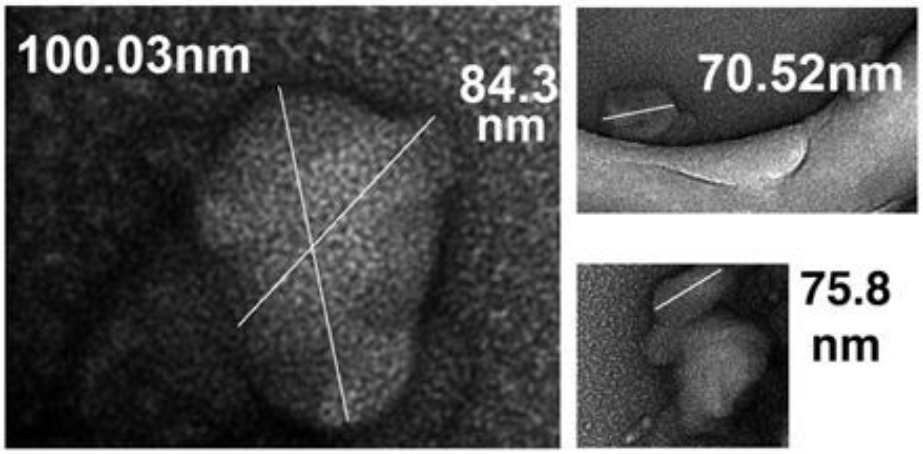

Figure 36 TEM images for polyplexes of plasmid and polymer 3a.

Polymer **3jj** (Structure described in Chapter 2) was made to allow for control of the overall charge of the material before fragmentation, since complete hydrolysis of the ester groups would provide a carboxylate anion for each pyridinium cationic center at neutral or basic pH.[75-76] Indeed, after incubation of **3jj** in 10 mM NaOH solution overnight, the ability of the resulting material to bind to DNA was significantly diminished relative to the starting esterified material Figure 37).

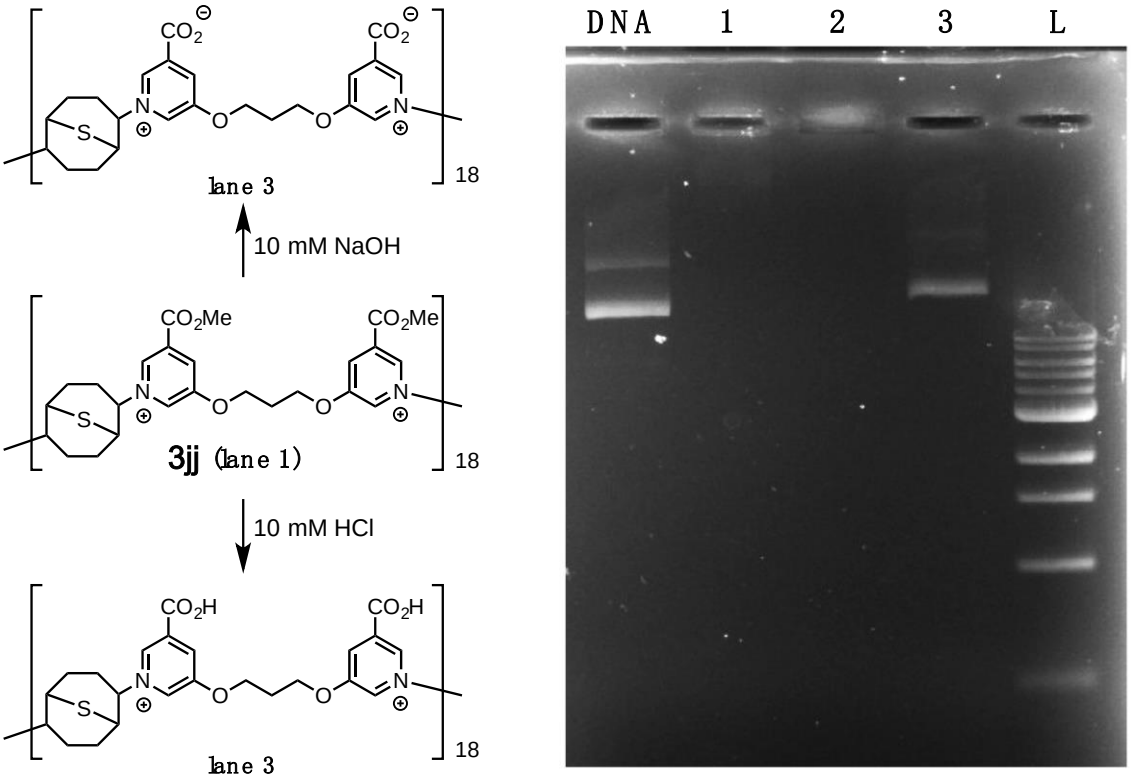

Figure 37 Efficiency of condensing DNA by 3jj, after 3jj had been treated with water (lane 1), HCl (lane 2), or NaOH (lane 3). Each mixture contained DNA at 50 μg/mL and 3jj at 1.6 mg/mL (N/P = 40).

3.3 Transfection of siRNA

The efficiency of both stable and fragmentable oligomers for the transfection of siRNA into HeLa cells was surveyed as shown in Figure 50, Figure 51. Much higher N/P ratios were required for siRNA transfection than for DNA complexation, and were constrained by the cytotoxicity of these new materials.

As shown in toxicity test (result shown in figures below), polymers **3a**, **3c**, and **3i** engendered significant toxicity after 24 hours treatment (red bar) at 2 μM, 200 μM and 12 μM respectively (concentrations refer to that of the chains, not the monomeric units,

calculated based on average molecular weights established by NMR); toxicities were much lower for 4 h exposure (black bar). At present, we do not understand what aspects of structure make for such different cytotoxic activities, but this is under investigation; it is possible that **3c** is unstable toward esterase in the cell or culture media. Polymers **3a** and **3c** should not fragment significantly by anchimeric substitution during 24 h incubation at 37 °C; **3i** may experience significant fragmentation over that time, since C-N bond breakage should occur to approximately 21% after 24 h.

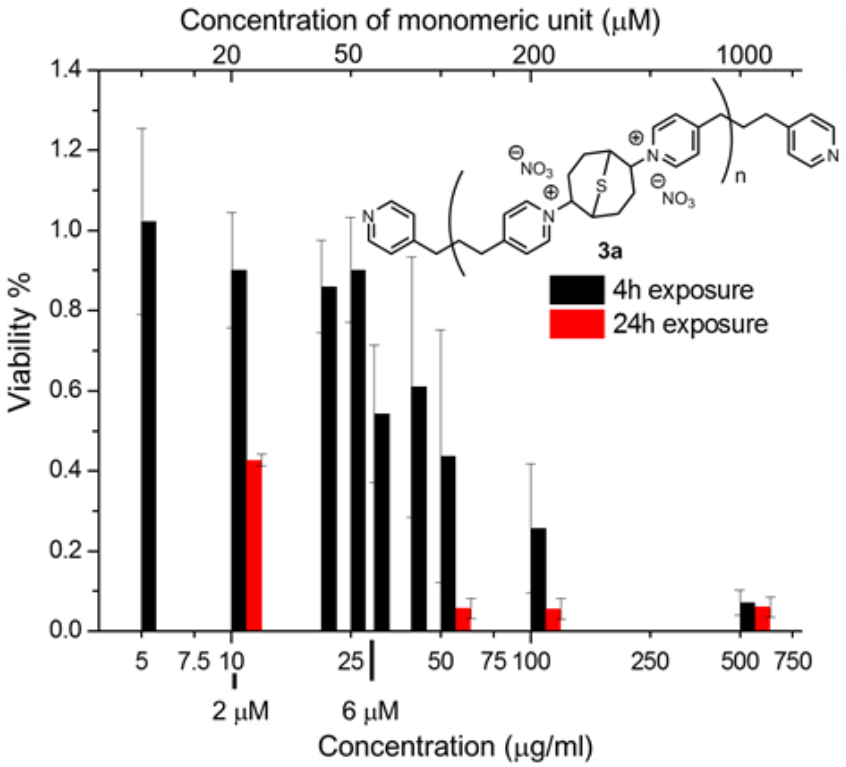

Figure 38 Cytotoxicity tests of BCN-based polymers 3a (M_n = 5 kDa) towards CHO-K1.

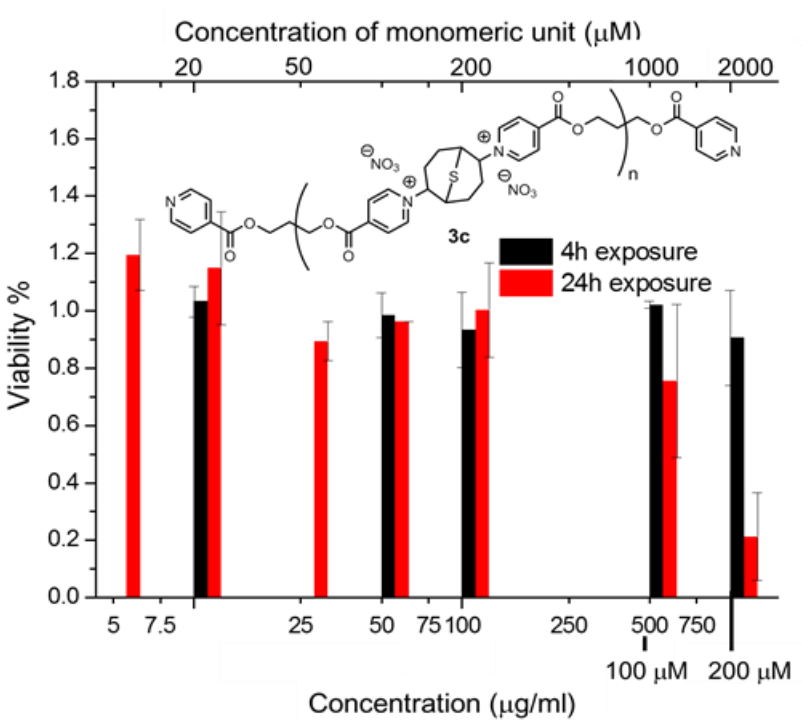

Figure 39 Cytotoxicity tests of BCN-based polymers 3c towards CHO-K1.

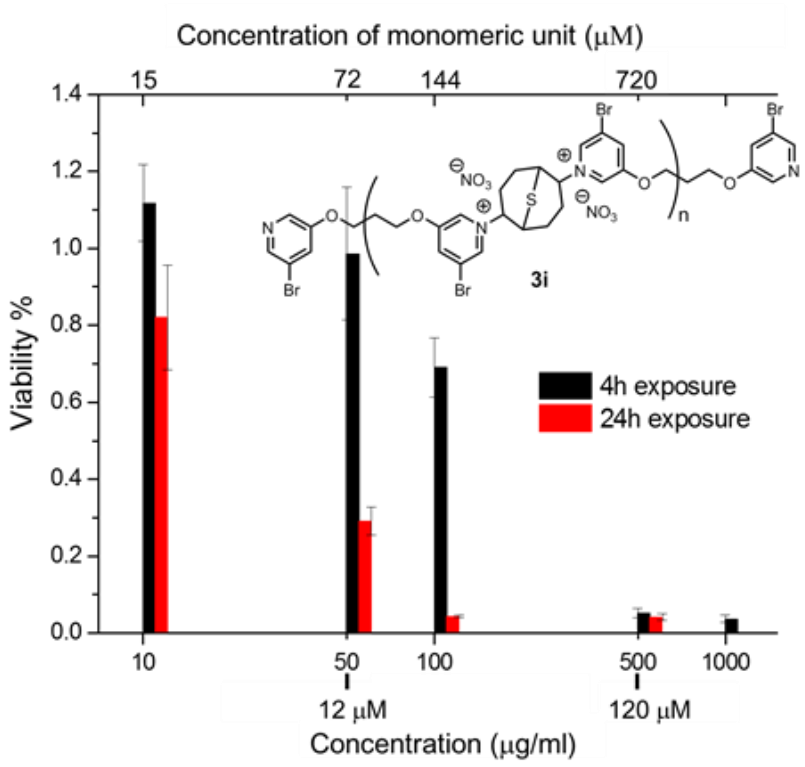

Figure 40 Cytotoxicity tests of BCN-based polymers 3i towards CHO-K1.

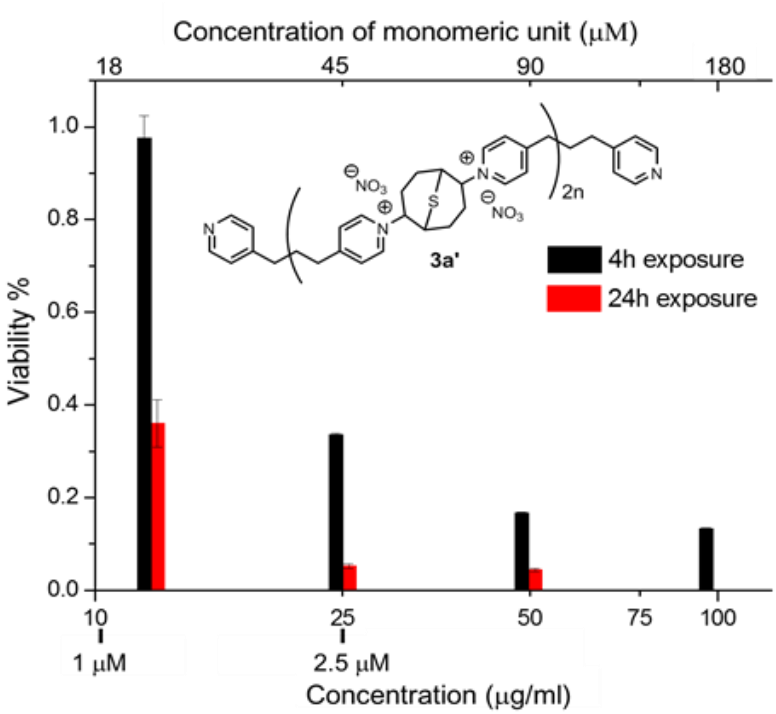

Figure 41 Cytotoxicity tests of BCN-based polymers 3a' (M_n = 10 kDa) towards CHO-K1.

In any event, the dipyridine monomers from which these polymers are constructed (**2a**, **2c**, and **2i**) were found to be nontoxic at concentrations below 500 μM, and the other decomposition product (diol **4**) had no effect on cellular viability up to 1 mM.

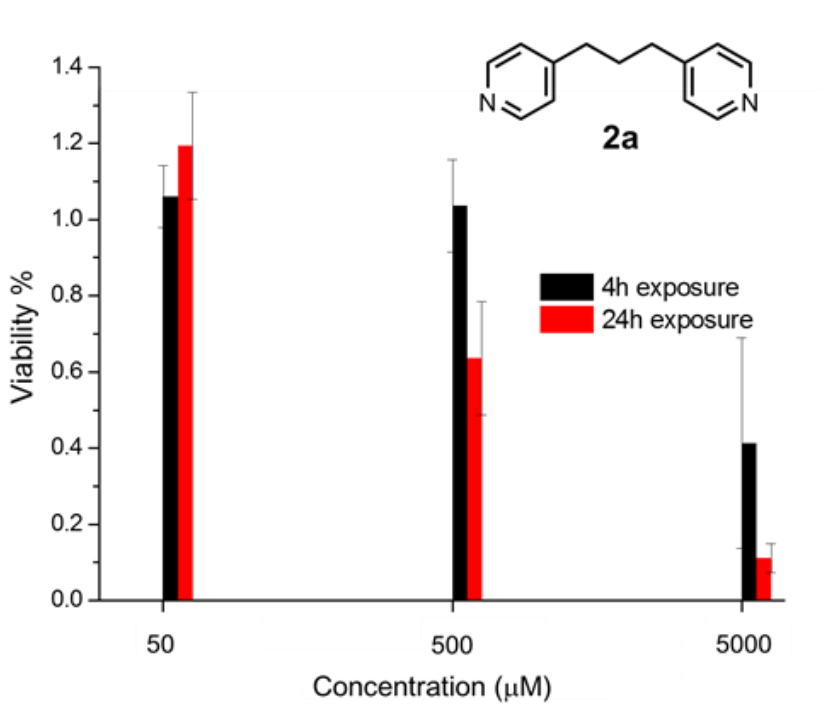

Figure 42 Cytotoxicity tests of BCN-based monomers/degradation product 2a towards CHO-K1.

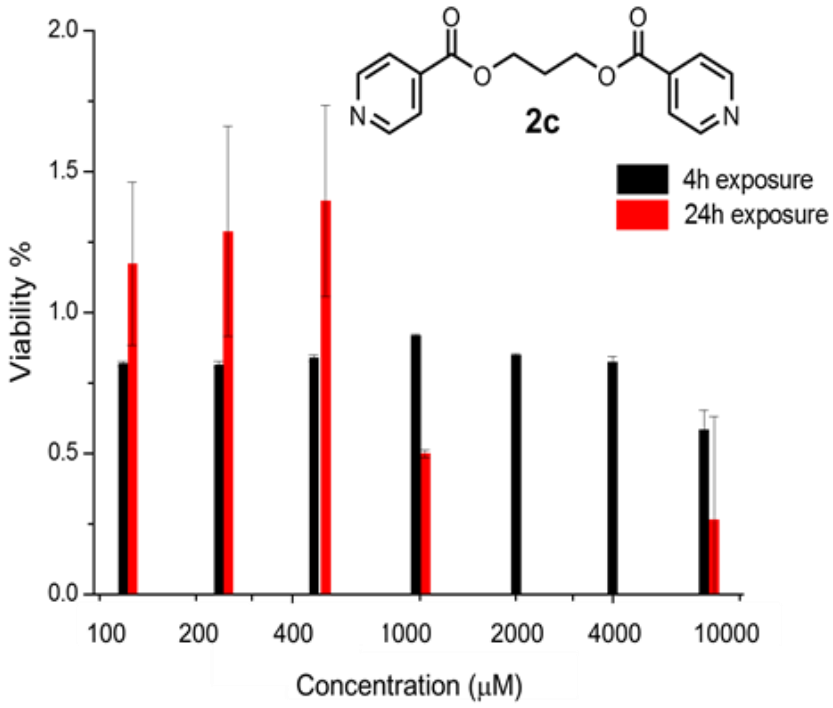

Figure 43 Cytotoxicity tests of BCN-based monomers/degradation product 2c towards CHO-K1.

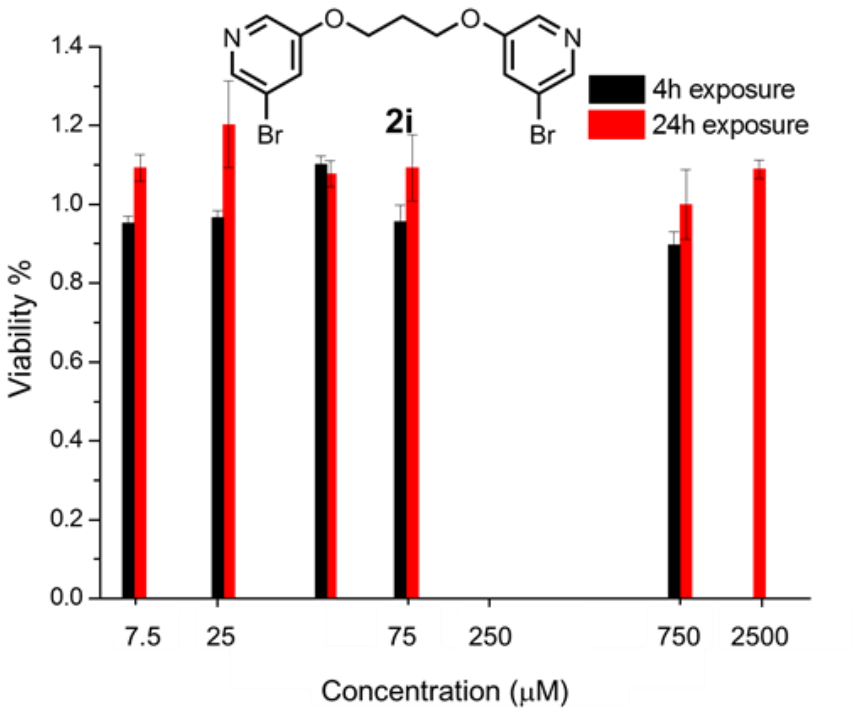

Figure 44 Cytotoxicity tests of BCN-based monomers/degradation product 2i towards CHO-K1.

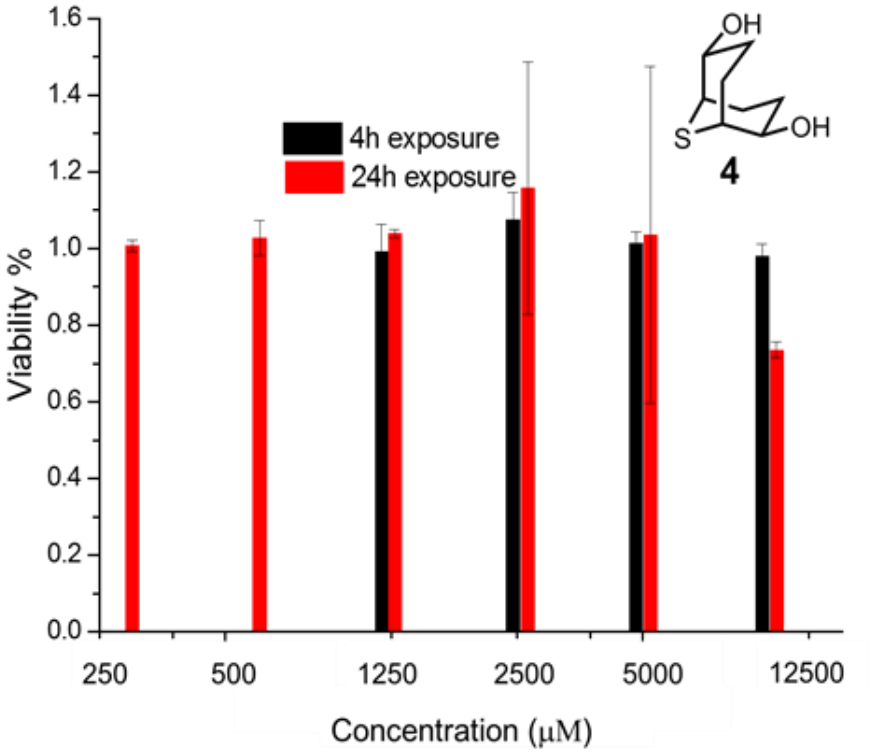

Figure 45 Cytotoxicity tests of BCN-based degradation product 4 towards CHO-K1.

Interestingly, the dicationic monomeric adducts **5a**, **5c**, and **5i** were much less toxic than their corresponding polymers (no effect up to 500 μM or greater), and a longer polymer (**3a'**, approximately 18 repeat units; Table 5, entry 7) was significantly more toxic than **3a** (approximately 10 repeat units) at 4 h exposure. These observations suggest that cytotoxicity is associated with the polymeric nature of these materials and therefore results from interactions with the cell membrane, rather than being a function of DNA alkylation. However, such mechanistic conclusions must await further studies.

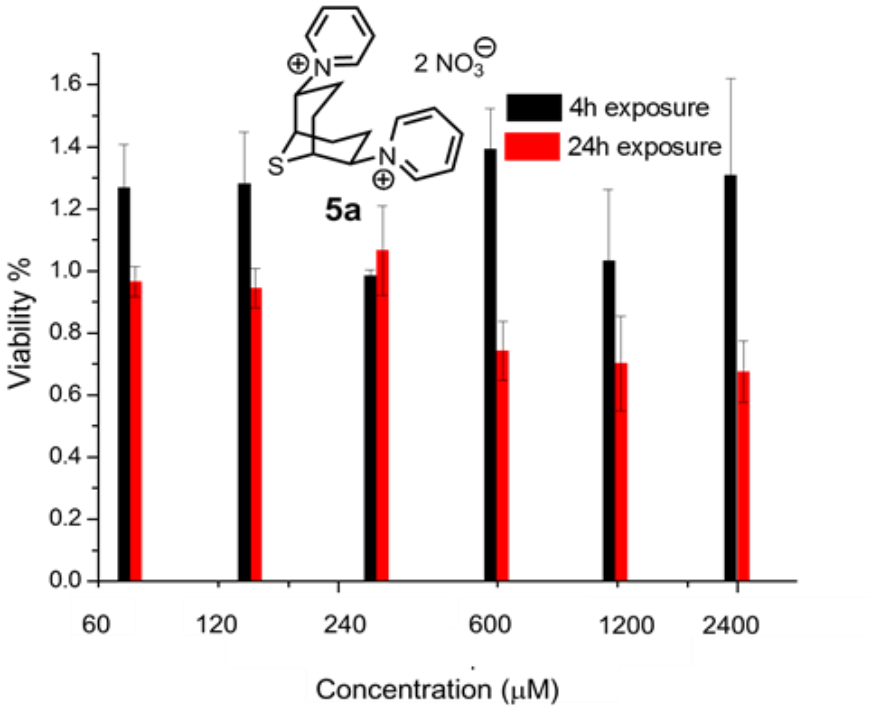

Figure 46 Cytotoxicity tests of BCN-based small-molecule adducts 5a towards CHO-K1.

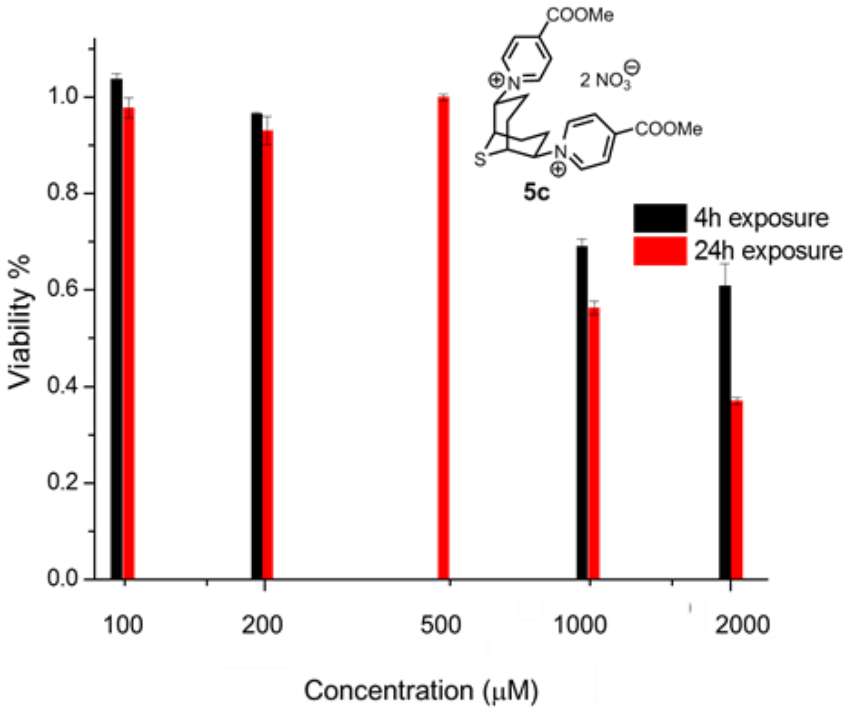

Figure 47 Cytotoxicity tests of BCN-based small-molecule adducts 5c towards CHO-K1.

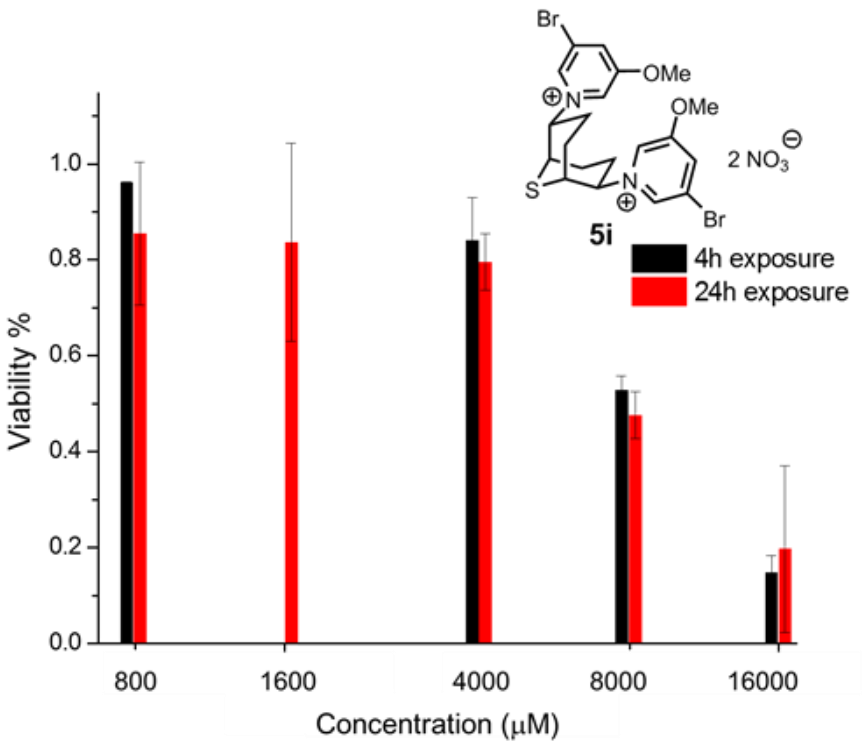

Figure 48 Cytotoxicity tests of BCN-based small molecule adducts 5i towards CHO-K1.

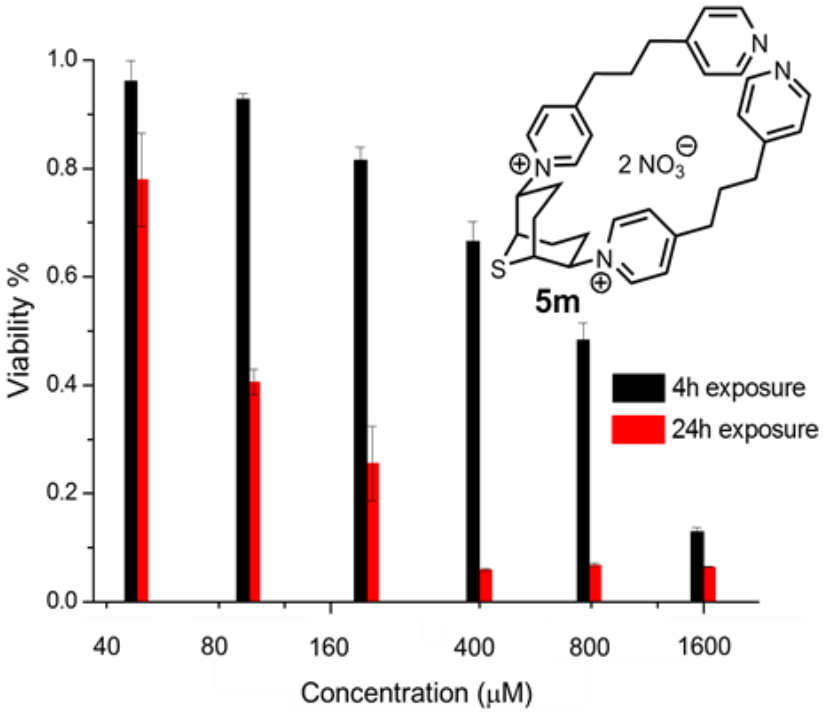

Figure 49 Cytotoxicity tests of BCN-based small-molecule adducts 5m towards CHO-K1.

At optimal N/P ratios of 55-65, polymer **3a** (1.2-1.5 μM) was able to mediate transfection with efficiencies near that of a standard commercial reagent (Lipofectamine, RNAiMAX) with similarly modest cytotoxicity (Figure 50), but these materials are, as discussed above, more toxic overall toward cultured cells. More readily degradable polymer **3i** exhibited no separation between cellular toxicity and apparent siRNA knockdown (starting from 6 μM shown in Figure 51). For clarity of demonstration, viability test of cells in the transfection trial has been outline independently with another box-and-whisker plot shown in Figure 52, Figure 53.

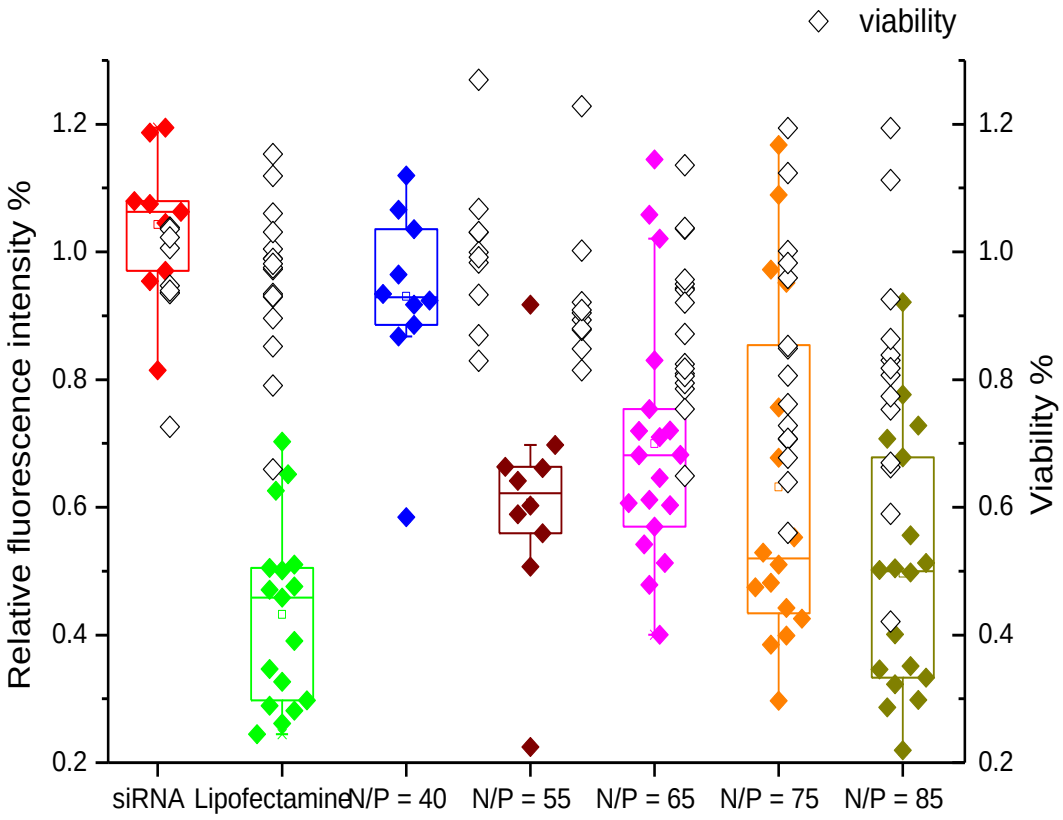

Figure 50 Box-and-whisker plot summarizing the results of siRNA transfection tests at various N/P ratios with polymer 3a.

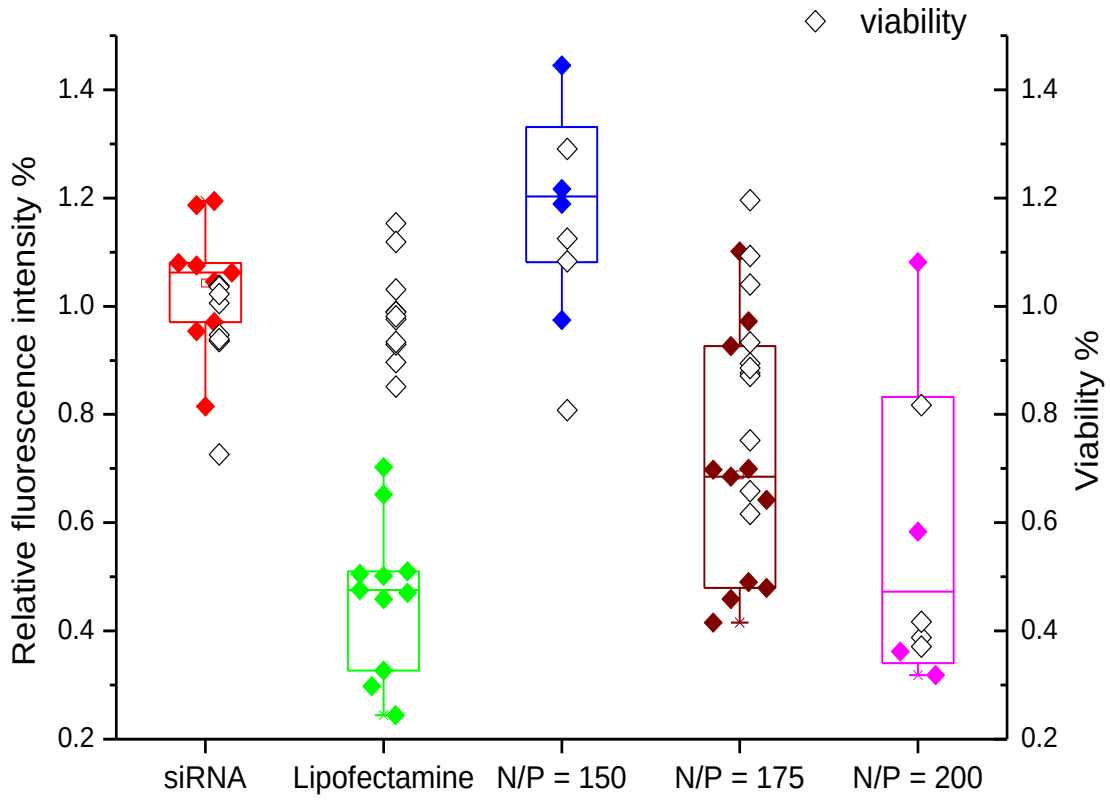

Figure 51 Box-and-whisker plot summarizing the results of siRNA transfection tests at various N/P ratios with polymer 3i.

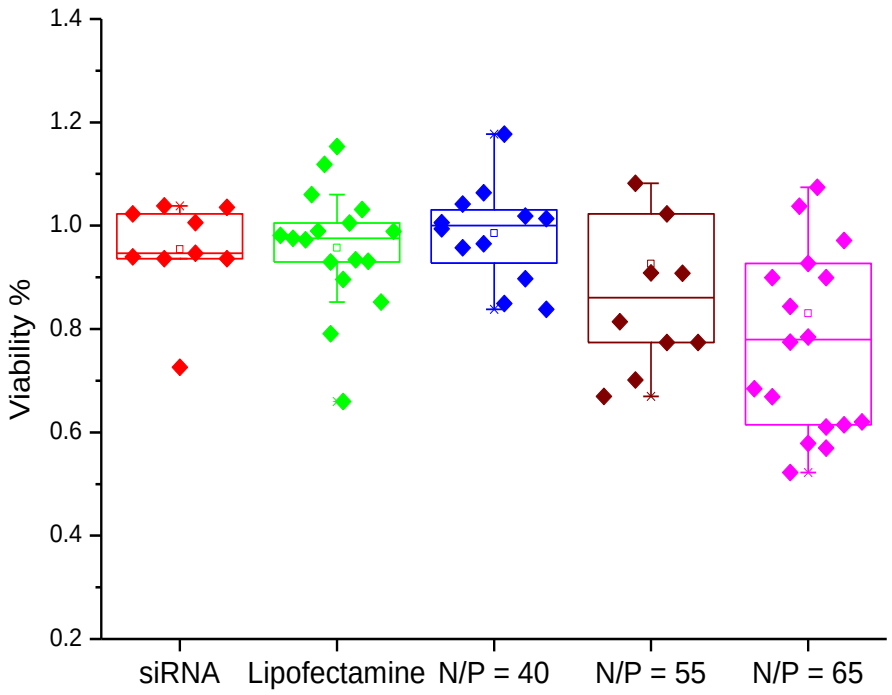

Figure 52 Box-and-whisker plot of viability test result for GFP-Hela at different N/P for polymer 3a in transfection experiment.

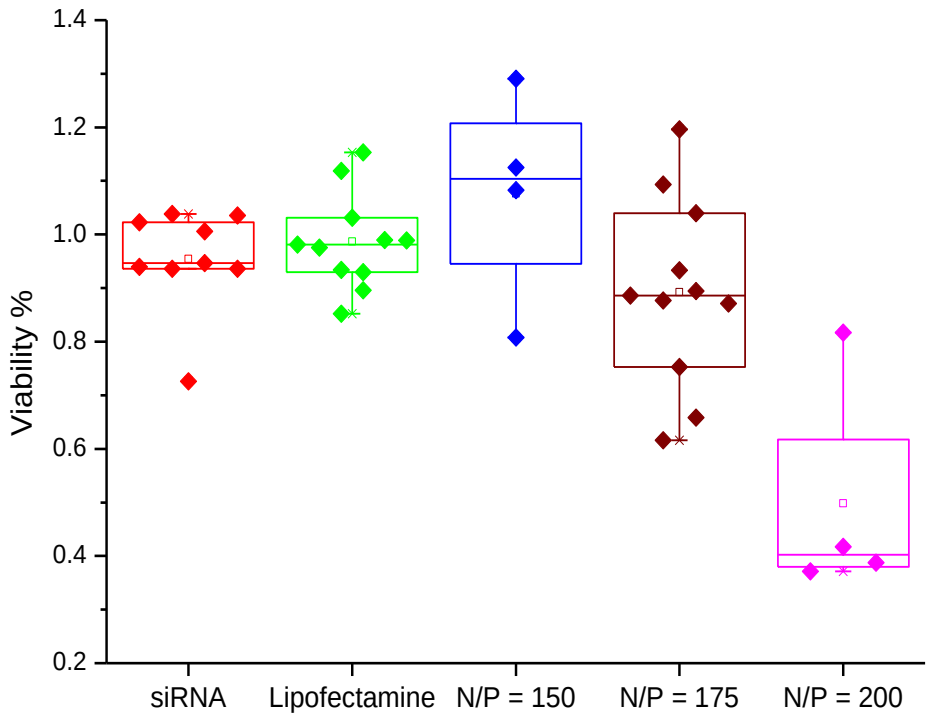

Figure 53 Box-and-whisker plot of viability test result for GFP-Hela at different N/P for polymer 3i in transfection experiment.

3.4 Transfection of plasmid DNA

Preliminary results in Figure 54 show that transfection and expression of plasmid DNA in HeLa cells could also be mediated by polymer **3a**. 200 ng of 6.2 kb plasmid responsible for GFP production has been transfected by treatment indicated in Figure 54.

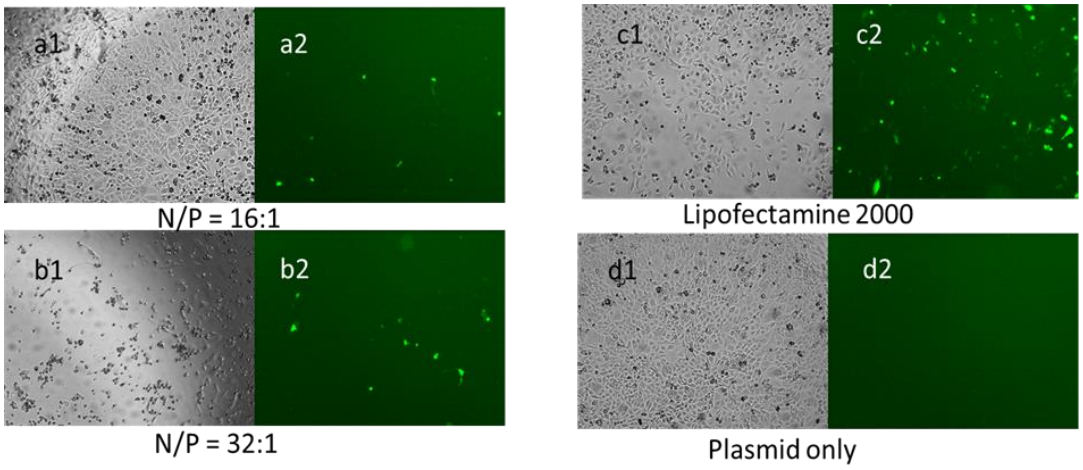

Figure 54 Fluorescence microscopy of HeLa cells transfected by polyplex made from BCN polymer 3a, lipofectamine and GFP plasmid only. Panels a1-d1 show brightfield images; a2-d2 show fluorescence emission images.

3.5 Design of hyperbranched polycations for higher siRNA transfection efficiency

Branched polyethylenimine(PEI) has been recognized as golden standard of transfection. However, there are very few reports on constructing polyionenes in hyperbranched architecture to be applied in gene delivery, in spite of their high potential. [90-93] Since BCN polycations has been modularly synthesized, it will be of interest to construct a library of hyperbranched polycations with similar linkages and compare their transfection potentials based on *in vitro* performance.

3.5.1 *Synthesis and characterization of hyperbranched BCN polycations*

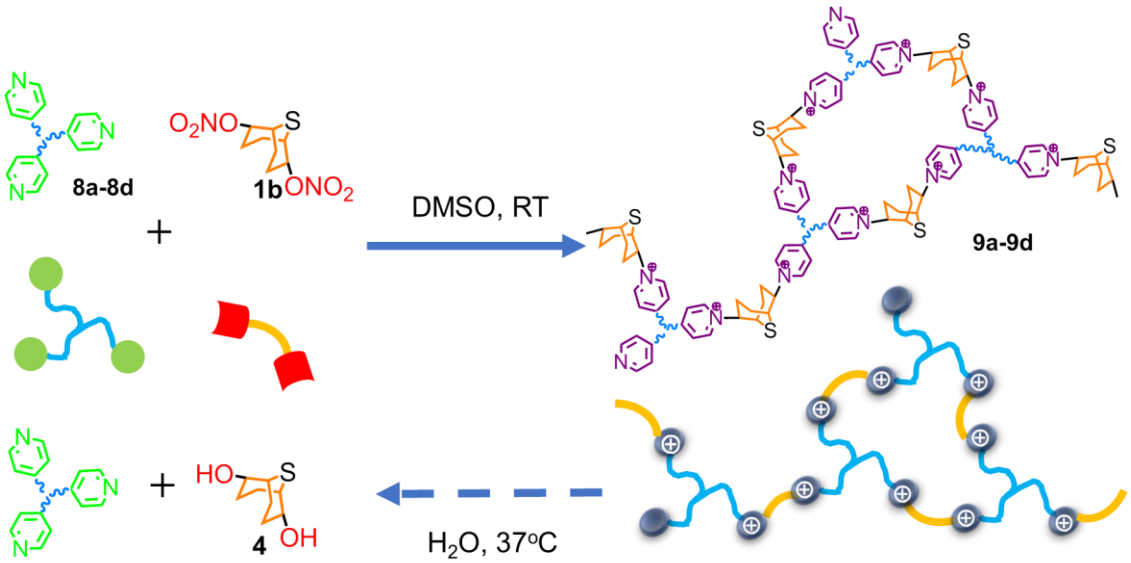

Figure 55 Schematic representation of condensation polymerization and depolymerization of BCN-based hyperbranched polycations, both processes taking place via anchimeric assistance.

Table 10 Components and characterization of hyperbranched BCN polycations.

nucleophile monomer	polymer	n [a]	M_n[b] (Da)	Half life (h) [c]
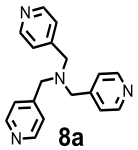 8a	9a	10	42000, 7200	-
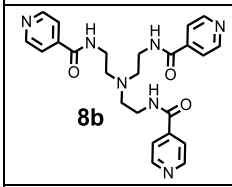 8b	9b	10	20000, 5400	400
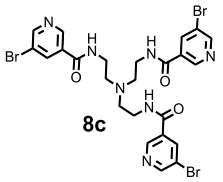 8c	9c	5	1600	6

Table 10 continued

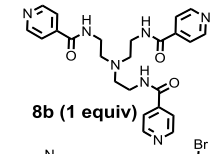 8b (1 equiv) 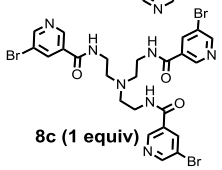 8c (1 equiv)	9d	5	3800	-
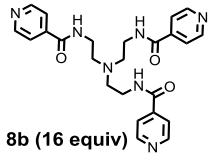 8b (16 equiv) 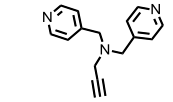 2bb (1 equiv)	9e	5	17000, 3000	-
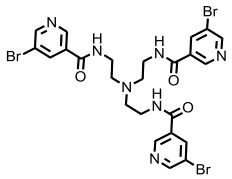 8c (16 equiv) 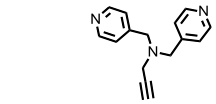 2bb (1 equiv)	9f	5	2300	-

a) n = ratio of alkylated (repeating units) to unreacted pyridine (chain end) determined by 1H NMR. b) M_n for major components (molecular for both peaks were estimated for bimodal trace) determined by GPC in 54/23/23 (v/v/v %) water/methanol/acetic acid containing 0.5 M NaOAc, calibrated with linear polyethylene glycol. c) half lives were estimated according to those of linear polycations reported before.

9-Thiabicyclo[3.3.1]nonyl electrophile **1b** was condensed with tripyridine trinucleophiles **8** at room temperature to provide novel hyperbranched polycations **9** in a

simple and scalable procedure (Figure 55). The nucleophilic components were prepared by reductive amination of pyridine-4-carboxaldehyde with amine linkers or condensation of trivalent amines to 4-pridinecarboxylic acid. After reaction with racemic BCN dinitrate **1b** under standard conditions with equimolar amounts of functionalities (electrophile **1b** concentration = 0.3 M, nucleophile **8** concentration = 0.2 M, dry dimethyl sulfoxide solvent, room temperature, 18 hours), the precipitated polycations were isolated by filtration and precipitation. Higher concentration of monomer (> 0.5 M) gave organogels which were difficult to purify.

Characterization of hyperbranched material was a challenge itself in addition to its being polyelectrolyte[94]. It was assumed the second substitution on each BCN core still to be faster than the first, as it did in step-growth polymerization to assemble linear polycations[95], so each branch was capped by the pyridine nucleophile. However, Average chain lengths was only roughly estimated by end-group analysis using ^{1}H NMR since the number of branches was missing (Table 10). Gel permeation chromatography (GPC) analysis in a high-ionic strength ternary composition aqueous-based mobile phase was also performed to provide a rough comparison of relative sizes among hyperbranched polyionens (Figure 56). All the prepared hyperbranched polycation and commercial available benchmark PEI displayed bimodal peaks in GPC traces (M_n located 10-400 kDa for 1st peak, 1-8 kDa for 2nd peak, shown in Figure 56), thus the absolute molecular weight determination is hard to acquire besides the lack of an appropriate standard and well-known interactions between the polyionenes and the stationary phase.

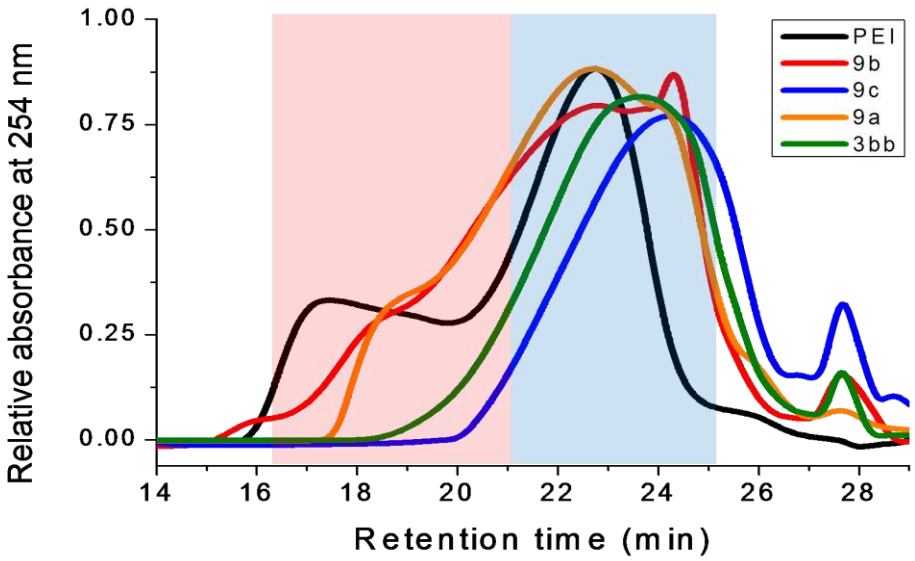

Figure 56 GPC curves of polymer 9a, 9b, 9c, PEI and L9d.

Using the same conditions, four hyperbranched polycations(**9a**-**9c**) were prepared from the tri(pyridine) linkers as shown in Table 1. The synthetic procedure proved to be modular, giving materials of similar size (n ≈ 10) except for monomer **8c** with two electron withdrawing group installed on the same pyridine to greatly reduce its nucleophilicity. According our previous study, these newly made linkages between monomers are highly dynamic at physiological condition and their half-lives were dictated by nucleophilicity of pyridine moiety. **9a** is not likely to fragment at all while **9b** and **9c** could be stable for tens and hundreds of hours in buffer of pH 7.4 at 37°C.

Random copolymers **9d-9f** were also prepared with two different trinulceophiles (**8b** and **8c)** or one trinucleophile and one dinucleohile (**8b,8c** and **8d)**. The polymerization degree was comparatively low (implied by smaller n, lower composition of pyridinium) compared with homopolymers prepared with same monomers**.** Constructed by pyridines

with different degrees of nucleophilicity, copolymer **9d** embraced a two-stage fragmentation. Within 22 hours, pyridinium peaks contributed by 3-bromo-5-amidopyridine in aromatic region shrunk to disappearance while the -CH_2-OH (on thiabicyclononane, around 4.2 ppm) peak resulted from hydrolysis kept growing until another 120 hours later (Figure 57). Additional functional group was incorporated by blending in 5% (composition in total pyridine moieties) of terminal alkyne containing monomer without altering property of original hyperbranched polycations. Functionality of "clickable" **9e** has been confirmed by successful conjugation of azide containing rhodamine molecules, indicated by colocalization of 254 nm (maximum for pyridine) and 540 nm (maximum for rhodamine) absorption peak at lower retention time (Figure 58).

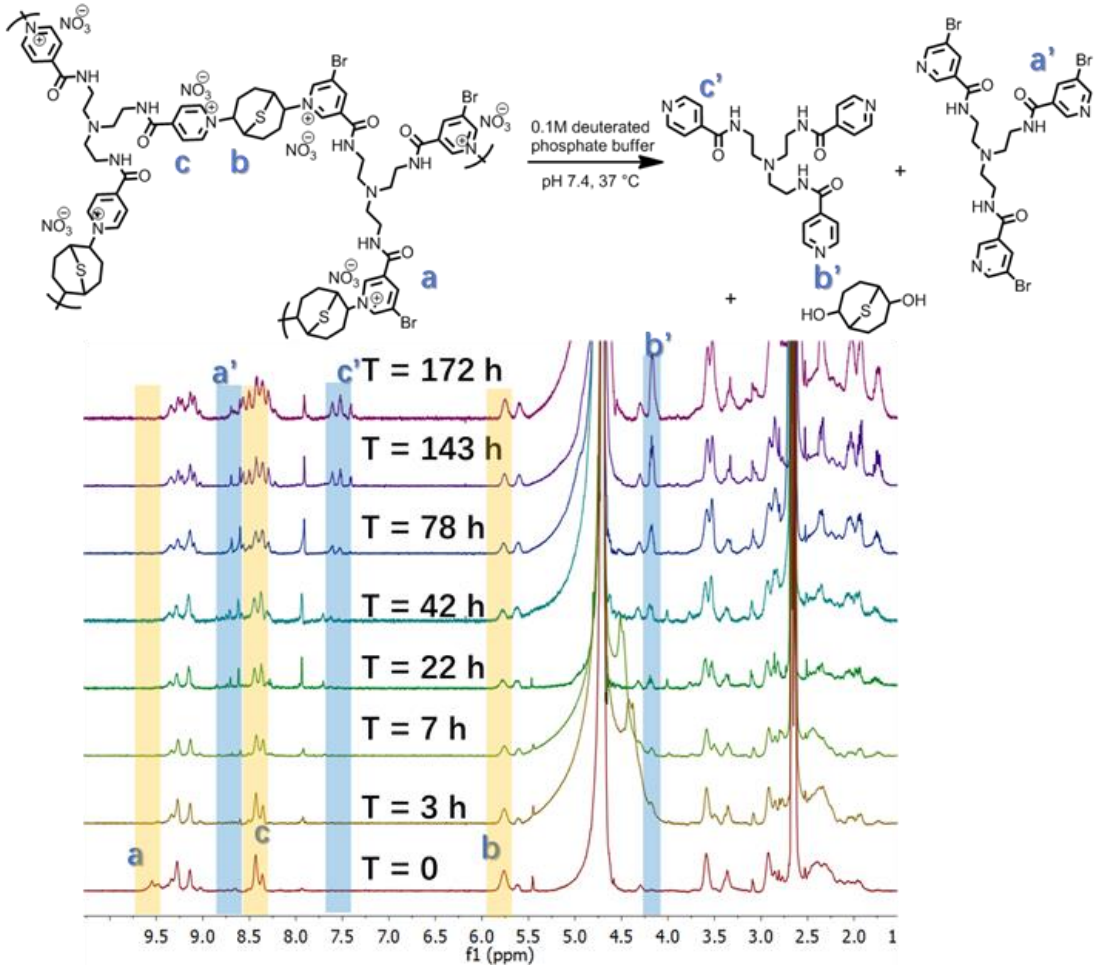

Figure 57 ^{1}H NMR spectra of polymer 9d in D_2O at 37 °C.

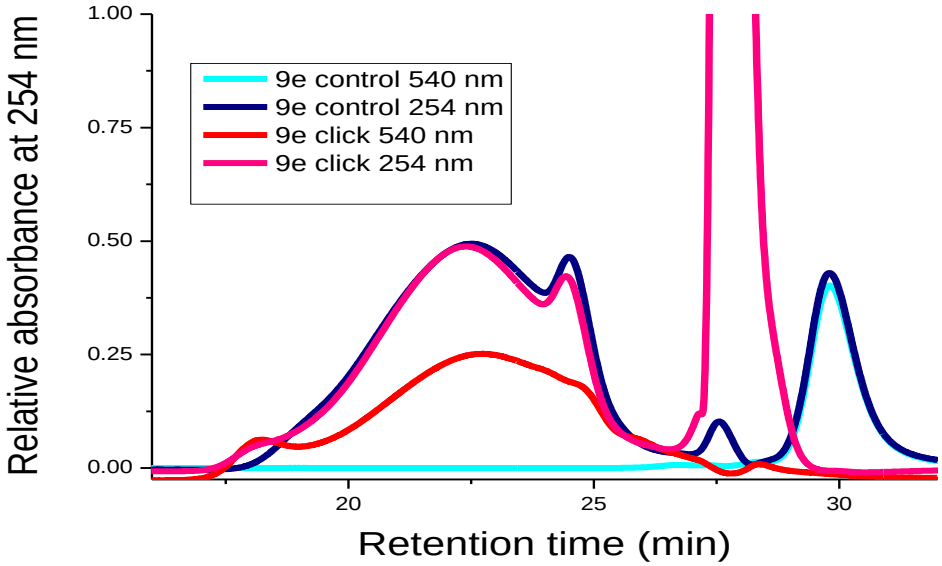

Figure 58 GPC traces of reaction mixture after 9e subjected to CuAAC reaction with ("click") and without (control) Cu^+ ion.

3.5.2 *Binding of DNA and siRNA to polycations*

Binding of DNA and hyperbranched polycation was firstly examined by agarose gel shift assay; a representative example is shown in Figure 59. Polyplex formation to completely inhibit the electrophoretic migration of a 6.2 kb double-stranded plasmid was observed with polymer **3b** at a N/P ratio as low as 7 and **9c** at N/P around 10.

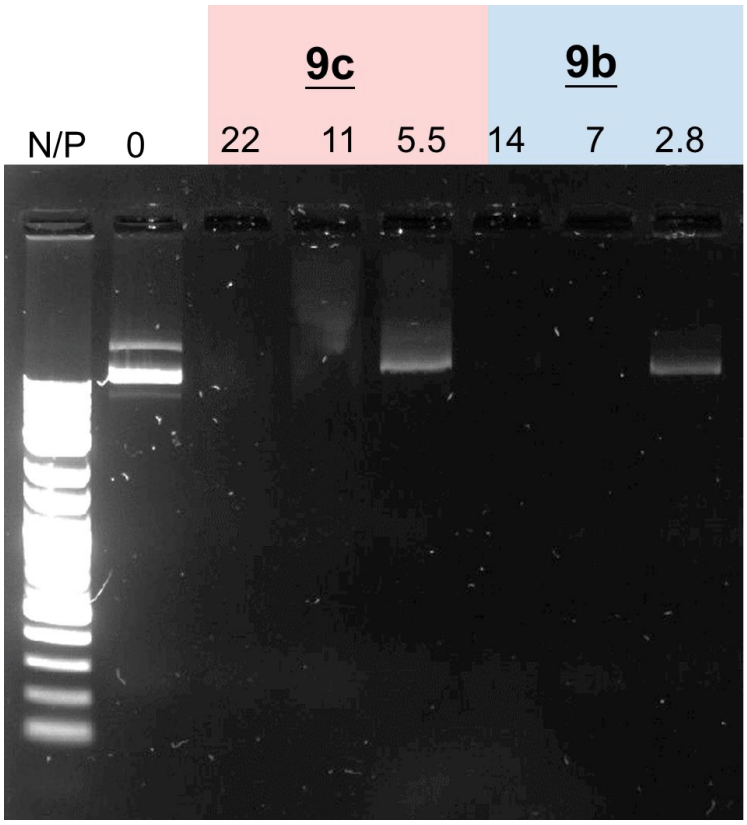

Figure 59 Agarose gel electrophoresis of plasmid DNA mixed with increasing amounts of polycation 9b,9c at various N/P.

Dynamic light scattering analysis showed the size of polyplexes assembled between hyperbranched polycations and 21-base-paired oligonucleoside (both DNA and RNA) fell between 80 nm and 160 nm. For polyplex assembled with DNA, the size would increase at higher N/P ratio while siRNA polyplex didn't have this obvious trend. Several hyperbranched BCN cationic polymer and commercial available branched PEI were employed to condense oligonucleotides into polyplex with consistent sizes at N/P = 28 while pure DNA nor polycations itself was observable at this concentration in DLS.

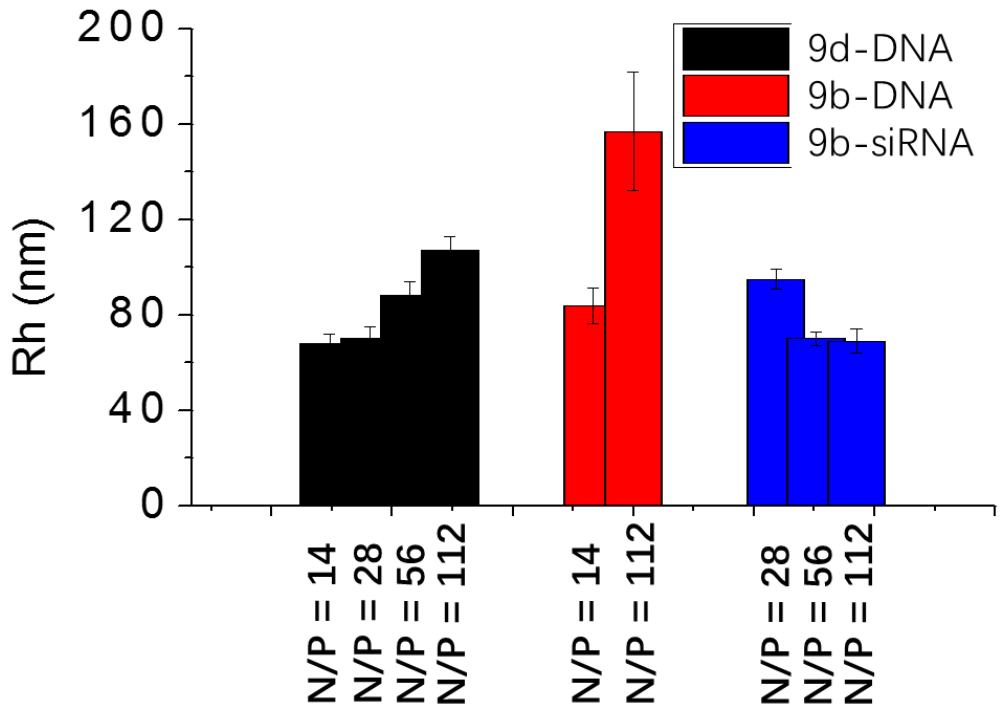

Figure 60 Hydrodynamic radius of polyplex assembled from hyperbranched BCN polycations and DNA/siRNA at different N/P.

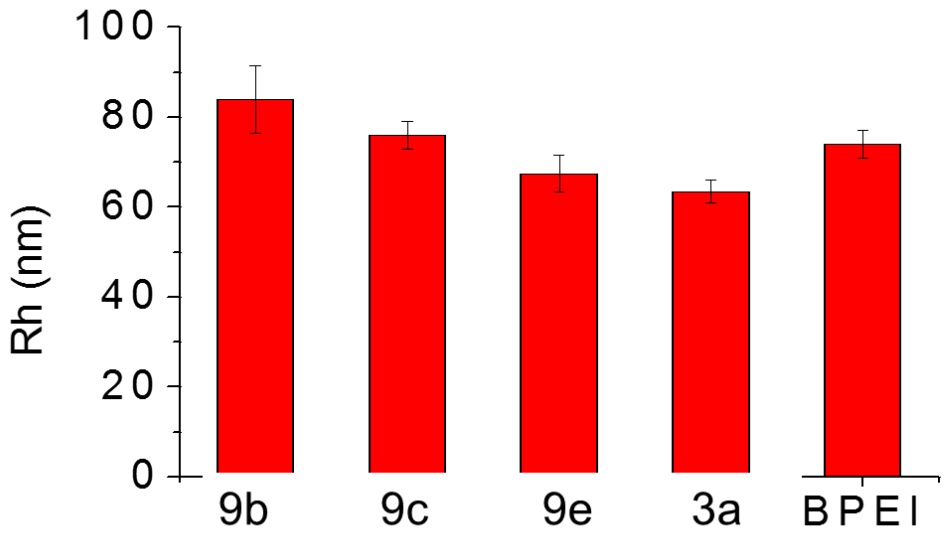

Figure 61 Hydrodynamic radius of polycation-oligo polyplexes acquired through dynamic light scattering at N/P ratio of 28/1. 3a stands for a linear BCN polycation referred in Chapter 2. PEI is commercial available with M_n of 60 kDa.

The polyplex formed with **9b** resisted heating at 37 °C for 48 hours, but would decompose after being treated at 60 °C for 24 hours, corresponding to the fragmentability profile of BCN polycations alone. Similarly, partial release of negatively charged plasmid has been observed on agarose gel after 48 hours incubation for polyplex formed with **9d**. Both implied high potentials of hyperbranched BCN polycations to intracellularly deliver nucleic acid in a controlled fashion.

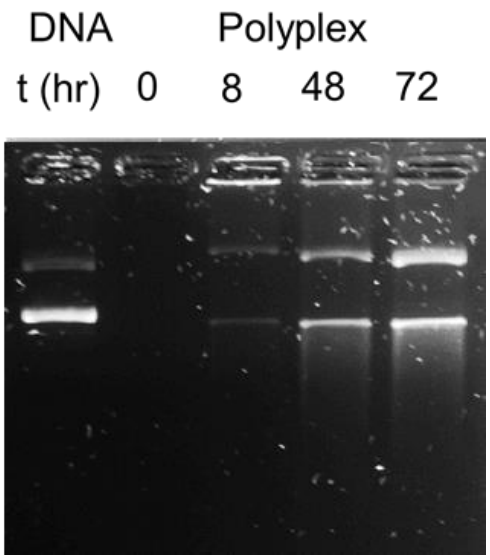

Figure 62 Agarose gel electrophoresis of polyplex assembled with plasmid and 9c incubated at 37 °C for different time.

3.5.3 *In Vitro Transfection Efficiency Evaluation of Polyplexes and comparison with linear polycations*

The efficiency of both stable and fragmentable hyperbranched polycations for the transfection of siRNA into HeLa cells was surveyed. as shown in Figures below. It is well known that polycationic material is universally toxic above certain concentration. Thus, a concentration screen for each polycation was performed while anchoring final siRNA concentration at 10 nM. Optimal N/P was determined for **3a-c** and PEI, where maximum transfection efficiency at similar level with positive control lipofectamine was achieved without sacrificing cell viability. Optimal N/P for each cationic material has been labeled on each graph with a blue square outside the data points. Viability below 80% (bolded blue line) is regarded as toxic entry. It was found 5-10 times higher N/P ratios were required for siRNA transfection than for DNA complexation. Since it was well known that behavior of

condensation polymers varied from batch to batch, a new batch of hyperbranched polycation 3b was made and tested for the transfection function and turned out to behave similarly with the previous batch, shown in Figure 64.

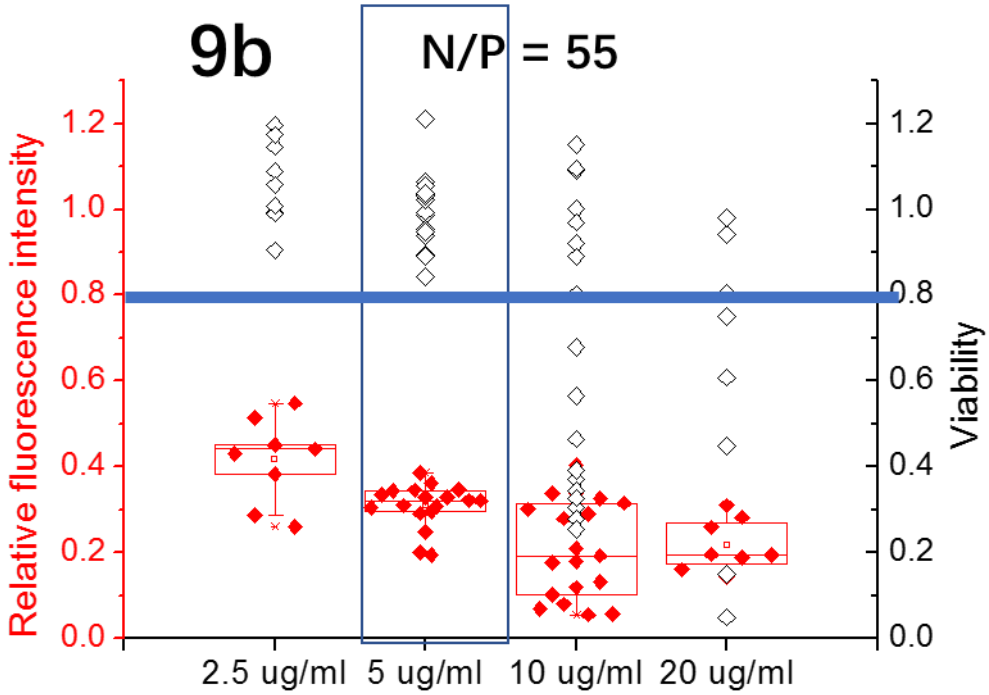

Figure 63 Box-and-whisker plots summarizing the results of transfection experiments for 9b at different N/P with 10 nM siRNA loading.

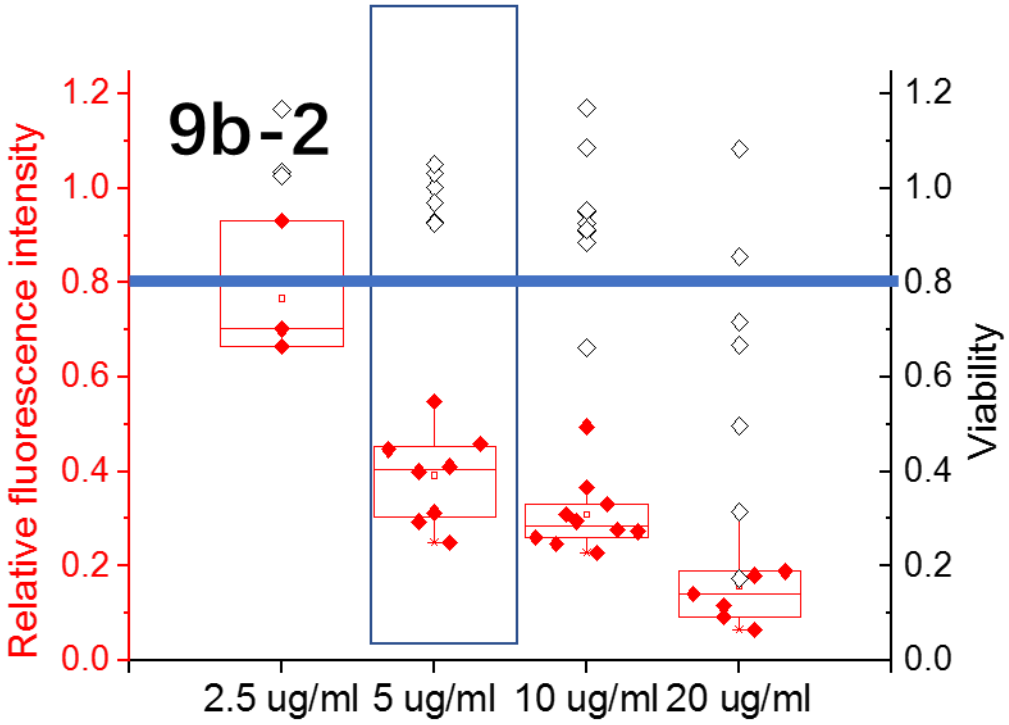

Figure 64 Box-and-whisker plots summarizing the results of transfection experiments for a different batch of 9b at different N/P with 10 nM siRNA loading.

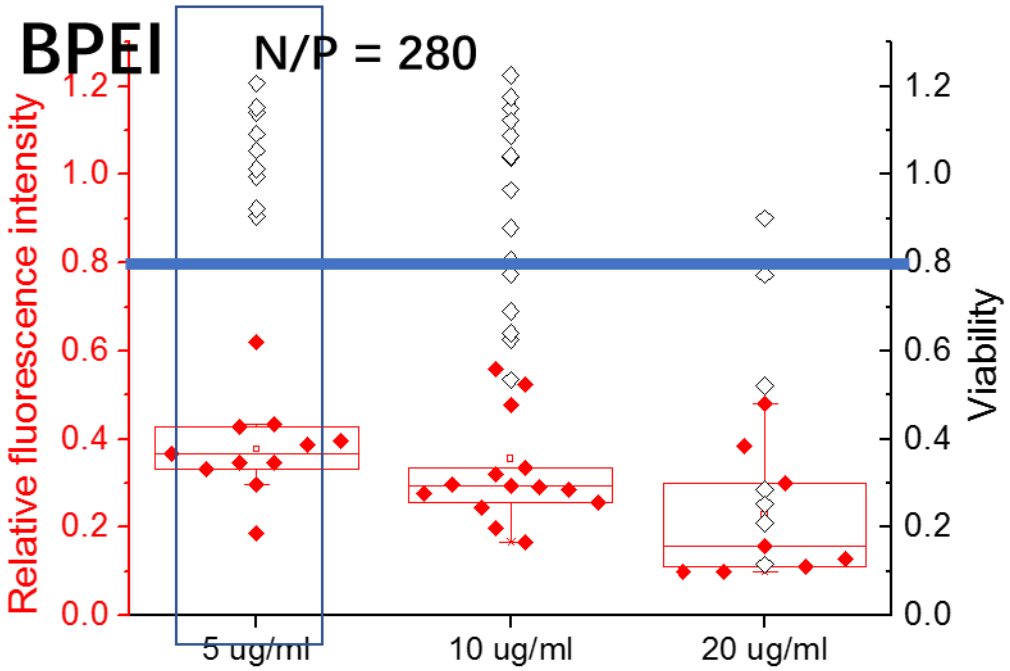

Figure 65 Box-and-whisker plots summarizing the results of transfection experiments for branched PEI (M_n = 60 kDa) at different N/P with 10 nM siRNA loading.

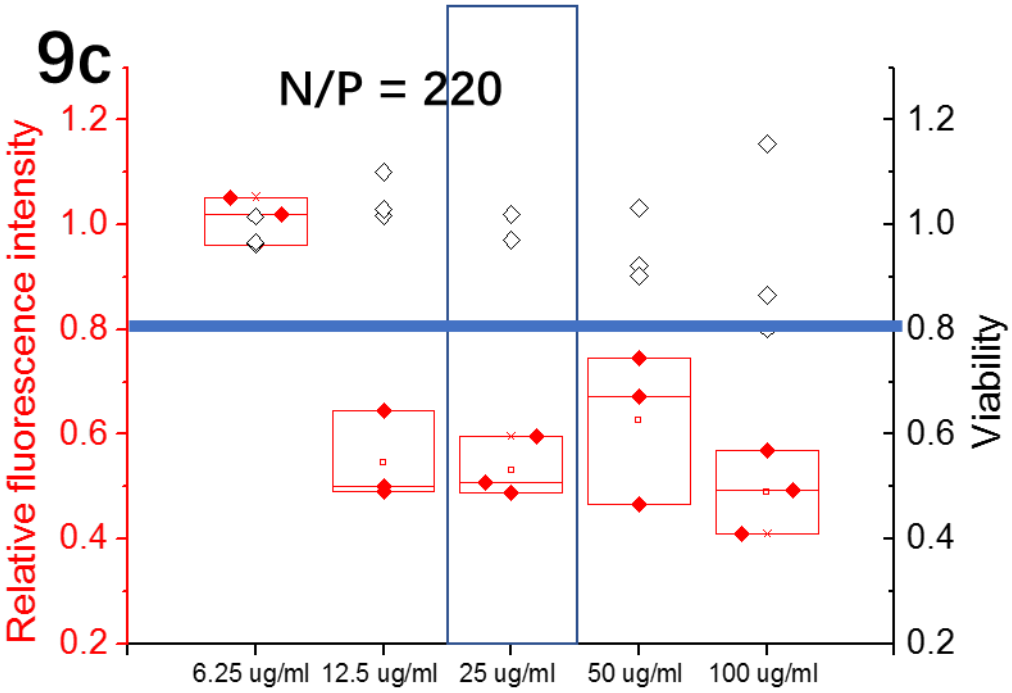

Figure 66 Box-and-whisker plots summarizing the results of transfection experiments for 9c at different N/P with 10 nM siRNA loading.

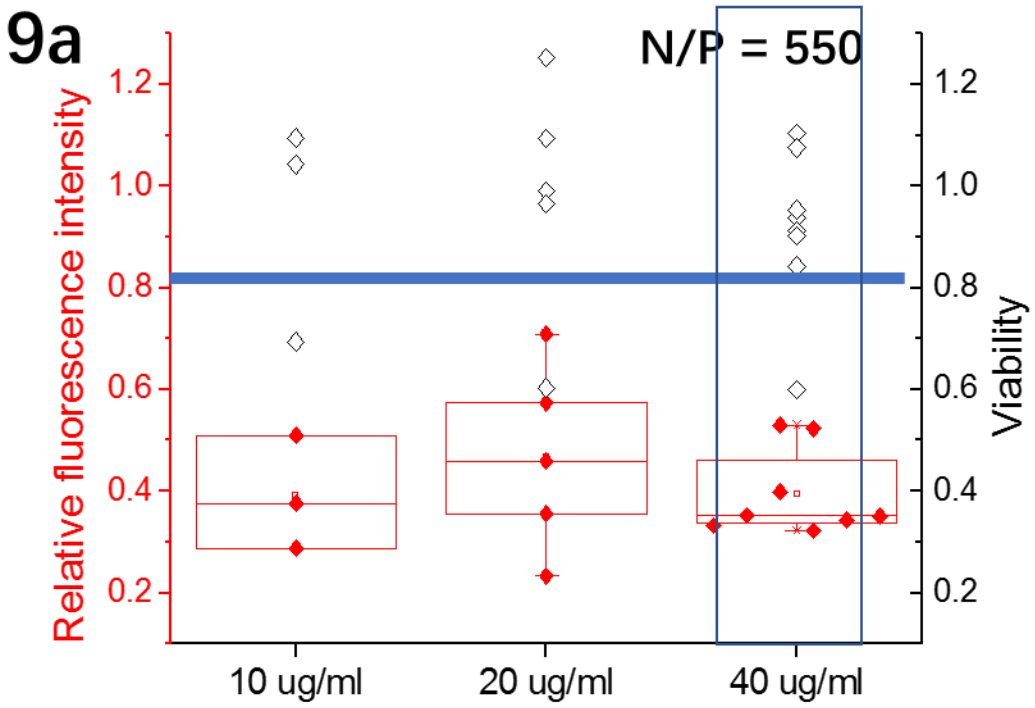

Figure 67 Box-and-whisker plots summarizing the results of transfection experiments for 9a at different N/P with 10 nM siRNA loading.

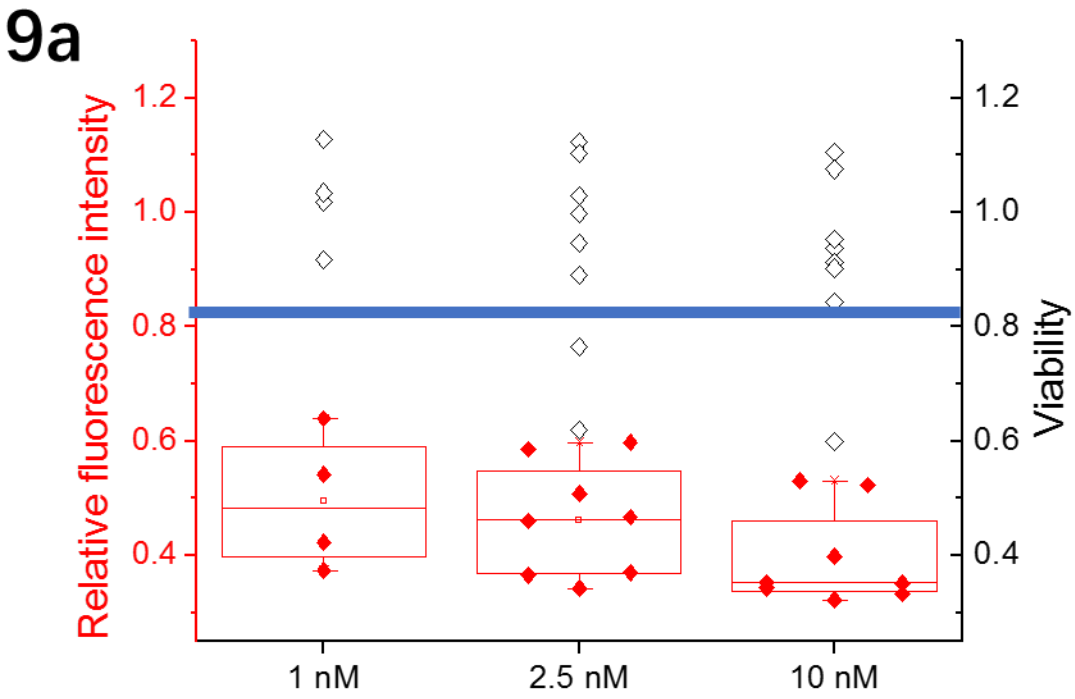

Figure 68 Box-and-whisker plots summarizing the results of transfection experiments for 9a at optimal N/P with various siRNA loading.

At optimal N/P, all of the material examined demonstrated more than 40% of transfection efficiency (respect to 60% of GFP intensity left). **9b** owned the most similar profile with Lipofectamine while **9a** and **9c** performed lower transfection efficiency than the other commercial available cationic polymer PEI. Example of linear polycations with amide linking pyridine rings has been approved to interact with cell membrane well according to our previous antimicrobial study associated with those polymers[68]. That might contribute to superior delivery efficiency of **9b** over **9a**. While what aspects of structure in

BCN polycations make for better transfection agents is still under investigation, good solubility, moderate stability toward nucleophile including water in the cell and comparatively high polymerization degree might be desirable, which **9c** lacked.

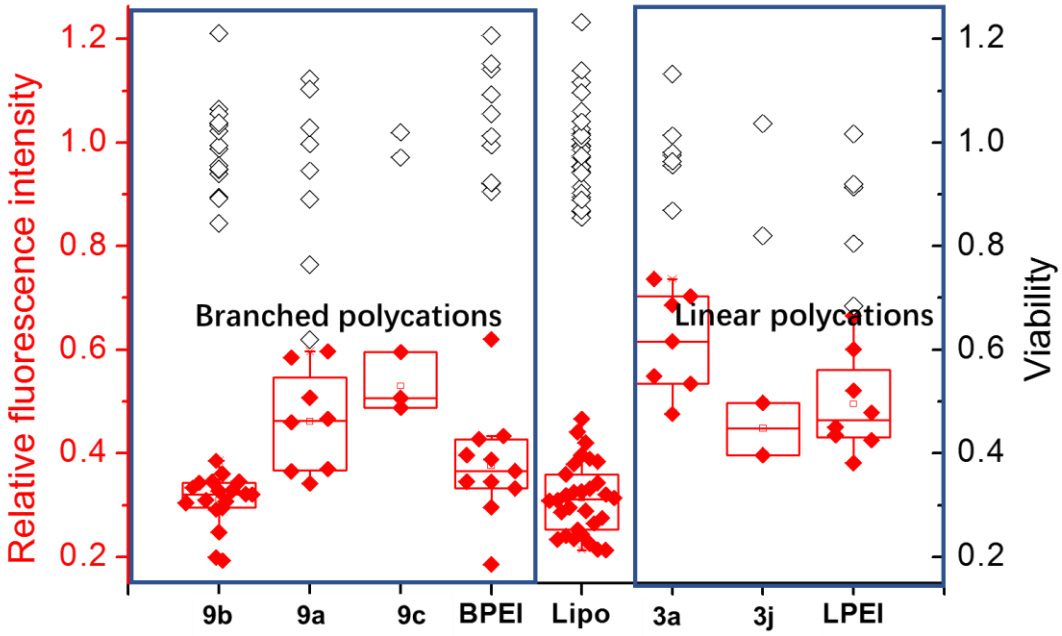

Figure 69 Box-and-whisker plots summarizing the results of transfection experiments at optimal N/P ratios for each polycationic materials.

Higher transfection efficiency has been achieved from hyperbranched PEI and **9a** compared with their linear counterparts at their respective optimal N/P ratios even though the size of polyplex is not dramatically different (Figure 61, Figure 69). This is consistent with the observation of hyperbranched architecture with higher capacity of buffering acidic pH and higher affinity to membrane for other cationic polycations.

In addition, with the decrease of siRNA loading, the transfection efficiency of **9b** didn't drop as quickly as commercial available standard PEI or lipofectamine (Figure 70). Even with 1nM of siRNA in final medium solution, which is recognized as a very low dosage[96-97], polyplex assembled with **9b** was still able to knockdown 60% of green fluorescence out of the whole cell population, indicating its superior potential for efficient non-viral transfection vehicle.

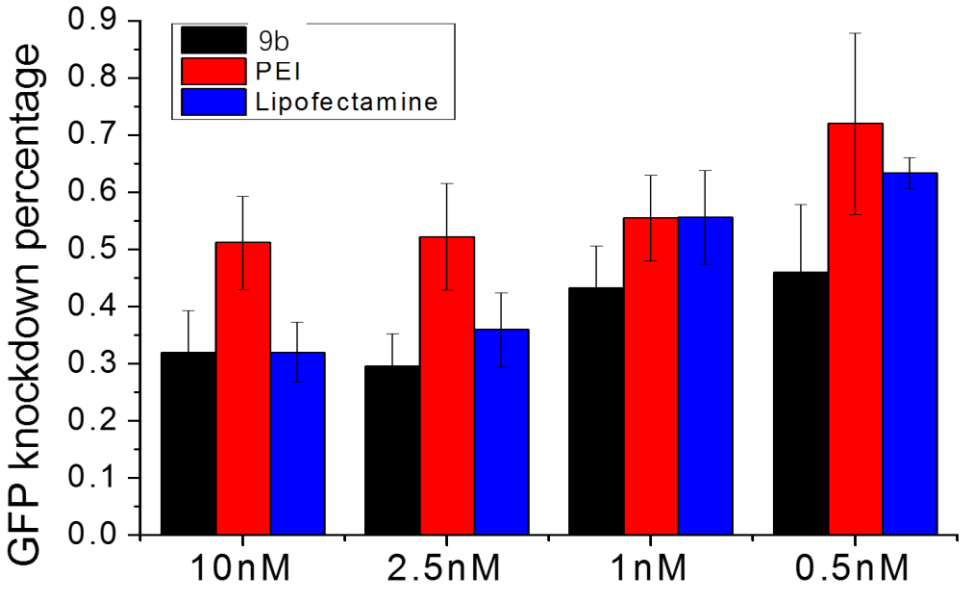

Figure 70 Comparison of transfection performance at lower siRNA loading between BCN polycation 9b and commercial available PEI and lipofectamine.

3.6 Intracellular trafficking of polycation and oligonucleotides

Fluorescence confocal microscopy imaging was employed to gain a deeper understanding of BCN-polycation-assembled polyplex trafficking inside cell. The Cy5

labeled oligonucleotides DNA was chosen as a visible cargo to mimic the siRNA in *in vitro* transfection study. It showed the polyplexes assembled at optimal N/P underwent efficient cell entry, and were seen to be clustered outside the nucleus. At an early stage, polyplex was partially colocalizing with the acidic endosome labeled with lysotracker, confirming its trafficking along the endosomal/lysosomal pathway.

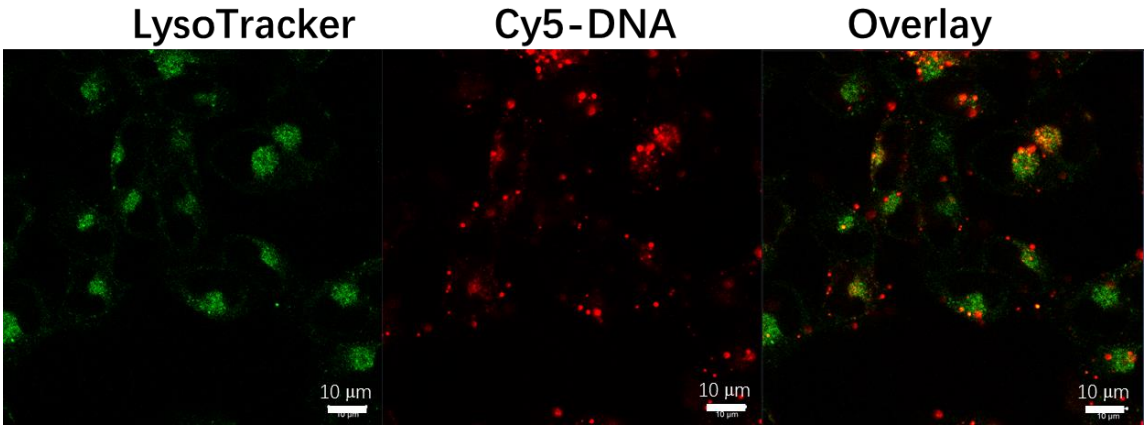

Figure 71 Confocal images of B16-F10 cells treated with 9b/Cy5-DNA polyplexes (red) for 4 h. The endosomes were stained with LysoTracker Green (green).

After 24 hours, the fluorescent pattern of cargo has turned from being punctate to diffusive indicating the successful endosome escape.

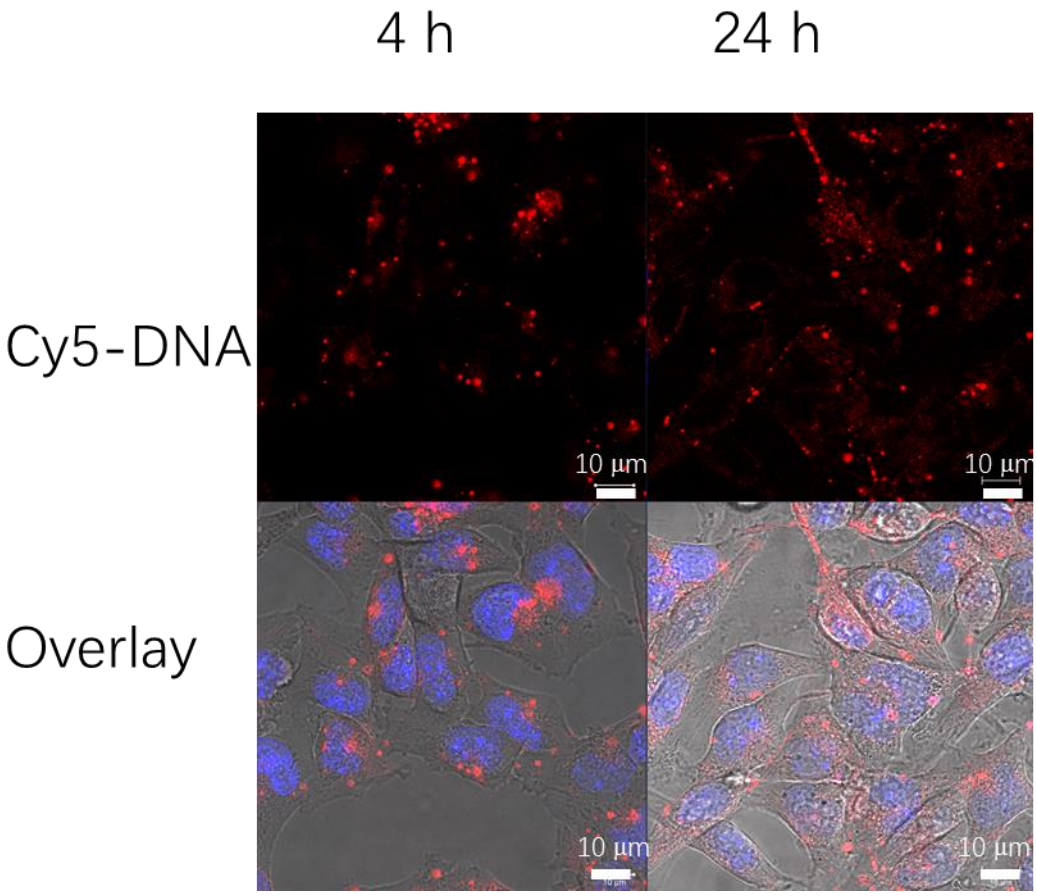

Figure 72 Confocal images of B16-F10 cells treated with 9b/Cy5-DNA polyplexes (red) for 4 and 24 h, respectively. The nuclei were stained with DAPI (blue).

With lower number of cells seeded in each well, nucleus entry was observed (Figure 73) implying the potential of transfecting DNA with therapeutic function. And the polyplex made from dye-labeled polycations and DNA colocalized well even after 24 hours taken up by cells, indicating the stability of the polyplex and protection provided to nucleotides cargo.

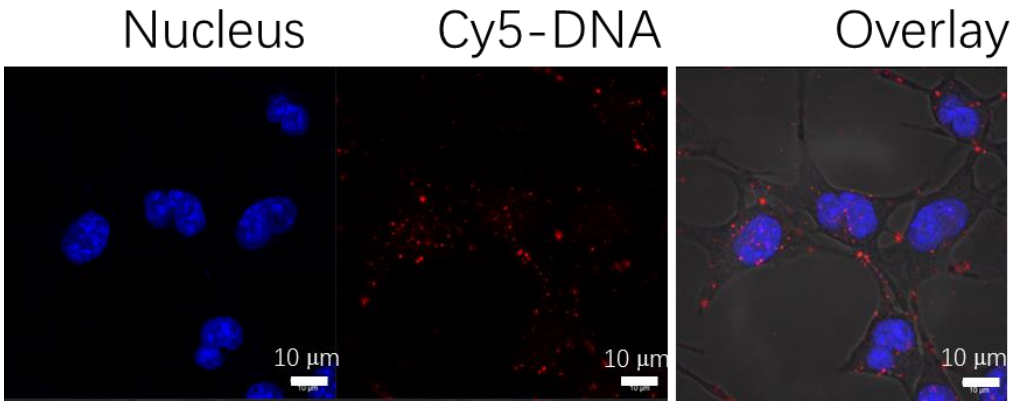

Figure 73 Confocal images of low seeding concentration of B16-F10 cells treated with 9b/Cy5-DNA polyplexes (red, middle) for 4 h; the nuclei stained with DAPI (blue, left) and overlay with bright field image (right).

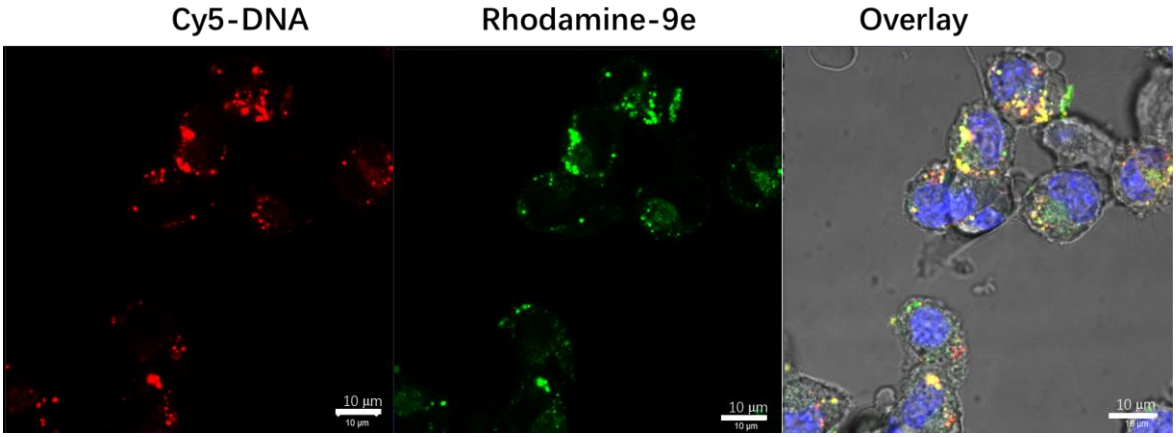

Figure 74 Confocal images of B16-F10 cells treated with 9e (green, middle)/Cy5-DNA (red, left) polyplexes for 24 h; with nuclei stained with DAPI (blue) and overlay with bright field image (right).

3.7 Conclusion

The BCN polymers were highly efficient in complexing DNA and showed functional behavior (transfection and cytotoxicity) normally associated with polycationic materials. The stability of polyplex assembled with the BCN polycations could be engineered by

tuning the basicity of the pyridine units to achieve controlled delivery. Compared with linear counterparts, hyperbranched BCN polymers demonstrated ability to transfect low dose siRNA, with higher efficiency than commercial available benchmarks. Further studies of structure-activity relationships are ongoing; this initial report suggests that these novel materials are worth exploring for biomolecular and materials applications, especially in gene delivery.

3.8 Experimental

3.8.1 *Cell culture*

All cell culture reagents were acquired from Life Technologies (Carlsbad, CA) unless noted otherwise. HeLa cells were purchased from ATCC (Manassas, VA). GFP-HeLa cells were a gift from the Schmid lab (University of Texas, Southwestern, Dallas, TX). Cells were grown and maintained in complete growth media: Dulbecco's Modified Eagle's Medium (DMEM), supplemented with 5% Fetal bovine serum (FBS), sodium pyruvate (1 mM), penicillin (100 units/mL), streptomycin (100 μg/mL), and GlutaMAX (2 mM). Cells were grown at 37 °C under humidified air with 5% CO_2. Glass-bottomed culture dishes were purchased form MatTek (Ashland, MA). Accutase was purchased from Innovative Cell Technologies, Inc. (San Diego, CA). 96-well microtiter plates were purchased from Thermo Fisher (Waltham, MA).

3.8.2 *Knockdown of green fluorescent protein in GFP-HeLa cells*

siRNAs were a gift from Integrated DNA Technologies (Coralville, IA), with the following sequences. GFP sense: 5'-CAAGCUGACCCUGAAGUUCUU, GFP antisense: 5'-GAACUUCAGGGUCAGCUUGUU. Approximately 1×10^4 GFP-HeLa cells/well were plated in a 96-well plate in 100 μL of complete growth media, and adhered overnight at 37 ^{o}C. For postitive control experiments, 10 nM double-stranded siRNA was transfected with Lipofectamine RNAiMAX according to the manufacturer's protocol. After 24 h, the media was replaced with complete growth media (100 μL/well). Fluorescence was measured 48 h post-transfection. For knockdown experiments with polyplexes (containing 10 nM siRNA in each well finally), cells were plated as described. 100 μL of oligomer/ds-siRNA complexes at indicated N/P ratios were added to cells. Media was again replenished after 24 h. Fluorescence was measured 48 h post-treatment.

3.8.3 *Viability of mammalian cells in the presence of BCN monomers and polymers*

Approximately 1×10^4 CHO-K1 cells/well were plated in a 96-well plate in 100 μL of complete growth media, and adhered overnight at 37 ^{o}C. The media was then replaced by 100 μL of polymer or monomer in serum-free media at the indicated concentration. Full media was replenished after 4 or 24 h. Viability was measured by MTT assay, with non-treated cells assigned as 100% viability.

3.8.4 *Synthesis of tripyridine linker*

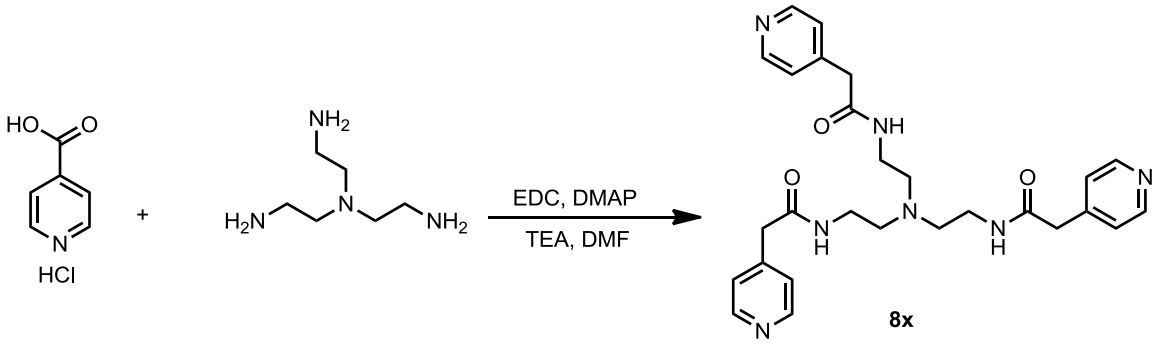

Isonicotinic acid hydrochloride (411 mg, 3 mmol, 3 equiv), 4-Dimethylaminopyridine (DMAP, 15.3 mg, 0.15mmol, 15% equiv), triethylamine (405 mg, 3 mmol, 3 equiv) and N1,N1-bis(2-aminoethyl)ethane-1,2-diamine were dissolved (146 mg, 1 mmol, 1 equiv) in 5 mL of DMF at 0 ^{o}C. 1-ethyl-3-(3-dimethylaminopropyl)carbodiimide hydrochloride (EDC, 570 mg 3 mmol, 3 equiv) were added in small batches. The solution was warmed to room temperature in 30 minutes and stayed overnight. Solvent was removed by rotary evaporation, basified by NaOH, and then purified by reverse phase column chromatography (3:7 water/acetonitrile elution). The desired product was obtained as pale yellow solid (112 mg, 22% yield).^{1}H NMR (700 MHz, MeOD) δ 8.45 (d, *J* = 6.0 Hz, 2H), 7.37 (d, *J* = 5.9 Hz, 2H), 3.57 (s, 2H), 3.23 (t, *J* = 6.2 Hz, 2H), 2.60 (t, *J* = 6.2 Hz, 2H). ^{13}C NMR (700 MHz, MeOD) δ 170.76, 148.63, 146.26, 124.84, 53.62, 41.51, 37.72.

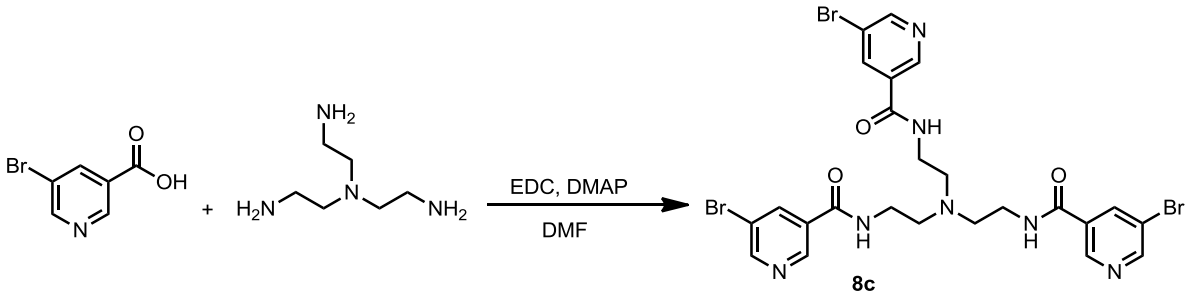

5-bromonicotinic acid (606 mg, 3 mmol, 3 equiv), 4-Dimethylaminopyridine (DMAP, 15.3 mg, 0.15mmol, 15% equiv) and N,N-bis(2-aminoethyl)ethane-1,2-diamine were dissolved (146 mg, 1 mmol, 1 equiv) in 5 mL of DMF at 0 ^{o}C. 1-ethyl-3-(3-dimethylaminopropyl)carbodiimide hydrochloride (EDC, 570 mg 3 mmol, 3 equiv) were added in small batches. The solution was warmed to room temperature in 30 minutes and stayed overnight. The solid was filtered, washed with 1 M NaOH solutions and dried. The desired product was obtained as a white powder (226 mg, 32% yield). ^{1}H NMR (700 MHz, DMSO) δ 8.87 (d, *J* = 1.5 Hz, 1H), 8.78 (dd, *J* = 2.1, 1.1 Hz, 1H), 8.64 (t, *J* = 5.2 Hz, 1H), 8.27 (dt, *J* = 3.1, 1.6 Hz, 1H), 3.39 (dd, *J* = 11.9, 6.1 Hz, 2H), 2.71 (t, *J* = 6.3 Hz, 2H). ^{13}C NMR (176 MHz, DMSO) δ 163.90, 152.78, 147.32, 137.59, 131.79, 120.42, 53.63, 38.25.

3.8.5 *Characterization of hyperbranched polycations*

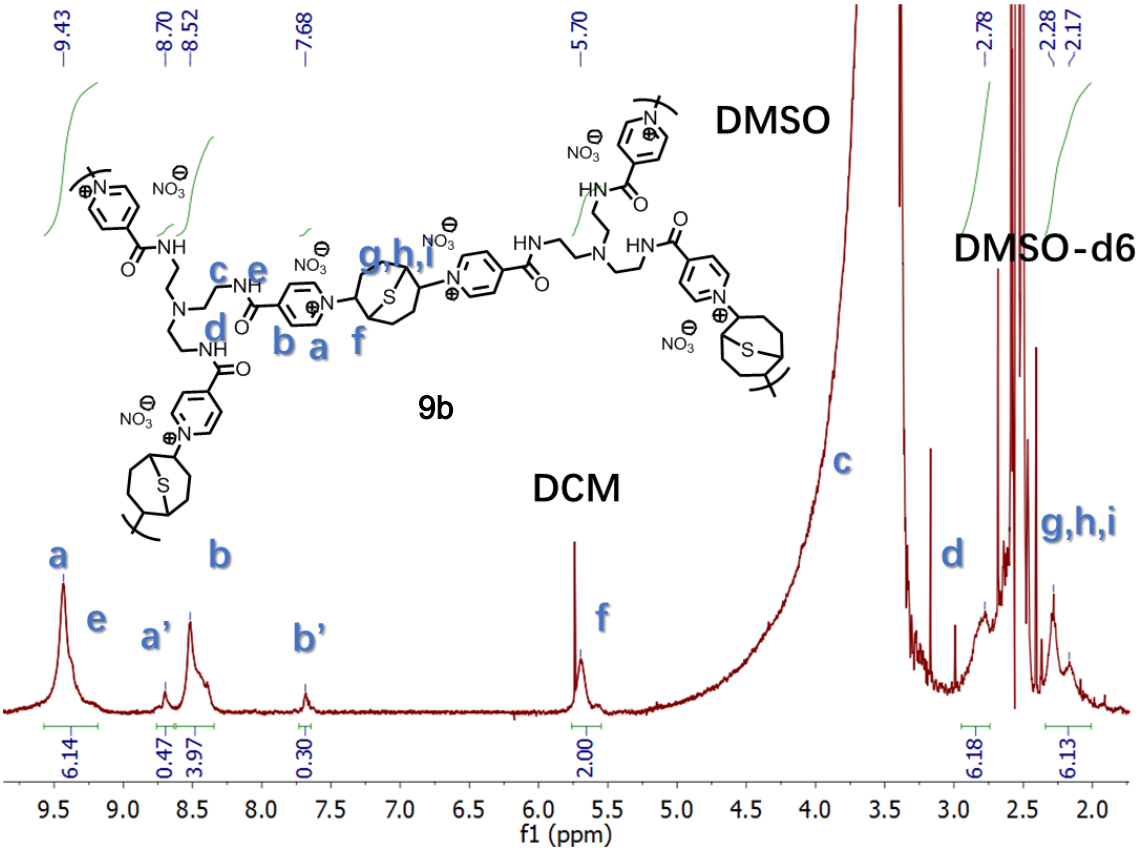

Figure 75 ^{1}H NMR spectrum of hyperbranched polycatoins made from 1b and 8b. (a' and b' referring to end group) (Table 10, entry 2)

CHAPTER 4. THIABICYCLONONANE-BASED ANTIMICROBIAL MATERIAL

（Chapter 4 is adapted with permission from
Geng, Z.; Finn, M. G., Thiabicyclononane-Based Antimicrobial Polycations. *Journal of the American Chemical Society* **2017,** *139* (43), 15401-15406.）

4.1 Introduction.

Antimicrobial drug resistance has emerged as an essential issue in modern healthcare.[56] Traditional small molecule antibiotics based on the inhibition of key enzymes are susceptible to the development and rapid dissemination of mutations in the target that confer resistance.[58] Bacteriocidal peptides, primarily cationic in nature, are a class of larger molecules often used by microorganisms for defensive purposes. While it has been stated or supposed that resistance to these agents is harder to develop,[98] their natural origin ensures that a variety of resistance mechanisms are known to exist or can be evolved.[63] These include modifications of the external surface of the bacterium[99-100] (including changes in capsular polysaccharide,[101-102] outer membrane proteins,[103-104] and other membrane adhesion systems[105]), proteolytic attack on the antimicrobial peptide,[106-107] and upregulation of transporters.[108] Small quaternary ammonium compounds have been similarly touted as being difficult to generate resistance against, but this, too, is proving to be incorrect.[61] Still, the very different mechanisms of action of natural antimicrobial peptides has inspired the development of many different types of charged synthetic oligomers or short polymers.[64-66] These are usually assumed to target bacterial membranes

and, because they can be engineered to resist some of the natural defense mechanisms, still represent a promising approach toward antimicrobial applications.

Much success has been achieved with carbon-chain polymers made by techniques such as ROMP[109] and ATRP,[110] using monomers with pendant cationic ammine/ammonium, phosphine/phosphonium, or metallocenium side chains,[66, 111-112] the most commonly employed being polyethyleneimine (PEI). Polyionenes, polymers with cationic centers in the main chain, are also common but are less diverse in structure, deriving usually from simple displacement reactions of tertiary amines on alkyl, allylic, and benzylic halide electrophiles, and are not biodegradable. Many are prepared under harsh conditions, giving modest molecular weights (6,000-20,000 g/mol) and broad molecular weight distributions, but interesting antibacterial function. [67, 86, 113]

4.2 Antibacterial activity and selectivity in solution.

The potency of BCN polycation was tested against a Gram-negative bacterium (*E. coli*), a Gram-positive bacterium (*B. subtilis),* and human red blood cells (RBCs) (Table 11). Cytotoxic selectivity was defined as the ratio of HC_{50} (the lowest polymer concentration that induces release of 50% of the hemoglobin from RBCs) to MIC_{90} (the lowest polymer concentration that inhibits 90% of bacterial growth);[65-66] the natural host-defense peptide magainin exhibits a selectivity value of 10.[109] Four antimicrobial standards were included for comparison: polyethelenimine, the small-molecule antibiotic ampicillin, the quaternary ammonium detergent cetylpyridinium chloride, and compound **7** (Figure

76), a recently-reported highly active polyionene from Hedrick, Yang, and coworkers (structure **1** in that work, synthesized using the reported protocol).[67]

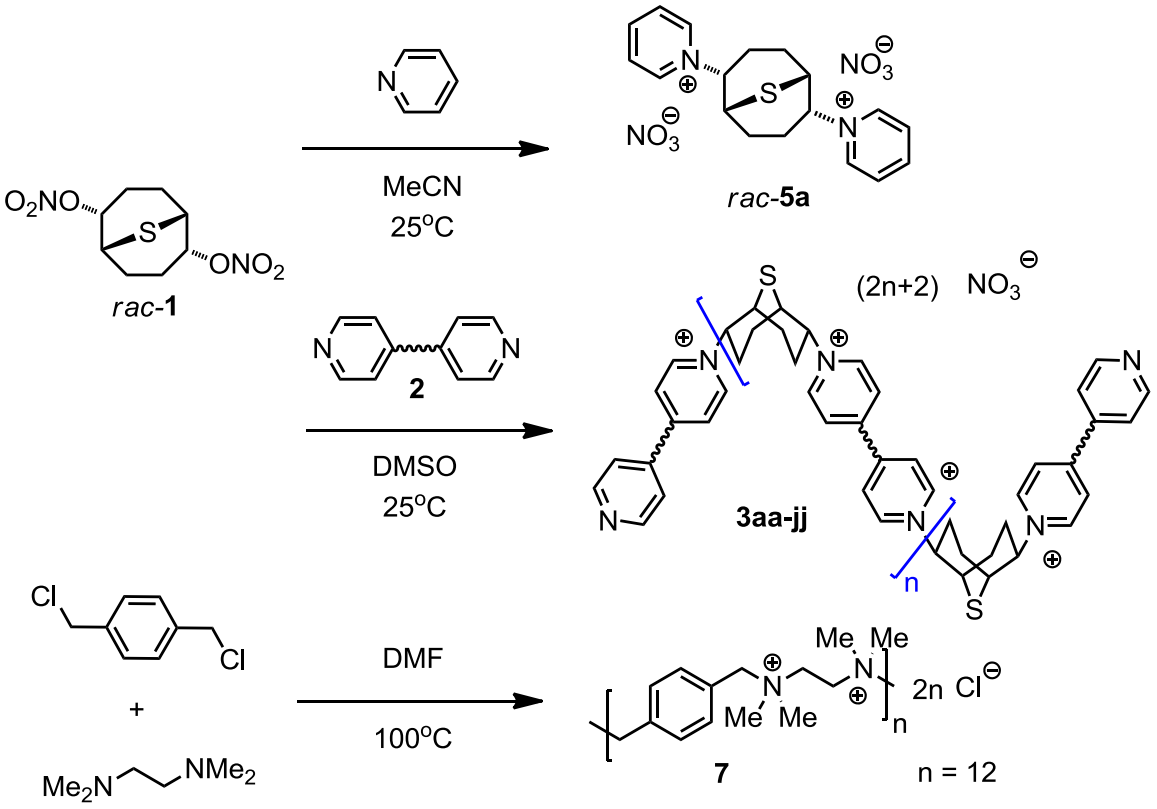

Figure 76 (*Top and middle*) General synthesis of substituted adduct and polycations based on BCN dinitrate *rac*-1. (*Bottom*) Example of a recently reported polyionene used for comparison.

Antibacterial activity was assessed in both buffer and rich media; most published reports use one or the other set of conditions. Similarly, while we measured hemolytic activity for the full range of materials in buffer as is usually done, we also assessed this parameter in media for selected agents. As expected, both MIC and HC values in rich media were higher than those measured in buffer, presumably because of interactions of the polycations with components other than the target cells. While all of the BCN-based

polycations were at least as potent against *E. coli* as PEI (MIC_{90} = 50 μg/mL), three materials were especially active against both bacteria and exhibited good selectivity vs. erythrocyte lysis; these are highlighted in Table 11.

Table 11 Survey of cytotoxic and membrane disruptive activity, with the most potent polymers highlighted.

Cpd	n	MIC_{90} in media (μg/mL) [a]				MIC_{90} in buffer (μg/mL) [b]		HC_{50} in media (μg/mL)	HC_{50} in buffer (μg/mL)	Selectivity			
		E. coli	B. subtilis	P. aeruginosa	S. aureus	E. coli	B. subtilis			*E. coli* (media) [c]	E. coli (buffer) [d]	B. subtilis (media) [c]	B. subtilis (buffer) [d]
3aa	20	12.5	3	25	12.5	0.12	0.12	350	65	28	540	117	542
3bb	12	50	25	50	100	0.5	0.5	2200	300	44	600	88	600
3cc	8	50	12.5						125	2.5 [e]		10 [e]	
3dd	10	50	15										
3ee	8	6.25	1.5	50	12.5	0.2	0.12	200	125	32	725	133	1041
3ff	8	40	40						18	0.45 [e]		0.45 [e]	
3gg	8	12.5	50						30	2.4 [e]		0.6 [e]	
3hh	3	10	10						100	10 [e]		10 [e]	
3ii	18	1.5	0.4	6	3	0.2	0.5	500	30	333	200	875	60
3jj	18	6.25	6.25			-			65	10.4 [e]		10.4 [e]	
3j	10	12.5	6.25	25	12.5	0.3	0.2	3000	150	240	500	480	750
5a	-	200	200			16			>1000		>63		
PEI	200	50	6.25			1.2		>25000	1250	>500	1000	>4000	
Amp		1	1			50							
CPC		2	1.5					12.5	6	6.25		4	
7	12	10	2.5			0.1		>25000	6000	>2500	60000	>10000	

a) Determined by method A in rich media. b) Determined by method B in PBS buffer. See experimental section for details. c) HC_{50}/MIC_{90}, both determined in media. d) HC_{50}/MIC_{90}, both determined in buffer. e) HC_{50}/MIC_{90}, with hemolysis measured in buffer and cytotoxicity in media; this is the most common method in the literature.

Longer polymer chain lengths (**3aa**, **3ii**) led to greater potency in terms of both mass and molar amounts. At the other extreme, a small-molecule dication mimic of polymer **3a** (compound **5a**, first shown in Chapter 2, Table 3) was far less active toward bacteria or red blood cell membranes. Except for the smallest example (n-octyl, polymer **3ee**), the addition of lipophilic side chains to **3bb** gave rise to poorer activity against bacteria and more efficient damage to erythrocytes. Besides making for poor solubility and greater likelihood of aggregation, these larger hydrophobic groups on the polycation repeat units decrease the charge density per unit mass (perhaps adversely affecting potency) and may penetrate membranes of both bacteria and mammalian cells (diminishing selectivity). [109]

The most active polymer, **3ii**, was made with a nucleophilic monomer containing a longer 5-atom bridge between pyridyl rings than most of the other structures. Polymer **3ii** was also unique in its performance in rich media, showing little to no loss in antibacterial potency, but a dramatic decrease in hemolytic activity, compared to buffer. This gave rise to outstanding overall performance (potency and selectivity) against both *E. coli* and *B. subtilis* in rich media, which of course more closely mimics biological environments than does buffer. Compared to the recently-reported acyclic polyionene **7**, polymer **3ii** was more cytotoxic but also more hemolytic.

A broad spectrum of activity was observed with four of the most effective polycations in this series (**3aa**, **3ee**, **3ii**, and **3i**, the last introduced in Chapter 2). All were found to be active against *S. aureus* (Gram-positive, kanamycin-resistant) and *P. aeruginosa* (Gram-negative, ampicillin-resistant), in addition to *E. coli* and *B. subtilis*, with roughly the same order of potency, **3ii** being the most active in every case. While we

observed Gram-positive bacteria to be somewhat more sensitive to polycations than Gram-negative, as expected,[65, 114-115] the observed magnitude of the difference was small (factors of approximately 2-4), and no significant difference was observed in buffer between *E. coli* and *B. subtilis*. Equipotency of this type has been reported for amphiphilic polymers made through ROMP and some polyionenes.[65, 109] and is particularly interesting when compared with the strong selectivity for Gram-positive bacteria strains exhibited by antimicrobial peptides[64, 116-117] and most quaternary ammonium compounds.[67, 117-122] The rigid and relatively hydrophobic nature of the thiabicyclononane building block is certainly different than for most polyionenes, and may contribute to the broad-spectrum potency of the derived polycations in ways yet to be determined. The assumption that these agents act by membrane disruption was supported by electron micrographs of treated cells (Figure 77)

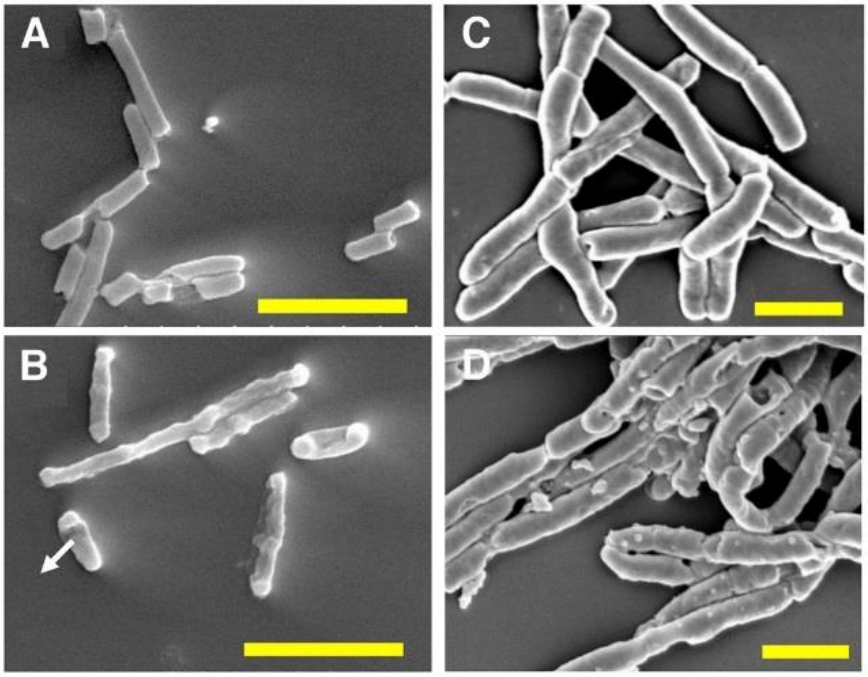

Figure 77 Morphology of bacteria before (A,C) and after (B,D) treatment with polycation 3aa. *E. coli* is shown on the left (A,B) and *B. subtilis* on the right (C,D). Scale bars = 2 μm.

4.3 Resistance development for polycations

Repeated exposure of bacteria to a sub-lethal amount of any cytotoxic agent induces the acquisition of resistance, a process that is usually faster with small-molecule agents than polycations.[67] We conducted a preliminary assessment of the development of *E. coli* resistance using a standard protocol involving repeated 12-hour cycles of treatment with a small molecule (CPC), the representative polycation **3aa**, and polymer **3j**, which undergoes hydrolytic decomposition to the uncharged dipyridyl and BCN diol fragments by anchimeric assistance with a half-life of slightly more than 9 hours at 37 °C.[95] (Note that the starting polymer architecture is much shorter-lived than this, since we monitor the appearance of the small molecules in this experiment, not the fate of the starting polymer.)

Such degradability would limit the exposure of the cells to the cytotoxic agent over the 12 hours of each cycle, and thus perhaps alter the appearance of a resistant phenotype.

In this test, polyionine **3j** induced the slowest appearance of resistance, denoted by a doubling in the MIC_{90} value (60 passages, 30 days), followed closely by **3a** (54 passages). MIC values started to shift much earlier against polyionine **7** and the small-molecule CPC[123] (33 and <28 passages, respectively). Interestingly, after passaging against **3j** for the two-week period, the resulting cells were found to be more sensitive to the other two agents, but not to **3j** itself (Table 12). The same phenomenon was not observed for the non-degradable polymer **3aa**. The culture medium (supernatant) from the cells made more resistant to CPC had no effect on CPC's toxicity toward fresh *E. coli* cells or toward cells evolved against **3j**, showing that a soluble excreted factor was not responsible for CPC resistance. The extent and mechanism of this apparent case of cross-sensitization remains to be explored.

Table 12 Sensitivity of *E. coli* cells against the indicated antimicrobial compound after two weeks (28 rounds) of exposure to sub-lethal doses.

Cells passaged against	CPC MIC_{90} (μg/mL)	**3aa** MIC_{90} (μg/mL)	**3j** MIC_{90} (μg/mL)
none	2	12.5	8
CPC	4	12.5	8
3aa	2	12.5	8
3j	1	6.2	8

4.4 Antimicrobial activity of polymer coatings

The ability to kill bacteria when adsorbed or attached to solid surfaces is useful in a number of contexts, including natural barrier membranes,[124-125] antimicrobial

packaging,[126-127] and infection control in healthcare settings.[128] Cationic peptides and polymers are certainly important in these efforts,[129] with a variety of examples showing that charge density and other factors are important.[130-132]

We tested a representative BCN-based polyionene for its contact cytotoxicity in the following way. Glass and crystalline silicon surfaces were rendered "clickable" by installation of azide groups via reaction of surface hydroxyl groups with azidopropyltriethoxysilane, and then addressed by CuAAC reaction with BCN polymer **3bb** bearing alkyne groups (Figure 78). Surface modification with the cationic polymer gave rise to expected increases in the C/N and C/Si atom ratios determined by X-ray photoelectron spectroscopy and a decrease in the water contact angle, consistent with the attachment of charged species.

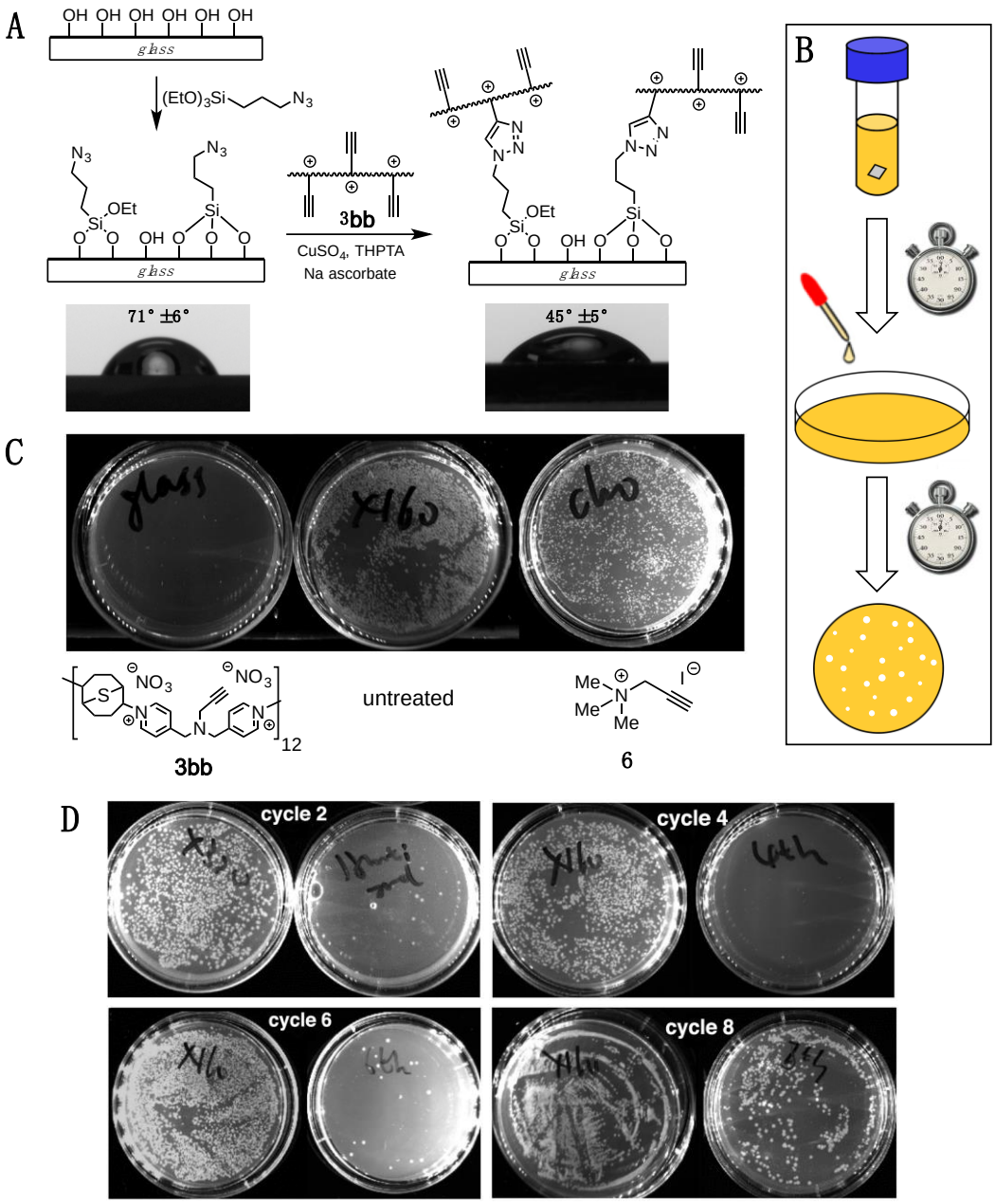

Figure 78 (A) Surface modification protocol for silica or glass substrate with alkyne-functionalized polycation 3bb. (B) Schematic representation of assay used to measure antibacterial properties of derivatized glass surfaces. (C) Photographs of agar plates 24 h (37 °C) after inoculation with *E. coli* suspensions incubated with a glass chip functionalized with the indicated molecule. (D) Reusable antimicrobial activity of a glass chip covalently modified with 3bb.

After extensive washing to ensure that only covalently anchored polymers remained on the surface, chips approximately 0.01 cm^2 in area (≈ 3 mm square) were incubated with 50 µL of buffer containing 3×10^5 *E. coli* cells at 37 °C for 4 hours, after which samples of each mixture were transferred to agar plates. The plates were incubated for 24 h and assessed for bacterial growth. Complete sterilization of the original solution occurred at a level of approximately 3×10^7 *E. coli* cells killed per cm^2 of glass or silicon surface within 4 h, comparable to the best result in a combinatorial assessment of contact killing by dense arrays of cationic brush oligomers or polymers grown from silicon wafer surfaces.[133] Most of the cytotoxic effect was observed after 30 minutes incubation, but the time course was not assessed.

To ensure that the observed antimicrobial activity of polycation-functionalized glass was a function only coming from the attached polymer, the cytotoxicity of various treated samples was assessed, summarized in Figure 79. The C/N ratios were measured by XPS for each sample after cysteine washing; toxicity against *E. coli* was assessed before and after the Cys wash referring to the incubation of the glass chip in a 1 mM solution of cysteine in buffer with sonication for 3 minutes in a standard benchtop glass-cleaning sonicating bath.

Condition	Active cpd	before Cys	C/N	after Cys
Water	None			1B
Cu^+, ligand	3bb	2A	5.3	2B
Cu^+, ligand	None	3A	2.5	3B
none	3bb		3	4B
Cu^+, ligand	**3a**	5A	4.4	1B
Cu^+, ligand	**6**		3.6	6B
$AgNO_3$	None	7A	2.1	7B
AgCl	None		2.2	8B

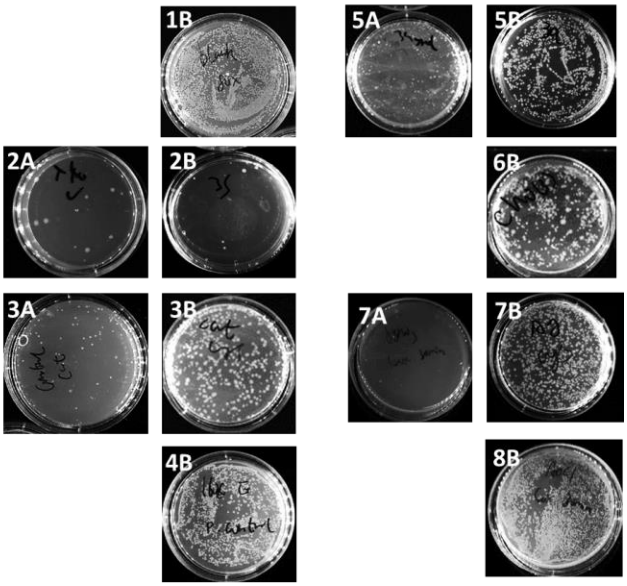

Figure 79 Control experiments with different surface treatment conditions and their respective antimicrobial activity before and after standard cleaning protocol.

Azide-modified glass samples exposed to CuAAC reaction conditions containing Cu^+ ions but no polycation (or the non-clickable **3aa**) initially showed antibacterial activity, but not after washing with cysteine to remove adsorbed metal ions (panels 3A-3B, 5A-5B). The same result was observed with $AgNO_3$ (panels 7A-7B), tested because of the potential to import silver ions from the polymer synthesis procedure. Only CuAAC reaction with the clickable polycation **3bb** gave rise to robust antibacterial activity after washing with cysteine (panels 2A-2B). The CuAAC attachment of small-molecule cation **6** (confirmed by a modest increase in observed C/N ratio) gave rise to only a small increase in antibacterial function.

Similar levels of cytotoxicity against *B. subtilis* and *P. aeruginosa* were observed in preliminary experiments (Figure 80). Glass chips modified by CuAAC attachment of a

small quaternary alkyne were ineffective, as were azide-functionalized chips treated with Cu(I) alone and with non-clickable polycation **3aa** Thus, the antibacterial property of the surface resulted from the covalent attachment of BCN polycations.

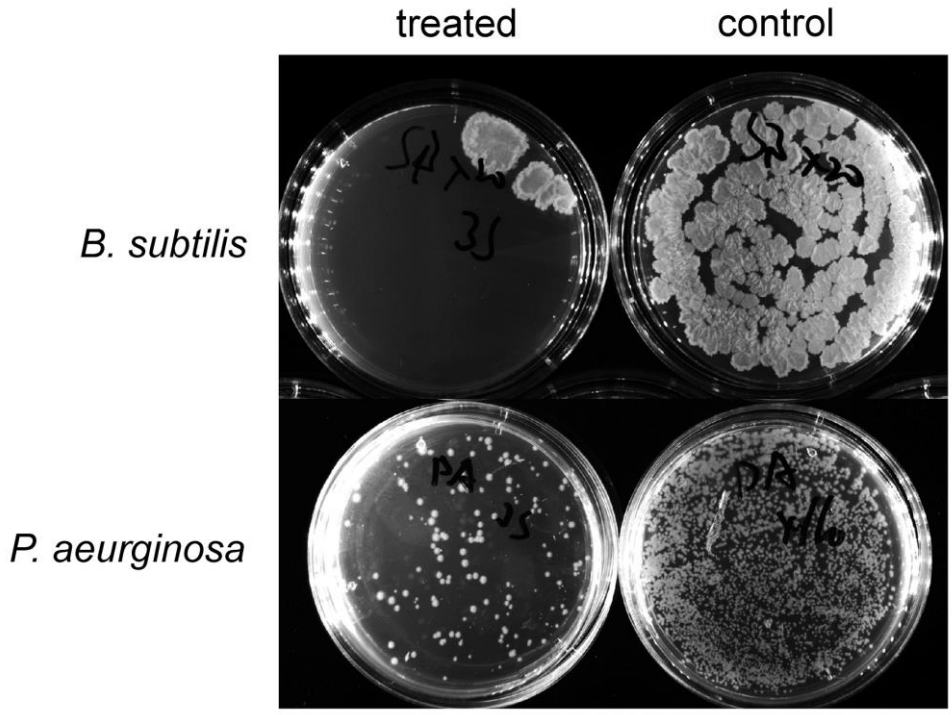

Figure 80 Demonstration of antibacterial activity against *B.subtilis* (top) and *P. aeruginosa* (bottom) of a glass surface bearing polycation 3bb.

The antibacterial property of these surfaces was retained by brief sonication in water for up to eight cycles, as shown in Figure 78. On the left of each image is the result from incubation with a new underivatized glass chip; on the right is the result from incubation with the **3bb**-modified chip. "cycle n" denotes the use of the same chip for the n^{th} time; after sonication for 3 minutes in a standard glassware-cleaning sonicator at room temperature between each incubation in *E. coli* culture. Complete eradication of viable

bacterial cells was observed through cycle 7, representing an activity of at least 1.5×10^7 cells per cm^2 of functionalized glass surface.

The integrity of the surface functionalization was confirmed by the maintenance of constant C/Si ratio and contact angle with each cycle (Table 13). However, these parameters were not predictive of antibacterial activity, as seen after cycle 7. When not washed or when harsher washing conditions were used between exposure to fresh batches of *E. coli* cells in buffer, effective killing was observed to the third cycle (Figure 81). Active antimicrobial glass chips were not cytotoxic toward cultured mammalian (Jurkat) cells under conditions similar to those used in antibacterial testing (details in experimental sections).

Table 13 Characterization of glass surfaces after each round of microbial challenge.

# bacterial challenges / washes	C/Si	C/N	Contact angle
2 / 1	1.7	2.3	43
3 / 2	1.8	2.6	36
4 / 3	1.7	2.5	37
5 / 4	1.3	2.4	41
6 / 5	1.8	2.3	42
7 / 6	1.5	2.7	39
8 / 7	1.3	2.6	44
9 / 8	1.4	2.2	43

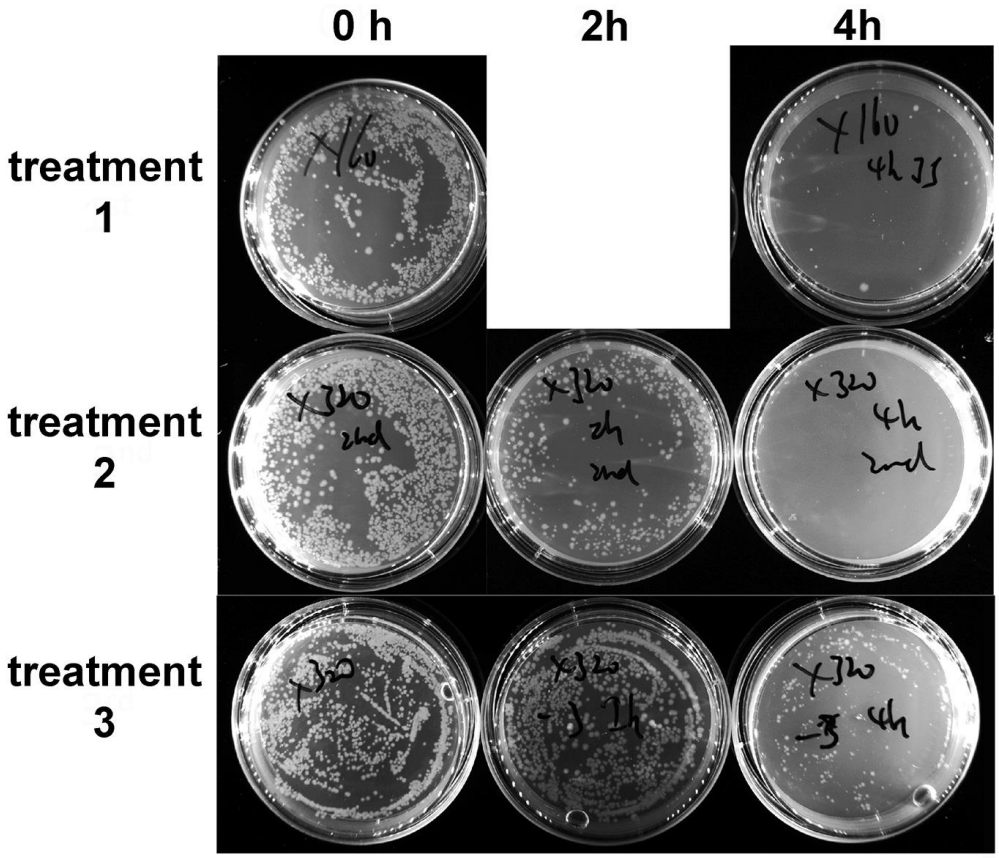

Figure 81 Viability of cells after being treated with single polymer coated glass chip at low initial concentration of *E. coli* (4×10^4 cells). The chip was repeatedly used without washing. Aliquots of the cell suspension were taken at the start (0 hours) and after 2 and 4 hours of incubation.

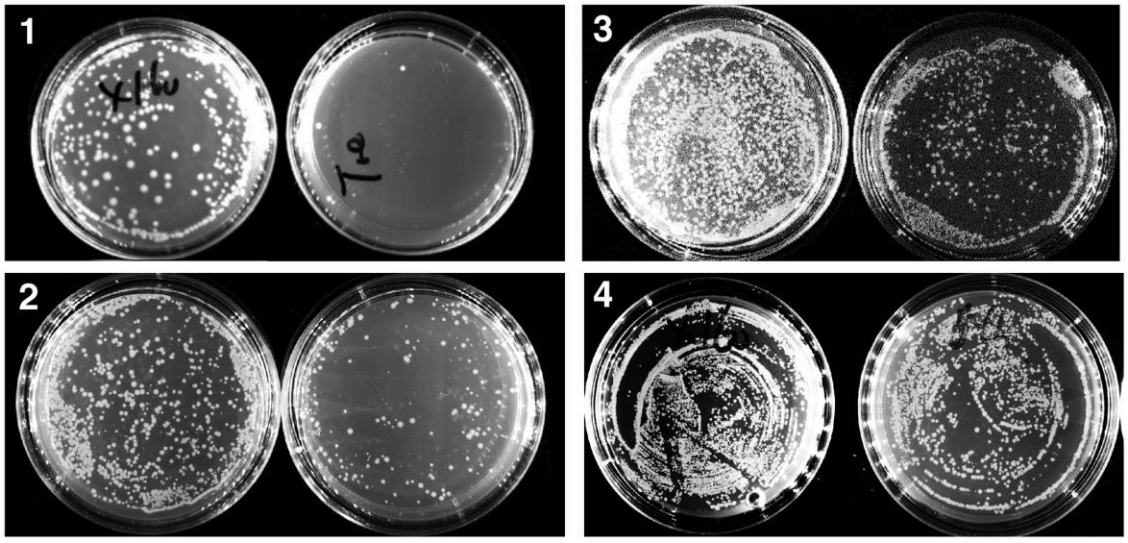

Figure 82 Antimicrobial activity in PBS buffer against *E.Coli* of glass beads derivatized with 3b and washed with the harsher two-hour protocol described in the experimental section. Each number refers to the wash cycle. Note that the last (4th) cycle was done with 1% Triton X-100.

Bulk materials made from synthetic polymers has also been coated with BCN polycations through three-step-method shown in Figure 83. PCL is demonstrated here as an example, first immersed in solution of polydopamine precursors at basic condition. The PDA-coated material was then attached with BCN polycations as described above via CuAAC conjugation. And the antimicrobial function was tested and compared with BCN-polycation-modified glass. While abolishing the whole bacteria broth after 1st time usage (bacteria colony number decreased by more than 3 order of magnitudes), starting from the 2nd cycle, the ratio of bacteria cells killed demonstrated by microdilution method sharply decreased to 200. In the 3rd cycle there is no difference of bacteria colony number between the treated and control group, indicating the non-covalently attached polydopamine might require more delicate washing protocol to retain the antimicrobial activity of attachment

layer above. However, this experiment provides a potential of a universal way of using BCN polycations as antimicrobial coating on any materials.

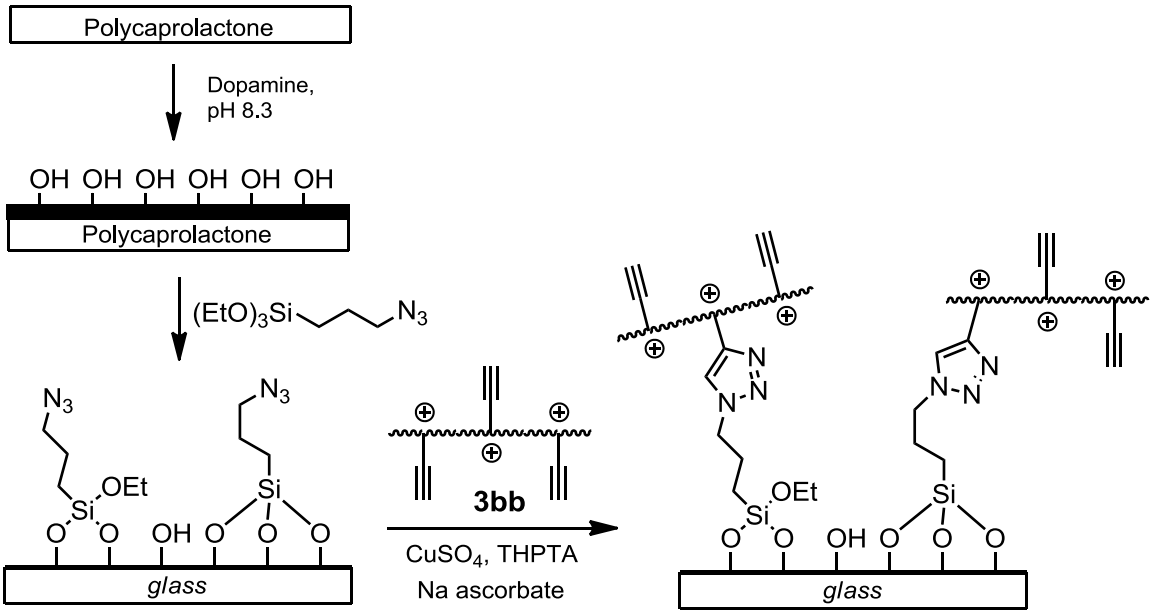

Figure 83 Surface modification protocol for polymer substrate with alkyne-functionalized polycation 3bb.

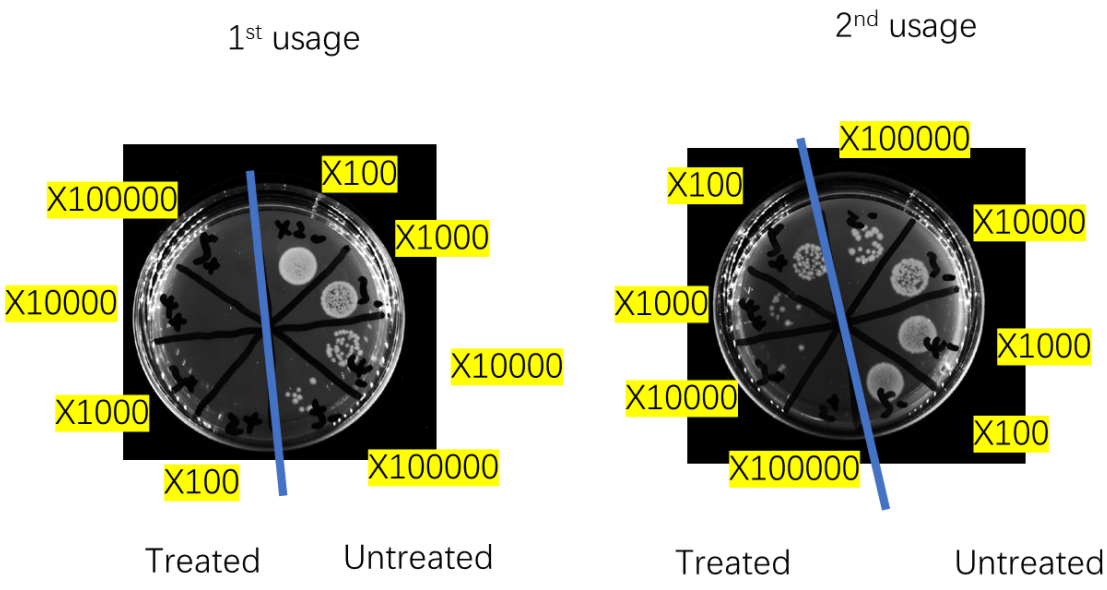

Figure 84 Photograph demonstrating antimicrobial activity in PBS buffer against *E. coli* of 3bb-coated PCL fiber and washed antimicrobial fiber.

4.5 Conclusion

An initial survey was presented here for a new class of antimicrobial BCN polyionenes, with favorable characteristics for further development. The novel structured polycations demonstrated high potency against four bacterial strains, two Gram-negative and two Gram-positive. Inhibition of the bacteria growth occurred at the μg/mL level and killed static bacterial cells at polymer concentrations of tens of ng/mL, with moderate-to-good selectivity with respect to lysis of red blood cells.

While resistance to the BCN polymers was developed only very slowly over multiple passages, a degradable version of the polycation was observed to make *E. coli* cells more susceptible to other quaternary ammonium based antimicrobials.

Solid substrates (glass and crystalline silicon) covalently functionalized with a representative BCN polycation were also able to repetitively kill bacteria in solution at high rates and with cleaning by simple sonication between exposures. Combined with polydopamine coating technique, this type of new membrane-active antimicrobials is able to be applied to majority of bulk materials.

Since these materials are the first examples of this subclass of polyionenes to be made and tested, their promising activity in both soluble and immobilized forms bodes well for further optimization of antimicrobial potency and selectivity.

4.6 Experimental

4.6.1 *Measurement of antimicrobial activity*

Bacteria suspensions (*E. coli* and *B. subtilis* subsp. Subtilis (Ehrenberg) Cohn (ATCC® 6051™)) were grown in Mueller-Hinton Broth (MHB) overnight at 37 °C. The resulting culture was used to inoculate a second culture in 2 mL of MHB medium until an optical density of 0.8 at 600 nm was reached.

Method A. The suspension was diluted with fresh MHB to an optical density at 600 nm (OD_{600}) of approximately 0.001. This suspension was mixed with different concentrations of freshly prepared polymer solutions in TRIS saline (pH 7.0) in a 96-well plate, and incubated overnight at 37 °C. The OD_{600} was measured for bacteria suspensions that were incubated in the presence *vs.* absence of polymer. Antibacterial activity was

expressed as minimal inhibitory concentration (MIC), the concentration at which more than 90% inhibition of growth was observed. All experiments were performed in triplicate.

Method B. The bacteria were collected by centrifugation at 4,000 × g for 3 min at 4 °C, washed with sterile PBS (pH 7.4) and suspended in PBS to a final concentration of 6 × 10^6 cells mL^{-1}. The glass/silicon substrate (0.01-0.04 cm^2 in area) or polymer solution was added to 50 μL of the bacterial suspension and gently shaken for 0.5-4 hours. Then 25 μL of suspension was spread onto a sterile Petri dish covered with a layer of LB medium containing 0.8% agar (previously autoclaved, and cooled to 37 °C). After overnight incubation at 37 °C, bacterial colonies became visible and were counted and compared with the untreated bacteria plate. The MIC was defined as the minimum concentration in the diluted series when the CFU number on the agar plate reached no more than 10% of the control plate.

4.6.2 *Measurements of hemolytic activity*

These were performed by a standard method,[65] with slight modifications. Freshly drawn human red blood cells (RBCs) were obtained by centrifuging a whole blood at 300g for 7 minutes (no brake) to remove plasma and white blood cells. A sample of the resulting RBC suspension (100 μL) was diluted with 3.9 mL TBS buffer (10 mM Tris buffer, pH = 7.0, 150 mM NaCl) to give a stock suspension of 0.25% RBCs. This stock (120 μL), TBS buffer (15 μL) and the polymer stock solutions (15 μL) (or control solutions) were added to a 1.5 mL tube and incubated at 37 °C for 1 hour. The tube was centrifuged at 10,000 rpm for 5 minutes. The supernatant (60 μL) was transferred to a 96-well plate and

hemolysis detected by measurement of absorbance of the released hemoglobin at 414 nm. 100% Hemolysis was obtained by adding 15 μL of Triton-X100 solution to sample RBC suspensions while 0% hemolysis was defined as the absorbance from suspension treated with TBS containing no polymer. A dilution series of polycation gave the HC_{50} value by linear interpolation of concentration inducing 50% hemolysis, as illustrated in the examples in Figure 85. All experiments were run in triplicate.

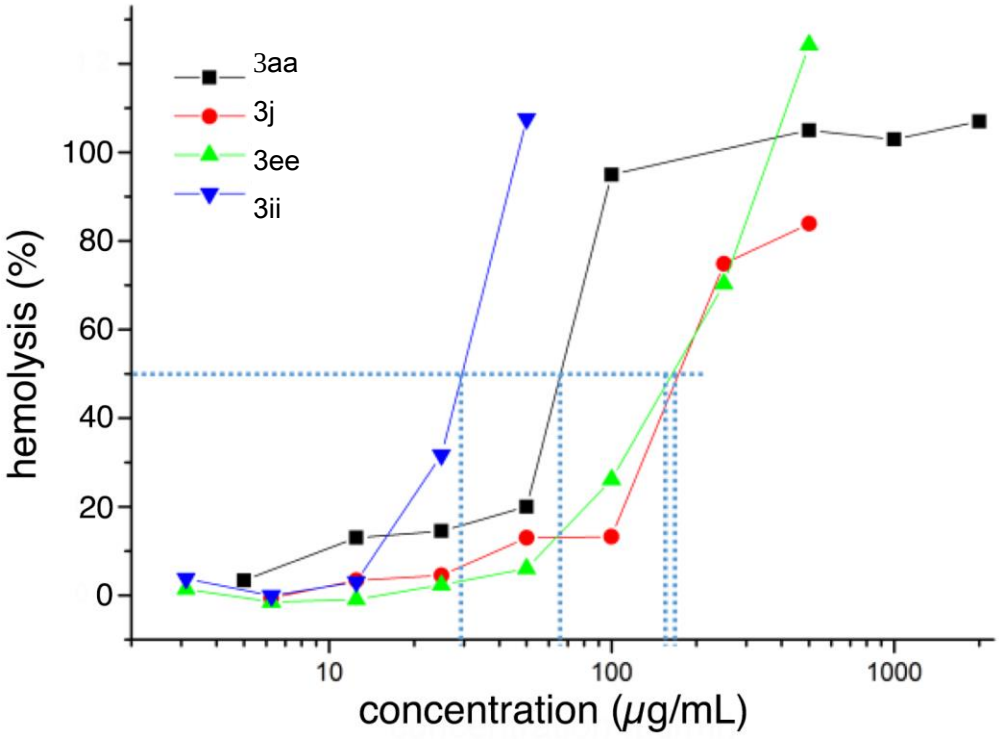

Figure 85 Representative hemolytic profiles of BCN polycations; this experiment was performed in PBS buffer. HC_{50} for each polymer is indicated by the line to the x-axis.

4.6.3 *Measurements of antimicrobial resistance*

Adapted from a standard assay method (Figure 86).[123, 134] An *E. coli* culture grown in MHB media overnight was inoculated into wells of a 96 well microtiter plate containing MHB media and two-fold dilutions of the candidate antimicrobial around the previously determined MIC_{90} value (designated MIC^{init}_{90}). These plates were incubated in gently rotating incubator-shaker at 37 °C. Every 12 hours, bacterial growth was assayed by reading absorbance of the solution at 600 nm on a plate reader, and an aliquot of bacterial culture was removed from the well containing the highest concentration of antimicrobial agent allowing observable bacterial growth, defined as an absorbance value greater than above 0.015, with background absorbance at 0.01). Each aliquot was diluted 100 times in fresh MHB media and distributed into wells containing the same concentration range of antimicrobial agent (freshly prepared). When MIC towards certain antimicrobial shifted, the MIC of those evolved cells towards other antimicrobials was also evaluated.

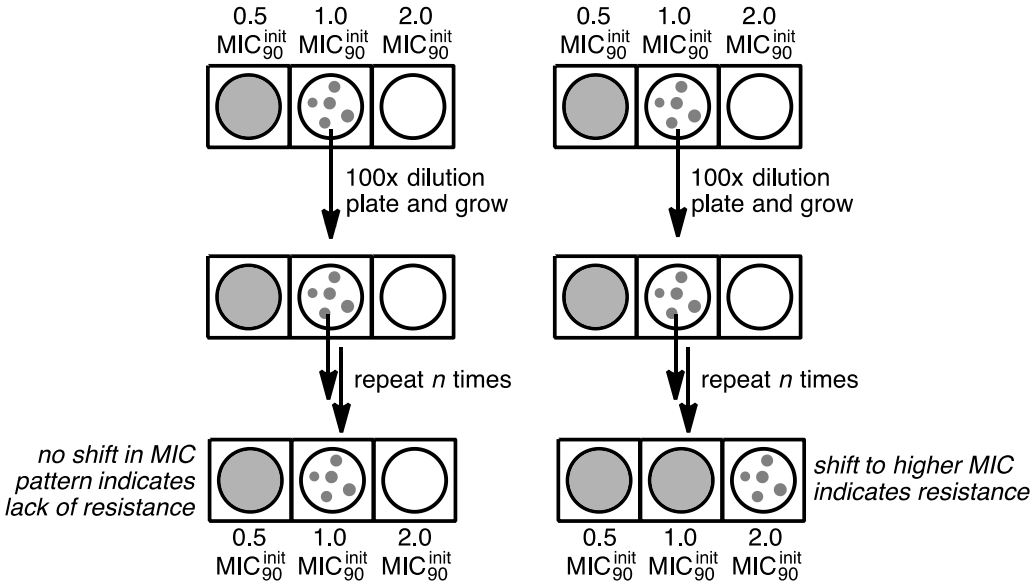

Figure 86 Protocol for assessment of *E. coli* resistance to antimicrobial agents of interest. Dilution and re-plating was done twice a day.

4.6.4 *Surface modification and characterization*

Silicon wafers (1 cm × 1 cm), glass chips (1 cm × 1 cm), or glass beads (0.25 cm in radius) were cleaned with piranha solution for 30 min, sonicated with deionized water for 30 min, rinsed with methanol, and dried with N_2. The cleaned substrate was immersed in a solution of 3-azidopropyl triethoxysilane (20 mM in toluene) overnight at room temperature.

The substrate was then washed with methanol, dried under a N_2 stream and immersed in solution of polycation **3bb** (1 mg/mL, 0.16 mM (3.2 mM in terms of monomer units), in 80/20 water/t-BuOH) with copper sulfate (5% equiv, 0.2 mM), sodium ascorbate (10% equiv, 0.4 mM) and THPTA ligand (5% equiv, 0.2 mM) overnight at room temperature in a closed vial.

After washing with water and then methanol, the surface was incubated in a 1 mM aqueous solution of cysteine for 1 hour to remove adsorbed metal ions. After a final wash with methanol and drying under N_2, the surfaces were characterized by XPS and contact angle measurements at three places with high reproducibility between these values. Each substrate was cut into smaller pieces before use in antimicrobial assays.

PDA coated PCL materials were provided by Dr. Jiajia Xue in Xia group. The covalent modification is performed in a similar way. Increased C/N (from 14 to 50) acquired from XPS spectrum confirmed the successful attachment of polycations to azide.

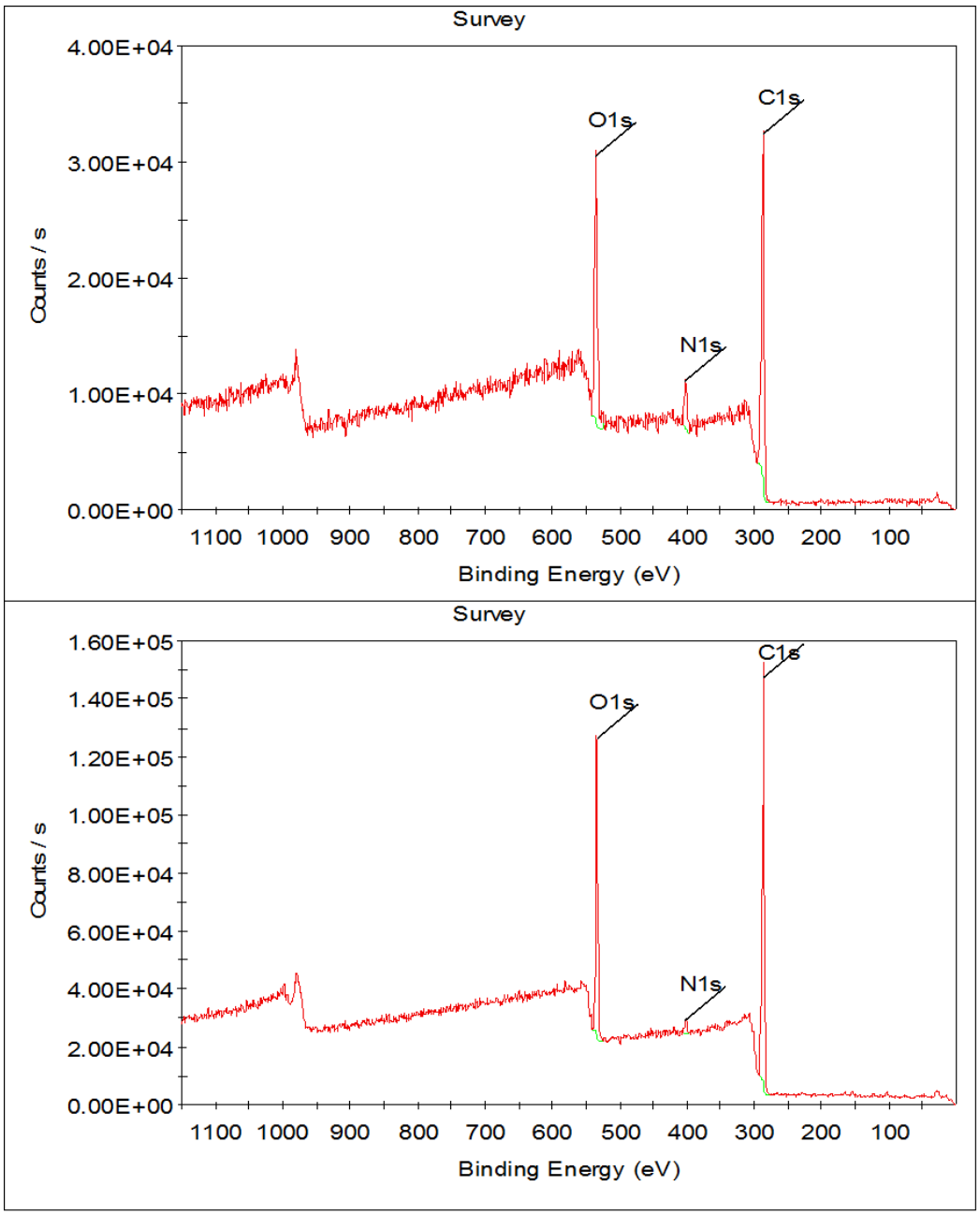

Figure 87 XPS spectrum of azide coated PCL before (bottom) and after (top) modification of 3bb.

4.6.5 *Mammalian cell viability in contact with derivatized glass chips*

Jurka cells (approximately 1×10^5 per well) were plated in a 96-well plate in 100 μL of complete growth media or PBS buffer at 37 °C. A glass chip coated with BCN polycation **3b** (approximately 0.01 cm^2 in area) was immersed in the cell suspension. After 4 or 24 h, cell viability was measured by MTT assay, with non-treated cells assigned as 100%. No cytotoxicity was observed, with both 4- and 24-hour incubations returning results showing 100 ± 5% viability.

4.6.6 *Scanning electron microscopy (SEM) measurements*

After treatment with the antimicrobial agent of interest, bacteria were immediately fixed with glutaraldehyde (0.5%) in PBS at room temperature for 30 min. The bacteria were centrifuged (3500 × *g* for 10 min) and the supernatant was removed, and the resulting pellet was suspended in sterile water. A 1 μL aliquot of the bacterial suspension was added to a clean piece of mica and allowed to dry in air. Immediately after drying, 0.1% glutaraldehyde was added for further fixation for 2 h. The resulting the specimen was washed with sterile water and dehydrated by addition of ethanol in a graded series (70% for 5 min, 90% for 5 min, and 100% for 5 min) and then dried in air. Finally, each specimen was sputtered with gold before examination with SEM (SU8230, Hitachi).

4.6.7 *Antimicrobial activity assay with different washing protocols for glass surface*

Repeat antimicrobial activity without washing

A glass chip covalently modified with **3bb** was used repeatedly but without the sonication cleaning step between each cycle. The results of agar plate culture of the

mixtures resulting from chip incubation for 0, 2, and 4 hours are shown in Figure 81. The antimicrobial efficiency increased with longer incubation in the presence of the chip. The approximate limit of killing efficiency at the third cycle was 4×10^6 cells per/ml.

Harsher washing conditions for reuse of derivatized glass

In addition to flat glass slides, glass beads were derivatized with polymer **3bb** to test antimicrobial activity. After one use in the antimicrobial assay by **method B** (with similar results as the glass slide), the beads were sonicated in PBS for 20 min, water for 20 min, acetone for 1 hour, and finally with water again for 20 min, comprising a washing cycle of 2 hours. This cycle of testing and washing was repeated a total of four times, with results shown in Figure 82.

CHAPTER 5. AZABICYCLONONANE-BASED FRAGMENTABLE CATIONIC ADDUCTS AND POLYCATIONS

9-Azabicyclo[3.3.1]nonane dihalides are potentially more interesting building blocks than their sulfur analogues, since they bear an additional attachment point at nitrogen, which could offer a variety of functions with appropriate selection of handle. A number of analogues involving aromatic and aliphatic amines with hydrochloride salts were isolated as pure solids. According to previous study, the nature of 9-aza substituent also contributed substantially to the substitution reaction rate in the expected order of nucleophilicity, N-heptyl > N-propargyl > N-phenyl, with a difference in rate of more than 800-fold between the slowest and fastest cases

5.1 Synthesis and characterization of cationic adduct and polycations

Since the starting dielectrophile 2,6-dichloro-9-azabicyclo[3.3.1]nonane is isolated as a hydrochloride salts and comparatively unstable in basic form, adding one equivalent of base is necessary to ensure high conversion of 9-azabicyclo[3.3.1]nonane dichloride to 9-azabicyclo[3.3.1]nonane dipyridinium. One extra equivalent of $AgNO_3$ is also added to be consumed by hydrochloride associated with tertiary ammonium in the core of azabicyclononane.

The reaction could also be performed in two steps, first deprotonating aza-BCN electrophile and then nucleophilic substitution under inert atmosphere. Chloride salt transformed from aza-BCN electrophile will be filtered after acid-base reaction. In this way,

only two equivalents of $AgNO_3$ are required, same as the thia-BCN version. A series of aza-BCN substituted adducts have been synthesized, purified and characterized.

In preparation for polycations based on aza-BCN electrophiles, choice of base must be carefully made. Tertiary ammine, such as triethylamine, N, N-diisopropylethylamine and potassium carbonate gave only small molecules (not able to be precipitated out from DCM) and turned solution into green colour. When NaH was picked up as nonnucleophilic base, 5-8 mer was obtained as a brown solid for heptylamino-BCN electrophiles. When the internal nucleophile was changed to propargyl amine or benzyl amine, smaller molecules were obtained again, indicated by almost 1:1 ratio of end group in NMR. This could be related to the activating ability of nitrogen affected by their neighboring groups.

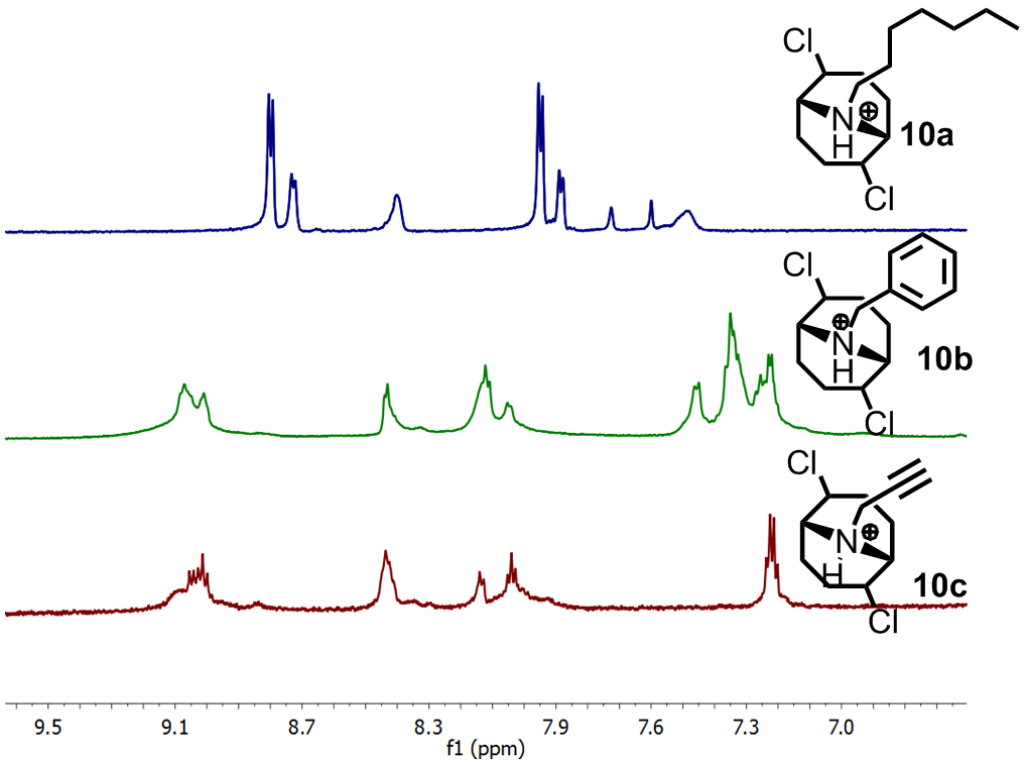

Figure 88 Aromatic region of ^{1}H NMR spectrum for oligomer made from various aza-BCN electrophiles with bis(pyridine) 2a.

As activated by its thia-counterparts, aza-BCN dichloride could also be turned into a more reactive intermediate. The Finkelstein reaction of **10a** with sodium iodide in acetone gave **10d** in moderate yield. Polycation with higher molecular weight was prepared with the new aza-BCN diiodide in the two-step procedure, in which NaI and potential excess of NaH was filtered out first. When the polymerization is carried out in one pot, polymerization is disturbed potentially by deprotonated DMSO or pyridinium since NaH is very reactive. Even in that case, the substitution still gave 5-mer which is no less effective than any polymerization starting from aza-BCN dichloride.

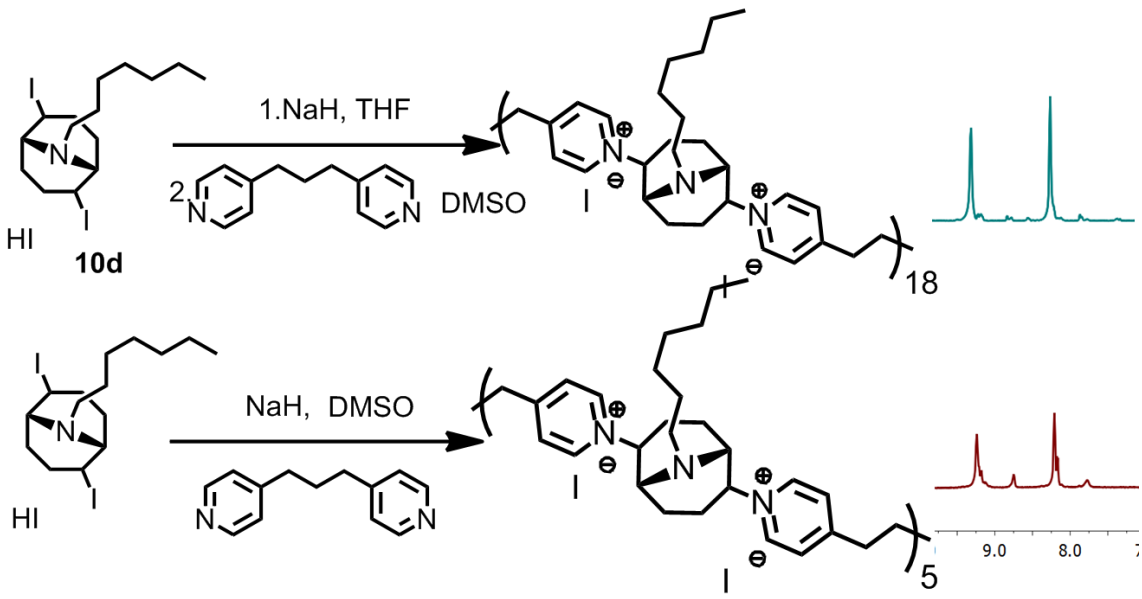

Figure 89 Polymerization of 10d and 2a in one pot (bottom) and two step fashion (top), polymerization degree determined by end group analysis in aromatic region of ^{1}H NMR spectrum (right).

5.2 Fragmentability

Since the internal nucleophilic nitrogen itself is pH sensitive, the extent of anchimeric assistance is controlled by protonation. Thus, it is highly promising to build up pH sensitive linker or materials based on this scaffold and find applications in biological systems. The stability of some representative aza-BCN pyridine adducts to fragmentation in buffer (acidic pH) at 37^{o}C was examined.

Fragmentation of heptylaminobicyclononane dipyridinium was monitored through NMR (example shown in Figure 90). The overall fragmentation progress was determined by tracking the disappearance of the azabicyclononane C-H resonance adjacent to the

pyridine group (position *e* in Figure 90) and the appearance of the corresponding resonance (*e''* at 4.3 ppm) for the diol product.

Different from fragmentation of thiabicyclononane dipyridinium, the aromatic region has three sets of peaks instead of two (belong to starting material and fragmentation product respectively). The newly added set comes from the protonation of tertiary amine of the starting pyridinium adducts. The simple acid-base reaction also took place in the same time scale of fragmentation reaction, thus resulting in pyridinium adduct not completely degraded under acidic condition within 48 hours even at 50 ^{o}C. As a comparison, the fragmentation at pH equals to 7.4 for the same substituted adduct took half of the time when it did at lower pH. This phenomenon is described in Figure 91, Figure 92. The kinetic constants were calculated based on the integration of characteristic peaks, shown in Figure 93, Figure 94.

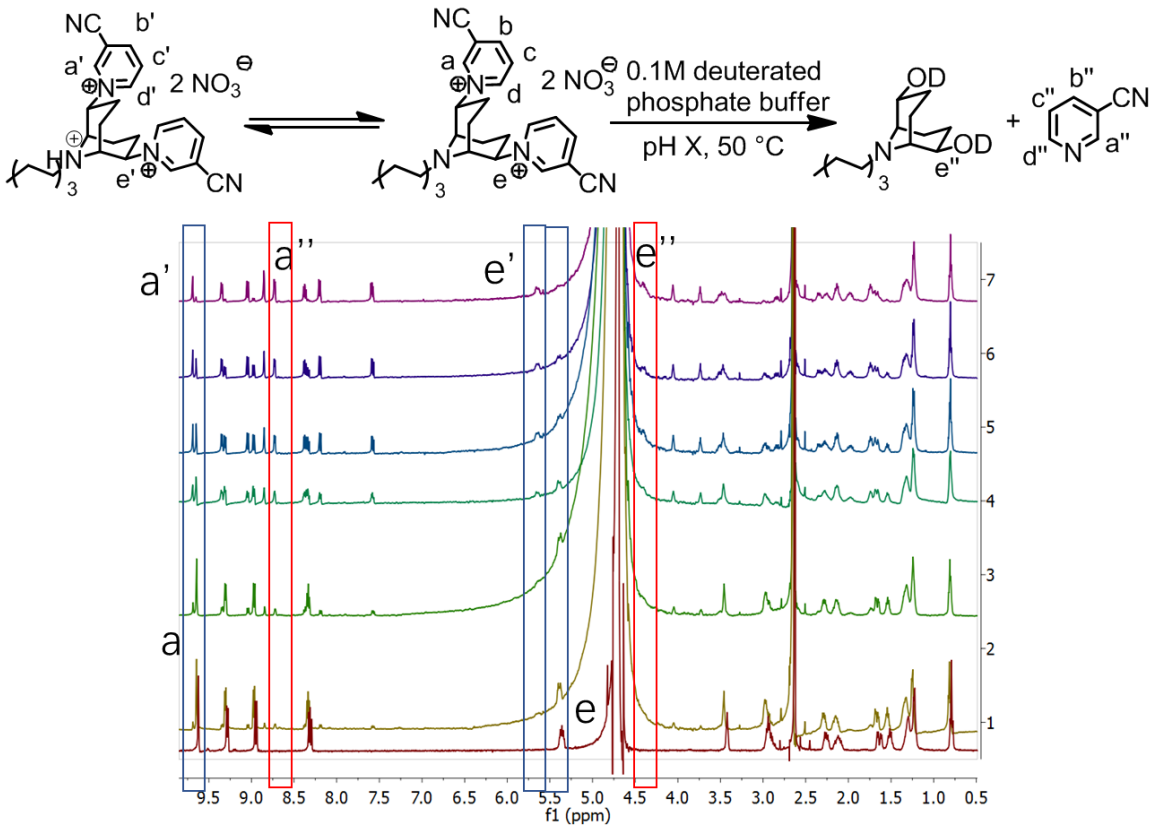

Figure 90 ^{1}H NMR spectra of representative heptylamino BCN adduct in deuterated aqueous phosphate buffer (pH 3.5) at 50 °C from t = 0 (bottom) to t = 42 h (top).

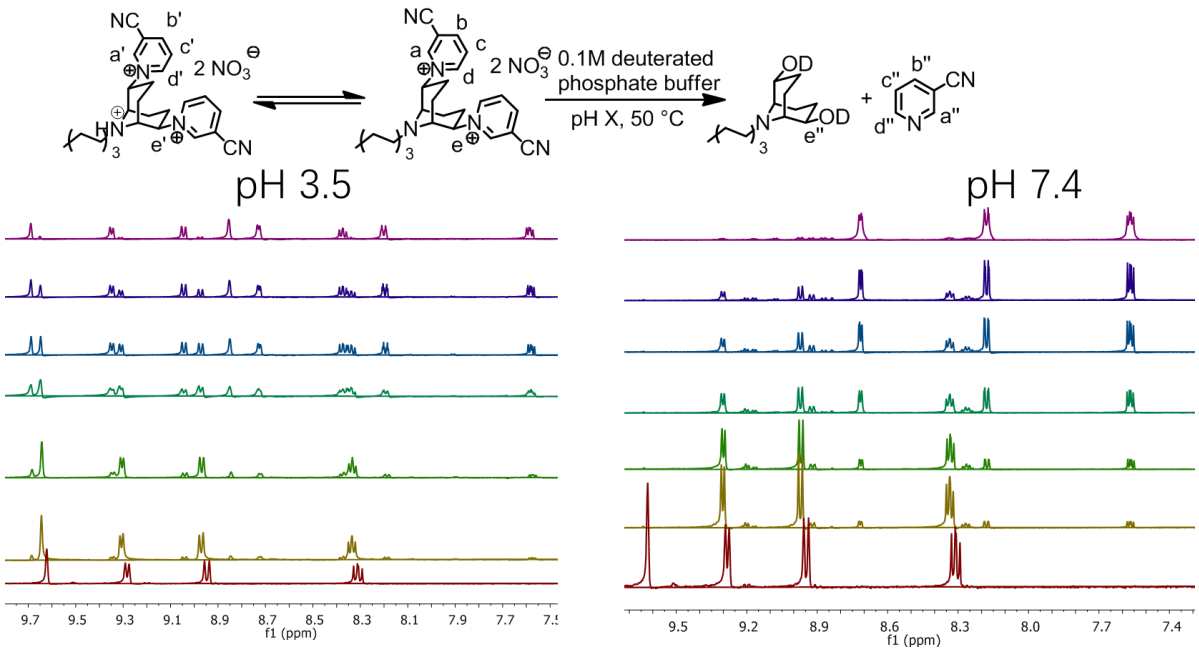

Figure 91 Aromatic region of ^{1}H NMR spectrum for representative heptylamino BCN dipyridinium adduct at different pH as fragmentation proceeds at 50 ^{o}C from t = 0 (bottom).

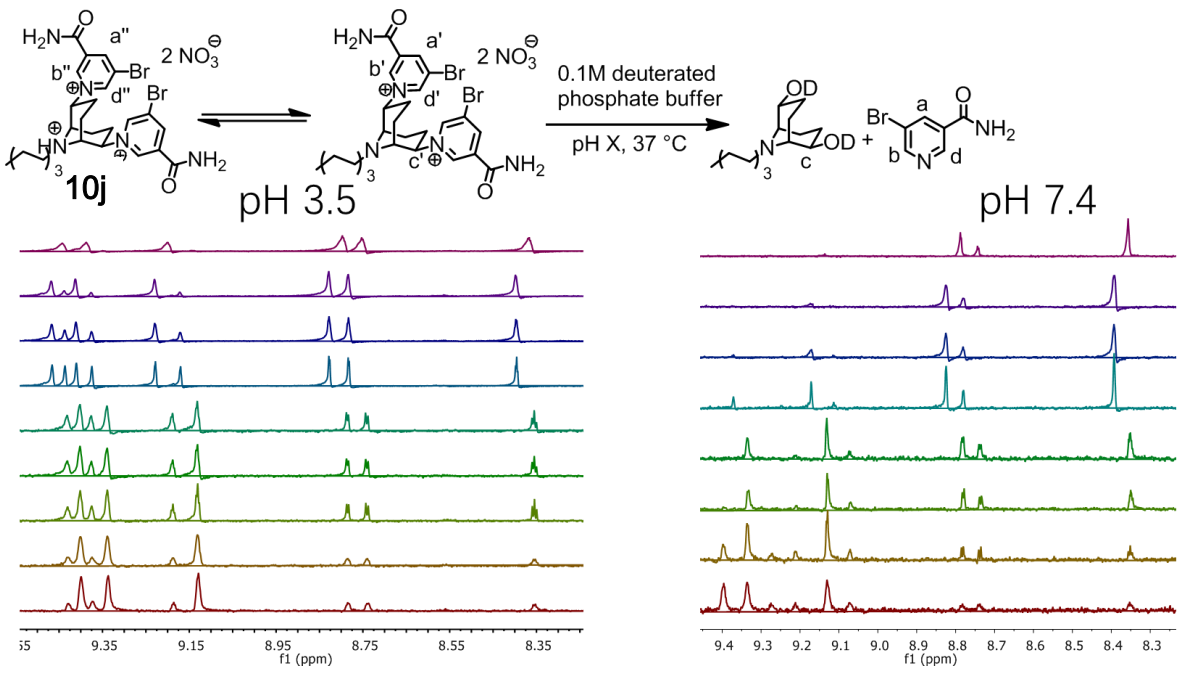

Figure 92 Aromatic region of ^{1}H NMR spectrum for representative heptylamino BCN dipyridinium adduct at different pH as fragmentation proceeds at 37 ºC from t = 0 (bottom).

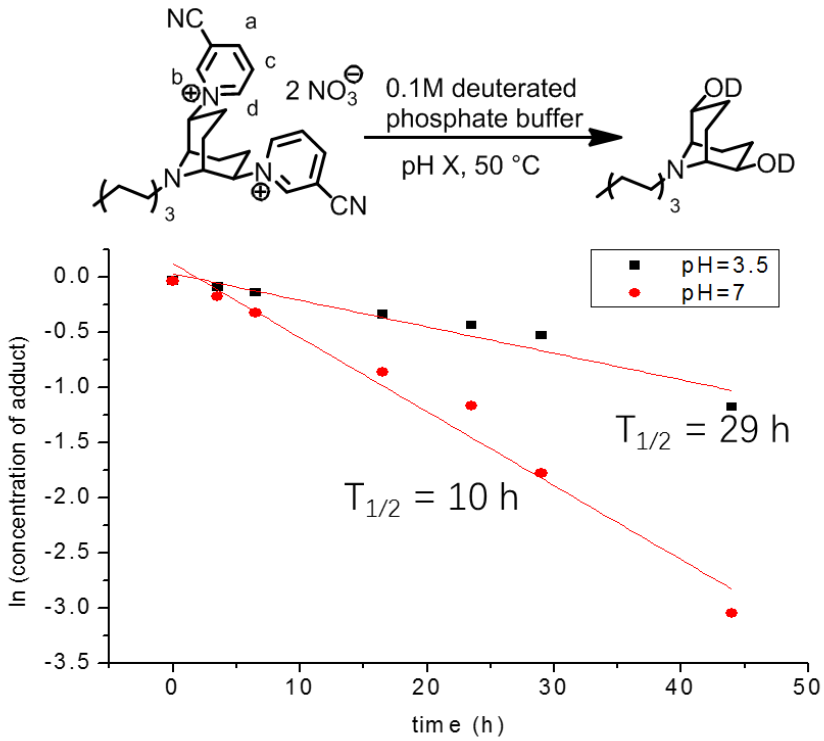

Figure 93 Pseudo-first order plot for pH dependent fragmentation of representative aza-BCN adduct at 50 ºC.

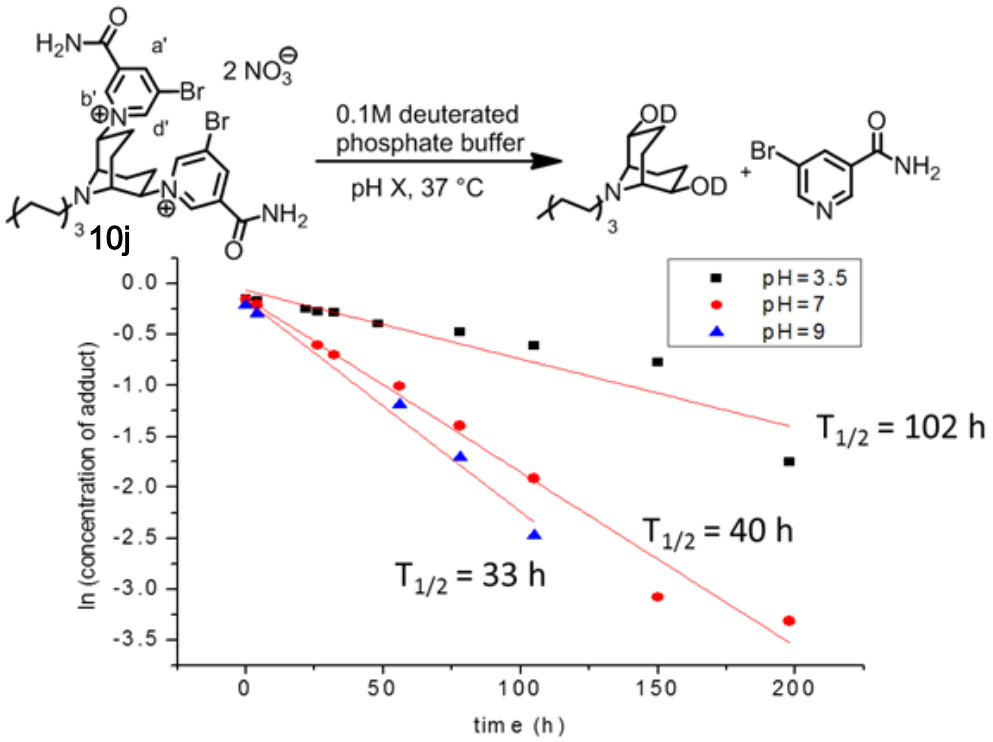

Figure 94 Pseudo-first order plot for pH dependent fragmentation of representative aza-BCN adduct at 37 ºC.

A series of fragmentable aza-BCN polycations were made and subjected to degradation test, with representative examples listed in Figure 96. As 9-aza substituents on BCN core, N-benzyl and N-heptyl made a difference on fragmentation rates for polycations. That provided another tunable handle for controlling material's property besides the choice of pyridine with different nucleophilicity.

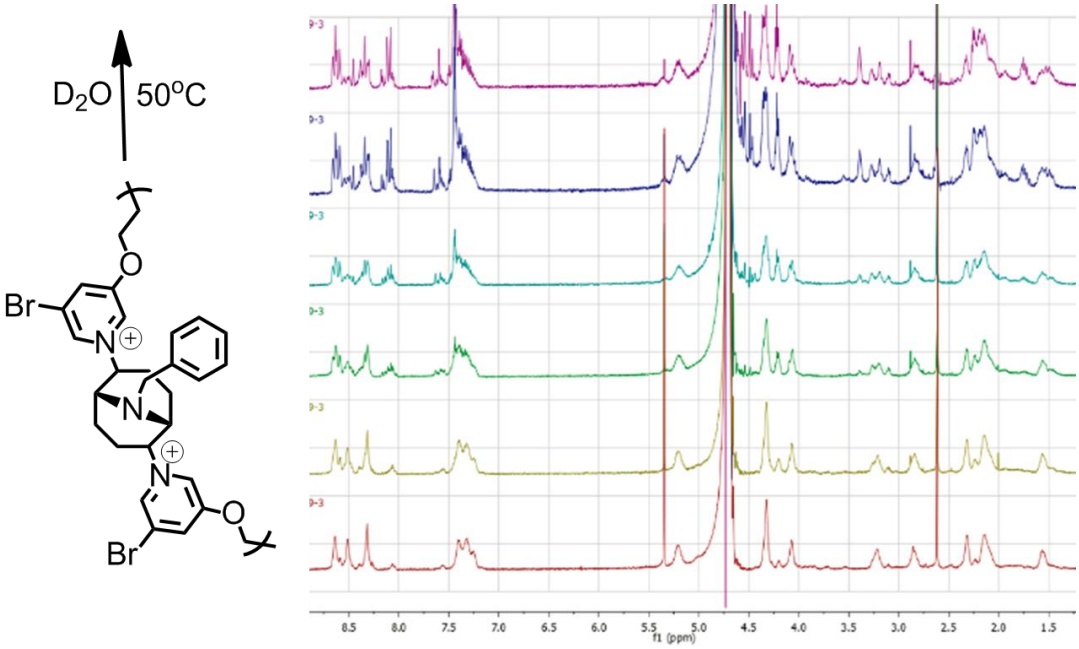

Figure 95 ^{1}H NMR spectra of fragmentation for representative aza-BCN polycations in deuterated aqueous phosphate buffer (pH 7.4) at 50 °C starting from t = 0 (bottom).

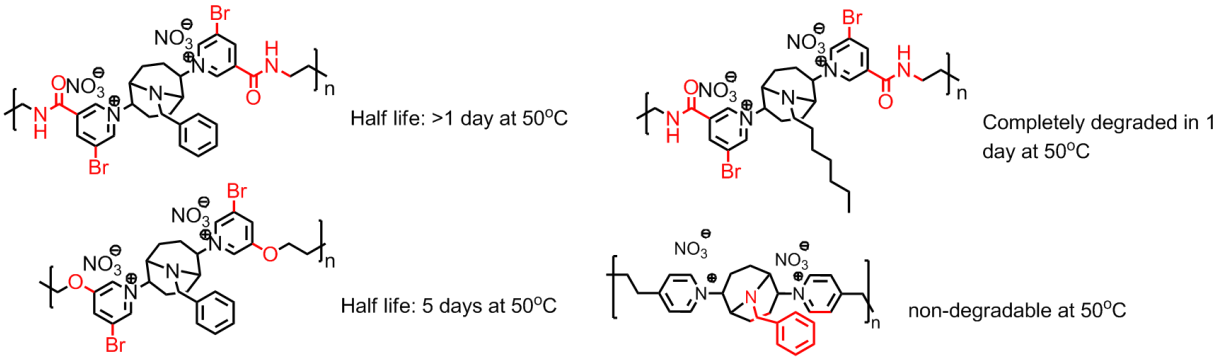

Figure 96 Representative aza-BCN polycations and their fragmentability at 50 °C.

5.3 Application of azabicyclononane-based cationic materials in antimicrobial

Heptylamino-BCN cationic adduct was expected to strongly interact with cell membrane. MIC of a series of pyridinium adducts with various of substitution R groups on

pyridine were acquired against *E. coli*. The adduct **10j** with unalkylated amide and bromo groups decreased MIC significantly compared with their thia-BCN counterparts or pyridine adducts without any EWGs. When the N-alkylation chain length was shortened the activity still retained. However, when sp^2 hybridized carbon was introduced, MIC increased to the level of thia-BCN adducts.

Table 14 Antimicrobial and hemolytic activity for thia-BCN and aza-BCN cationic adducts.

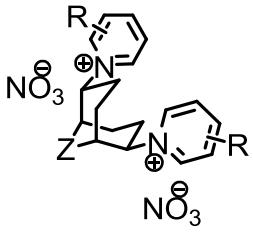

R	Z	MIC_{90} (μg/ml)	HC_{50} (μg/ml)
H	S	250	2500
3-$CONH_2$	S	500	850
3-Br	S	100	520
3-CN	S	125	-
3-CF_3	S	125	6000
3-Br, 5-$CONH_2$	S	50	>5000
H	N-heptyl	>100	-
3-Br	N-heptyl	6.25	-
3-$CONH_2$	N-heptyl	6.25	250
3-CONHMe	N-heptyl	>100	-
3-Br, 5-$CONH_2$	N-heptyl	12.5	500
3-Br, 5-$CONH_2$	N-ethyl	12.5	400
3-$CONH_2$	N-Oligoetheleneglycol	<3.12	-
3-$CONH_2$	N-propargyl	100	-

Oligocations based on aza-BCN electrophiles and various bis(pyridines) were also prepared and subjected to antimicrobial and hemolytic assay. All of the heptylamino-BCN polycations showed simultaneously low MIC_{90} and HC_{50} (lower than 10 μg/ml) except for when using bis(imidazoles) as nucleophile (HC_{50} at 75 μg/ml), resulting from strong hydrophobicity associated with greasy alkylation chain on aza-BCN core.

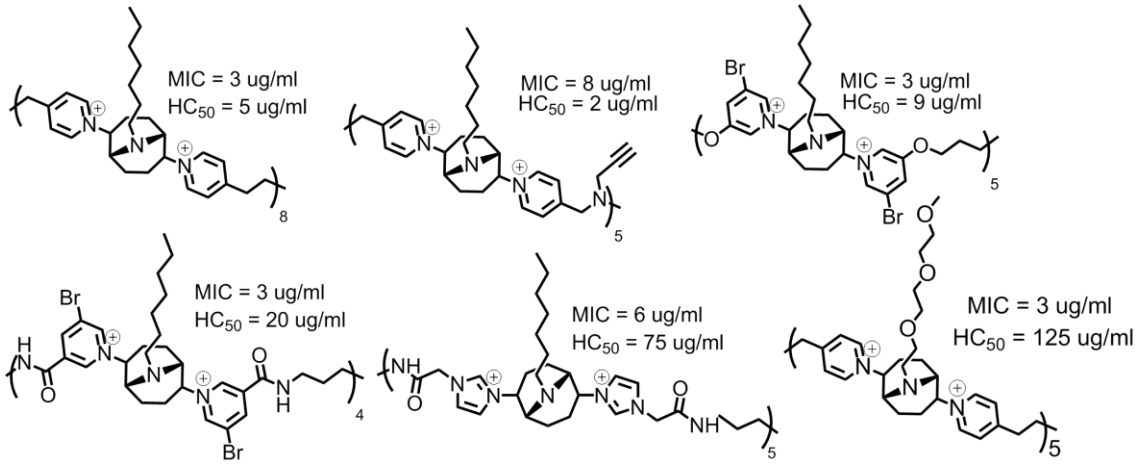

Figure 97 Antimicrobial and hemolytic activity for aza-BCN polycations.

These observations implied small molecule adduct killed bacteria via a different mechanism from polycations, which is nonselectively rupturing cell membrane. Since the ability to inhibit bacteria growth differed a lot among species of substituted pyridinium adducts, the complexed mechanism was hypothesized to be DNA alkylation by this BCN adduct after permeation across the cell membrane. This hypothesis was supported by observations listed below.

According to previous study, heptylamino BCN dichloride was more reactive than thia-BCN dichloride as an electrophile[15]. As a result, the heptylamino BCN substituted

adducts were more labile towards nucleophiles such as base pairs of nucleotides. Besides, the heptyl chain also facilitated the uptake of the BCN alkylation reagents. That explains the toxicity difference between thia-BCN and aza-BCN adducts, pyridine adducts and pyridine adducts with EWGs.

To confirm the alkylation ability of BCN adducts, PCR reactions were performed for the plasmid incubated with adducts, polycations or known alkylation reagents as positive control. The PCR products were examined by agarose-gel-shift assay. It is shown in Figure 98 that dimethylsulfate, an aqueous soluble alkylation reagent, started to inhibit PCR reaction at 25 μg/ml (major product band on agarose gel shifted). The product band for thia-BCN adducts was not observable at concentration even lower than 1 μg/ml while aza-BCN adducts completely disturbed the PCR reaction only above 5 μg/ml. The alkylation of DNA by BCN-based substitution was further confirmed by non-disturbed PCR reaction after treating plasmid with nonfragmentable cationic adduct **5a**. Fragmentable polycation **3j** was also demonstrated to alkylate DNA in similar assay above 20 μg/ml which is beyond its MIC towards bacteria cells, potentially caused by less accessibility of macromolecules to base pairs. All the treated plasmids were transformed into healthy bacteria cells and grown on agar plate containing streptomycin. Sine the plasmid carried a sequence on antibiotics resistance, survival on the plate indicated the ability of bacteria cells to recruit plasmid in addition to the integrity of the treated plasmid itself. That all the alkylated plasmid implied by PCR assay couldn't be recruited by bacteria either, further confirmed occurrence of DNA alkylation reaction.

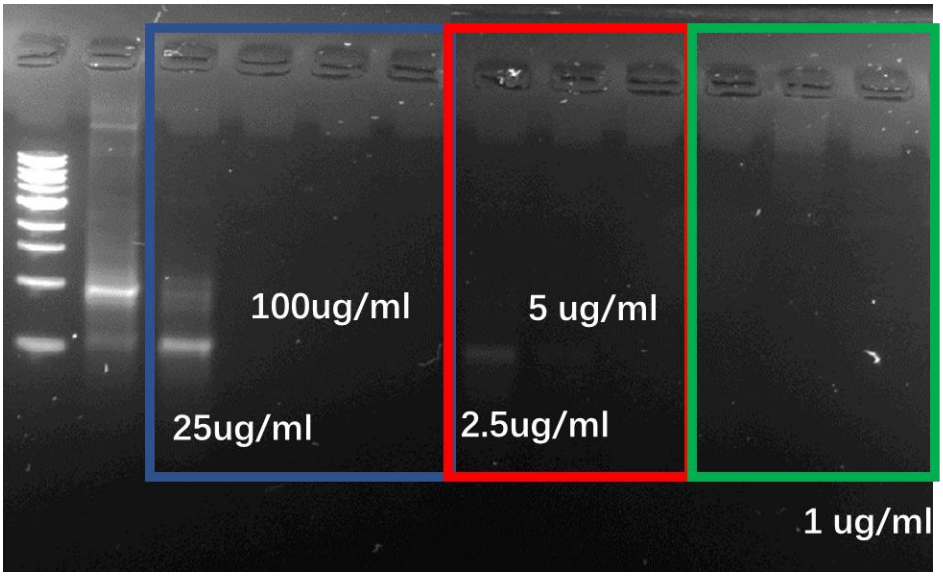

Figure 98 Agarose gel electrophoresis of PCR products from plasmid DNA incubated with increasing amounts of alkylation reagent: dimethylsulfate (in blue box), representative aza-BCN adduct 10j (in red box), representative thia-BCN adduct 5j (in green box). Critical concentration of alkylation reagent was marked in white for important lanes. Product of plasmid treated with only solvent is run at 2nd lane.

Another confirmation experiment is conducted towards four different deletion strains of *E. coli* MG1655 (a generic and commonly used strain). *ΔlacZ*::Kmr is a control strain. Δ*uvrD*::Kmr (nucleotide excision repair mutant), Δ*recA*::Kmr (homologous recombination mutant) and LexA(S119A)::Kmr (SOS-uninducible) are strains with deletion of DNA repair pathways. The reduction of MIC towards these strains will indicate DNA damaging mechanism. The preliminary results were shown in Figure 99. Since Ciprofloxacin is inhibiting DNA gyrase, its antimicrobial activity is also associated with disturbance of DNA amplification which makes it comparable to BCN adducts if DNA alkylation is involved. It was observed Δ*recA*::Kmr had dramatic lower tolerance towards both Ciprofloxacin and thia-BCN adduct among other strains, indicated by lower MIC

determined by OD detection after 24 hours growth. However, aza-BCN adducts affected four strains equally with an overall lower MIC, which might be dominantly attributed to dramatic membrane disruption.

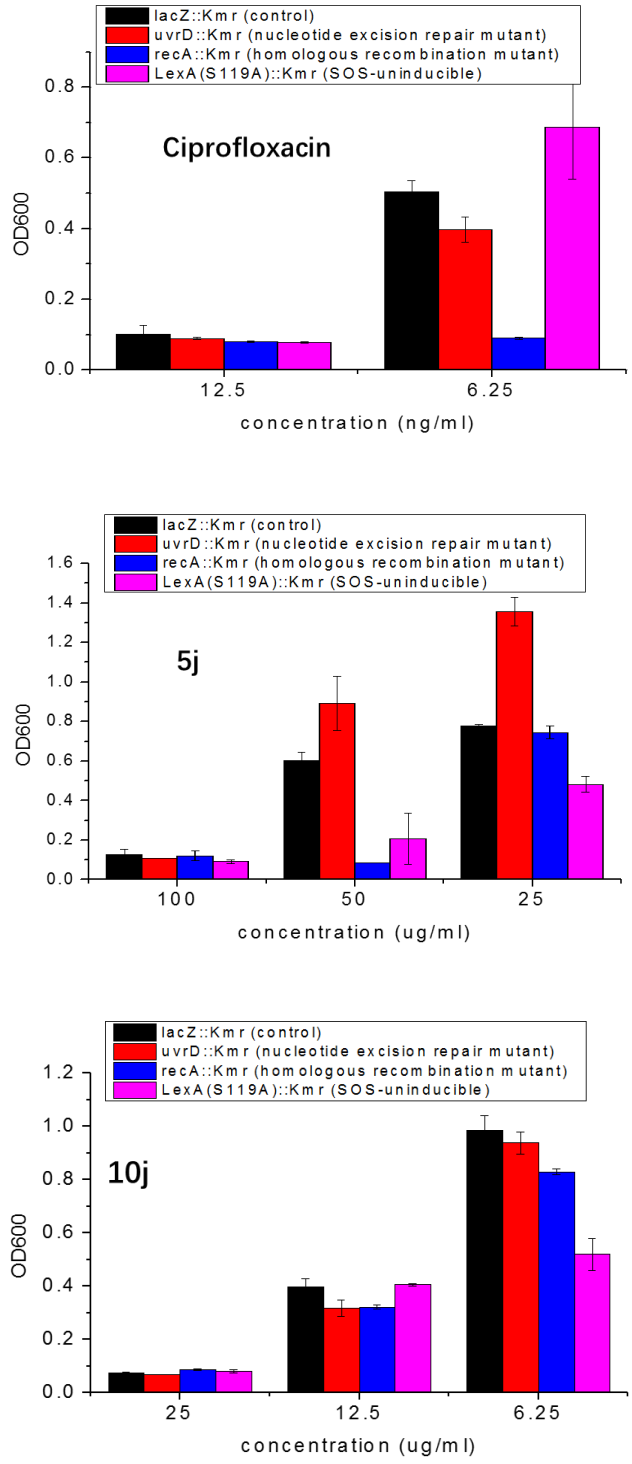

Figure 99 MIC comparison towards strains with deletion of DNA repair pathways for representative antimicrobials in each type (Ciprofloxacin for small molecule antibiotics, 5j for thia-BCN adducts, 10j for aza-BCN adducts).

It was hypothesized the unalkylated amide group played an essential role in interacting with cell membrane through H-bonding since the methylnicotinamide derivatives didn't display antimicrobial activity at similar level.

The detailed mechanism will be shed light upon if more analogues of this family of adducts are synthesized, such as phenylamino BCN adducts or stable pyridine adducts with bromo or amide groups on the pyridine ring.

5.4 Conclusion

A new type of fragmentable cationic adducts and oligocations has been developed through nucleophilic substitution of aza-BCN scaffolds by pyridines and imidazoles. The efficiency of this process depends on the leaving group ability of the group being substituted. Degrees of polymerization was enhanced by selecting NaH as base to release lone pair of aza-BCN electrophile or starting with iodide as a leaving group. pH dependent fragmentability of cationic materials based on aza-BCN was also established to demonstrate their potentials to be used as a robust linker under acidic condition, which is desirable in certain biomedical applications.

An initial survey of antimicrobial activity and hemolytic activity was presented for this new class of cationic material, both macromolecular and of low molecular weight. It was proposed aza-BCN substituted adducts and oligocations function through different antimicrobial mechanisms, also accompanied with different level of selectivity and potency. Efforts have been made to confirm DNA alkylation ability of BCN pyridinium

adducts. More detailed molecular biology experiments were required to explain the behavior of new cationic material.

CHAPTER 6. CONCLUSION AND OUTLOOK

Most of the useful functional materials developed nowadays are made by just a few reactions. When new reactions can be applied to materials synthesis, new worlds of potential function open up. This is especially true for construction of cationic materials, the synthesis of which are dominated by inefficient and energy-demanding traditional substitution reactions.

The anchimeric-assisted reaction involved with substrates containing bicyclononane structure was developed decades ago and was optimized in this thesis work to adapt to requirements of building polymeric materials. This facile nucleophilic substitution by pyridine derivatives are able to give polycationic material with molecular weight as large as 10 kDa at room temperature after optimization.

Not only providing a new method of constructing polycations, the new materials produced by this novel reaction also own valuable properties other traditional polycations lack. The tunable fragmentability of the polycations, rooting from reversible-bond-formation character of BCN-based substitution, is desirable for a number of biomedical application. The observation that pyridine basicity serving as a good guide to fragmentation rates builds up the bridge between physical organic fundamentals and practical requirements for biomaterials. pH dependent fragmentability of aza-BCN linker will also make a special addition to the general toolbox of biodegradable linkers already containing acid-sensitive esters, imines and acetals. It is of interest to apply the acid-robust BCN linker to drug delivery in stomach.

The successful realization of random copolymerization, incorporation of "clickable" handle for post-modification and constructing polymers with both linear and hyperbranched architecture all broadened the scope of cationic materials this novel substitution reaction can make. Variety of functional material could be obtained through these strategies. The examples not covered but might be desirable to be demonstrated include end group modification of polycation chain (so that larger molecules could be assembled through block polymerization), incorporation acrylate/methacrylate into BCN monomer for radical polymerization with precise control of cationic polymer's polydispersity.

The thia-BCN polymers were highly efficient in complexing DNA and showed functional behavior (transfection and cytotoxicity) normally associated with polycationic materials. This new polycation is standing out from traditionally made polyionenes in controlled release of oligonucleotides. The stability of polyplex assembled with the thia-BCN polycations could be engineered by tuning the basicity of the pyridine units. Compared with linear counterparts, hyperbranched thia-BCN polymers demonstrated ability to transfect low dose siRNA, with higher efficiency than commercial available benchmarks. Further details of structure-activity relationships should be disclosed with more diversified examples. The time-resolved study is especially important to shed light on ideal time scale for fragmentation to facilitate delivery and more importantly to realize the function of cargos.

Another common application of polyionenes, antimicrobial, has also been well performed by novel linear thia-BCN polycations. An initial survey was presented with

favorable characteristics for further development. The novel structured polycations demonstrated high potency against broad spectrum of bacterial strains. Inhibition of the bacteria growth occurred at the μg/mL level and killed static bacterial cells at polymer concentrations of tens of ng/mL, with moderate-to-good selectivity with respect to lysis of red blood cells. While resistance to the BCN polymers was developed only very slowly over multiple passages, a degradable version of the polycation was observed to make *E. coli* cells more susceptible to other quaternary ammonium based antimicrobials. The disclosure of mechanism for this phenomenon would potential give a new direction for design of next generation antimicrobials.

Solid substrates (glass and crystalline silicon) covalently functionalized with a representative thia-BCN polycation were also able to repetitively kill bacteria in solution at high rates and with cleaning by simple sonication between exposures. Combined with polydopamine coating technique, this type of new membrane-active antimicrobials was able to be applied to most classes of bulk materials. The next step is to develop smart self-cleaning surface by transitioning from charged killing status to zwitterionic repelling status. Since most bacteria growth will induce pH drop in surrounding environment, the pH dependent fragmentability of aza-BCN polycaitons might have the chance to shine again.

After all, since these novel BCN materials are the first examples of this subclass of fragmentable polyionenes to be made and tested, their promising activity in both soluble and immobilized forms, both transfection and antimicrobial bodes well for a wide range of biomedical applications.

REFERENCES

1. Winstein, S.; Buckles, R. E., The Role of Neighboring Groups in Replacement Reactions. I. Retention of Configuration in the Reaction of Some Dihalides and Acetoxyhalides with Silver Acetate1. *J. Am. Chem. Soc.* **1942,** *64* (12), 2780-2786.

2. Winstein, S.; Lindegren, C. R.; Marshall, H.; Ingraham, L. L., Neighboring Carbon and Hydrogen. XIV. Participation in Solvolysis of Some Primary Benzenesulfonates1. *J. Am. Chem. Soc.* **1953,** *75* (1), 147-155.

3. Morita, H.; Oae, S., The effect of α-epoxy and episulfide groups in the solvolytic reaction. *Tetrahedron Lett.* **1969,** *10* (17), 1347-1349.

4. Gassman, P. G.; Hall, J. B., Testing for symmetry in neighboring group participation in carbocation formation. An insight into double bond participation via trifluoromethyl group substitution. *J. Am. Chem. Soc.* **1984,** *106* (15), 4267-4269.

5. Grob, C. A.; Seckinger, K.; Tam, S. W.; Traber, R., Nucleophilic displacement at tertiary carbon. *Tetrahedron Lett.* **1973,** *14* (32), 3051-3054.

6. Page, M. I., The energetics of neighbouring group participation. *Chem. Soc. Rev.* **1973,** *2* (3), 295-323.

7. Miller, R. J.; Kuliopulos, A.; Coward, J. K., Alkyltransferase model reactions: synthesis of sulfonium and ammonium compounds containing neighboring nucleophiles. Kinetic studies of the intramolecular reaction of amino, hydroxy, phenoxy, and mercapto onium salts. *The Journal of Organic Chemistry* **1989,** *54* (14), 3436-3448.

8. Lakshmana Rao, P. V.; Vijayaraghavan, R.; Bhaskar, A. S. B., Sulphur mustard induced DNA damage in mice after dermal and inhalation exposure. *Toxicology* **1999,** *139* (1–2), 39-51.

9. Weil, E. D.; Smith, K. J.; Gruber, R. J., Transannular Addition of Sulfur Dichloride to Cyclooctadienes. *J. Org. Chem.* **1966,** *31* (6), 1669-1679.

10. Corey, E. J.; Block, E., New Synthetic Approaches to Symmetrical Sulfur-Bridged Carbocycles. *J. Org. Chem.* **1966,** *31* (6), 1663-1668.

11. Lautenschlaeger, F., The Reaction of Sulfur Dichloride with cis,cis-1,5-Cyclooctadiene. *Can. J. Chem.* **1966,** *44* (23), 2813-2817.

12. Converso, A.; Burow, K.; Marzinzik, A.; Sharpless, K. B.; Finn, M. G., 2,6-Dichloro-9-thiabicyclo[3.3.1]nonane: A Privileged, Bivalent Scaffold for the Display of Nucleophilic Components. *J. Org. Chem.* **2001,** *66* (12), 4386-4392.

13. Vincent, J. A. J. M.; Schipper, P.; de Groot, A.; Buck, H. M., Neighboring group participation of sulfur in carbonium ions. Observation of a sulfurane-like intermediate. *Tetrahedron Letters* **1975,** *16* (24), 1989-1992.

14. Converso, A.; Saaidi, P.-L.; Sharpless, K. B.; Finn, M. G., Nucleophilic Substitution by Grignard Reagents on Sulfur Mustards. *J. Org. Chem.* **2004,** *69* (21), 7336-7339.

15. Accurso, A. A.; Cho, S.-H.; Amin, A.; Potapov, V. A.; Amosova, S. V.; Finn, M. G., Thia-, Aza-, and Selena[3.3.1]bicyclononane Dichlorides: Rates vs Internal Nucleophile in Anchimeric Assistance. *J. Org. Chem.* **2011,** *76* (11), 4392-4395.

16. Nemoto, N.; Xu, X.; Sanda, F.; Endo, T., Cationic Ring-Opening Polymerization of Cyclic Monothiocarbonates: Varying the Polymer Main Chain by Neighboring Group Participation. *Macromolecules* **2001,** *34* (22), 7642-7647.

17. Trachsel, A.; de Saint Laumer, J.-Y.; Haefliger, O. P.; Herrmann, A., Parameters Influencing the Release of Tertiary Alcohols from the Surface of "Spherical" Dendrimers and "Linear" Stylomers by Neighbouring-Group-Assisted Hydrolysis of 2-Carbamoylbenzoates. *Chemistry – A European Journal* **2009,** *15* (12), 2846-2860.

18. Zussman, M. P.; Tirrell, D. A., Backbone-assisted reactions of polymers. . Poly[(chloromethyl)thiirane]. *Macromolecules* **1981,** *14* (5), 1148-1153.

19. Singer, S. J.; Nicolson, G. L., The Fluid Mosaic Model of the Structure of Cell Membranes. *Science* **1972,** *175* (4023), 720-731.

20. Martin, K. R. G.; Klein, R. L.; Quigley, H. A., Gene delivery to the eye using adeno-associated viral vectors. *Methods* **2002,** *28* (2), 267-275.

21. Samal, S. K.; Dash, M.; Van Vlierberghe, S.; Kaplan, D. L.; Chiellini, E.; van Blitterswijk, C.; Moroni, L.; Dubruel, P., Cationic polymers and their therapeutic potential. *Chem. Soc. Rev.* **2012,** *41* (21), 7147-7194.

22. Mintzer, M. A.; Simanek, E. E., Nonviral Vectors for Gene Delivery. *Chem. Rev. (Washington, DC, U. S.)* **2008,** *109* (2), 259-302.

23. Yamada, H.; Loretz, B.; Lehr, C.-M., Design of Starch-graft-PEI polymers: an effective and biodegradable gene delivery platform. *Biomacromolecules* **2014**.

24. Wu, Y.; Wang, M.; Sprouse, D.; Smith, A. E.; Reineke, T. M., Glucose-Containing Diblock Polycations Exhibit Molecular Weight, Charge, and Cell-Type Dependence for pDNA Delivery. *Biomacromolecules* **2014**.

25. Wang, M.; Liu, H.; Li, L.; Cheng, Y., A fluorinated dendrimer achieves excellent gene transfection efficacy at extremely low nitrogen to phosphorus ratios. *Nat. Commun.* **2014,** *5*, 4053/1-4053/8.

26. Li, R. Q.; Niu, Y. L.; Zhao, N. N.; Yu, B. R.; Mao, C.; Xu, F. J., Series of New β-Cyclodextrin-Cored Starlike Carriers for Gene Delivery. *ACS Appl Mater Interfaces* **2014,** *6* (6), 3969-78.

27. Akinc, A.; Anderson, D. G.; Lynn, D. M.; Langer, R., Synthesis of Poly(β-amino ester)s Optimized for Highly Effective Gene Delivery. *Bioconjugate Chem.* **2003,** *14* (5), 979-988.

28. Lynn, D. M.; Langer, R., Degradable Poly(β-amino esters): Synthesis, Characterization, and Self-Assembly with Plasmid DNA. *J. Am. Chem. Soc.* **2000,** *122* (44), 10761-10768.

29. Russ, V.; Elfberg, H.; Thoma, C.; Kloeckner, J.; Ogris, M.; Wagner, E., Novel degradable oligoethylenimine acrylate ester-based pseudodendrimers for in vitro and in vivo gene transfer. *Gene Ther.* **2007,** *15* (1), 18-29.

30. Won, Y.-Y.; Sharma, R.; Konieczny, S. F., Missing pieces in understanding the intracellular trafficking of polycation/DNA complexes. *J. Controlled Release* **2009,** *139* (2), 88-93.

31. Yue, Y.; Wu, C., Progress and perspectives in developing polymeric vectors for in vitro gene delivery. *Biomaterials Science* **2013,** *1* (2), 152-170.

32. Benfer, M.; Kissel, T., Cellular uptake mechanism and knockdown activity of siRNA-loaded biodegradable DEAPA-PVA-g-PLGA nanoparticles. *European Journal of Pharmaceutics and Biopharmaceutics* **2012,** *80* (2), 247-256.

33. Cai, J.; Yue, Y.; Rui, D.; Zhang, Y.; Liu, S.; Wu, C., Effect of Chain Length on Cytotoxicity and Endocytosis of Cationic Polymers. *Macromolecules* **2011,** *44* (7), 2050-2057.

34. Schaffer, D. V.; Fidelman, N. A.; Dan, N.; Lauffenburger, D. A., Vector unpacking as a potential barrier for receptor-mediated polyplex gene delivery. *Biotechnol. Bioeng.* **2000,** *67* (5), 598-606.

35. Deng, R.; Yue, Y.; Jin, F.; Chen, Y.; Kung, H.-F.; Lin, M. C. M.; Wu, C., Revisit the complexation of PEI and DNA — How to make low cytotoxic and highly efficient PEI

gene transfection non-viral vectors with a controllable chain length and structure? *J. Controlled Release* **2009,** *140* (1), 40-46.

36. Jones, N. A.; Hill, I. R. C.; Stolnik, S.; Bignotti, F.; Davis, S. S.; Garnett, M. C., Polymer chemical structure is a key determinant of physicochemical and colloidal properties of polymer–DNA complexes for gene delivery. *Biochimica et Biophysica Acta (BBA) - Gene Structure and Expression* **2000,** *1517* (1), 1-18.

37. Katav, T.; Liu, L.; Traitel, T.; Goldbart, R.; Wolfson, M.; Kost, J., Modified pectin-based carrier for gene delivery: Cellular barriers in gene delivery course. *J. Controlled Release* **2008,** *130* (2), 183-191.

38. Zhang, C.; Gao, S.; Jiang, W.; Lin, S.; Du, F.; Li, Z.; Huang, W., Targeted minicircle DNA delivery using folate–poly(ethylene glycol) ‑ polyethylenimine as non-viral carrier. *Biomaterials* **2010,** *31* (23), 6075-6086.

39. Gilleron, J.; Querbes, W.; Zeigerer, A.; Borodovsky, A.; Marsico, G.; Schubert, U.; Manygoats, K.; Seifert, S.; Andree, C.; Stoter, M.; Epstein-Barash, H.; Zhang, L.; Koteliansky, V.; Fitzgerald, K.; Fava, E.; Bickle, M.; Kalaidzidis, Y.; Akinc, A.; Maier, M.; Zerial, M., Image-based analysis of lipid nanoparticle-mediated siRNA delivery, intracellular trafficking and endosomal escape. *Nat Biotech* **2013,** *31* (7), 638-646.

40. Burke, P. A.; Pun, S. H.; Reineke, T. M., Advancing Polymeric Delivery Systems Amidst a Nucleic Acid Therapy Renaissance. *ACS Macro Letters* **2013,** *2* (10), 928-934.

41. Sonawane, N. D.; Szoka, F. C.; Verkman, A. S., Chloride Accumulation and Swelling in Endosomes Enhances DNA Transfer by Polyamine-DNA Polyplexes. *J. Biol. Chem.* **2003,** *278* (45), 44826-44831.

42. Tang, M. X.; Redemann, C. T.; Szoka, F. C., In Vitro Gene Delivery by Degraded Polyamidoamine Dendrimers. *Bioconjugate Chem.* **1996,** *7* (6), 703-714.

43. Kwon, Y. J., Before and after Endosomal Escape: Roles of Stimuli-Converting siRNA/Polymer Interactions in Determining Gene Silencing Efficiency. *Acc. Chem. Res.* **2011,** *45* (7), 1077-1088.

44. Strand, S. P.; Lelu, S.; Reitan, N. K.; de Lange Davies, C.; Artursson, P.; Vårum, K. M., Molecular design of chitosan gene delivery systems with an optimized balance between polyplex stability and polyplex unpacking. *Biomaterials* **2010,** *31* (5), 975-987.

45. Knorr, V.; Russ, V.; Allmendinger, L.; Ogris, M.; Wagner, E., Acetal Linked Oligoethylenimines for Use As pH-Sensitive Gene Carriers. *Bioconjugate Chem.* **2008,** *19* (8), 1625-1634.

46. Kim, Y. H.; Park, J. H.; Lee, M.; Kim, Y.-H.; Park, T. G.; Kim, S. W., Polyethylenimine with acid-labile linkages as a biodegradable gene carrier. *J. Controlled Release* **2005,** *103* (1), 209-219.

47. Lin, C.; Zhong, Z.; Lok, M. C.; Jiang, X.; Hennink, W. E.; Feijen, J.; Engbersen, J. F. J., Novel Bioreducible Poly(amido amine)s for Highly Efficient Gene Delivery. *Bioconjugate Chem.* **2006,** *18* (1), 138-145.

48. Kozielski, K. L.; Tzeng, S. Y.; Green, J. J., A bioreducible linear poly([small beta]-amino ester) for siRNA delivery. *Chem. Commun. (Cambridge, U. K.)* **2013,** *49* (46), 5319-5321.

49. Kozielski, K. L.; Tzeng, S. Y.; Hurtado De Mendoza, B. A.; Green, J. J., Bioreducible Cationic Polymer-Based Nanoparticles for Efficient and Environmentally Triggered Cytoplasmic siRNA Delivery to Primary Human Brain Cancer Cells. *ACS Nano* **2014**, *8* (4), 3232-3241.

50. Kulkarni, A.; Badwaik, V.; DeFrees, K.; Schuldt, R. A.; Gunasekera, D. S.; Powers, C.; Vlahu, A.; VerHeul, R.; Thompson, D. H., Effect of Pendant Group on pDNA Delivery by Cationic-β-Cyclodextrin:Alkyl-Polyvinyl Alcohol-Polyethylene Glycol Pendant Polymer Complexes. *Biomacromolecules* **2014,** *15* (1), 12-19.

51. Shcharbin, D.; Janaszewska, A.; Klajnert-Maculewicz, B.; Ziemba, B.; Milowska, K.; Ionov, M.; Bryszewska, M.; Dzmitruk, V.; Halets, I.; Loznikova, S.; Shcharbina, N.; Shakhbazau, A., How to study dendrimers and dendriplexes III. Biodistribution, pharmacokinetics and toxicity in vivo. *J Control Release* **2014,** *181C*, 40-52.

52. Tian, H.; Guo, Z.; Lin, L.; Jiao, Z.; Chen, J.; Gao, S.; Zhu, X.; Chen, X., pH-responsive zwitterionic copolypeptides as charge conversional shielding system for gene carriers. *J Control Release* **2014,** *174*, 117-25.

53. Hu, Q.; Wang, J.; Shen, J.; Liu, M.; Jin, X.; Tang, G.; Chu, P. K., Intracellular pathways and nuclear localization signal peptide-mediated gene transfection by cationic polymeric nanovectors. *Biomaterials* **2012,** *33* (4), 1135-1145.

54. Wei, J.; Jones, J.; Kang, J.; Card, A.; Krimm, M.; Hancock, P.; Pei, Y.; Ason, B.; Payson, E.; Dubinina, N.; Cancilla, M.; Stroh, M.; Burchard, J.; Sachs, A. B.; Hochman, J. H.; Flanagan, W. M.; Kuklin, N. A., RNA-Induced Silencing Complex-Bound Small Interfering RNA Is a Determinant of RNA Interference-Mediated Gene Silencing in Mice. *Mol. Pharmacol.* **2011,** *79* (6), 953-963.

55. Yang, Y.-Y.; Wang, X.; Hu, Y.; Hu, H.; Wu, D.-C.; Xu, F.-J., Bioreducible POSS-cored star-shaped polycation for efficient gene delivery. *ACS Appl. Mater. Interfaces* **2014,** *6* (2), 1044-52.

56. Levy, S. B.; Marshall, B., Antibacterial resistance worldwide: causes, challenges and responses. *Nature Med.* **2004,** *10* (12), S122-S129.

57. Taubes, G., The Bacteria Fight Back. *Science* **2008,** *321* (5887), 356-361.

58. Holmes, A. H.; Moore, L. S. P.; Sundsfjord, A.; Steinbakk, M.; Regmi, S.; Karkey, A.; Guerin, P. J.; Piddock, L. J. V., Understanding the mechanisms and drivers of antimicrobial resistance. *Lancet* **2016,** *387* (10014), 176-187.

59. Choi, O.; Deng, K. K.; Kim, N.-J.; Ross, L.; Surampalli, R. Y.; Hu, Z., The inhibitory effects of silver nanoparticles, silver ions, and silver chloride colloids on microbial growth. *Water Research* **2008,** *42* (12), 3066-3074.

60. Denyer, S. P., Mechanisms of action of antibacterial biocides. *International Biodeterioration & Biodegradation* **1995,** *36* (3), 227-245.

61. Jennings, M. C.; Minbiole, K. P. C.; Wuest, W. M., Quaternary Ammonium Compounds: An Antimicrobial Mainstay and Platform for Innovation to Address Bacterial Resistance. *ACS Infect. Dis.* **2015,** *1* (7), 288-303.

62. Tezel, U.; Pavlostathis, S. G., Role of Quaternary Ammonium Compounds on Antimicrobial Resistance in the Environment. In *Antimicrobial Resistance in the Environment*, John Wiley & Sons, Inc.: 2011; pp 349-387.

63. Joo, H. S.; Otto, M., Mechanisms of resistance to antimicrobial peptides in staphylococci. *Biochim. Biophys. Acta - Biomembranes* **2015,** *1848* (11), 3055-3061.

64. Chakraborty, S.; Liu, R.; Hayouka, Z.; Chen, X.; Ehrhardt, J.; Lu, Q.; Burke, E.; Yang, Y.; Weisblum, B.; Wong, G. C. L.; Masters, K. S.; Gellman, S. H., Ternary Nylon-3 Copolymers as Host-Defense Peptide Mimics: Beyond Hydrophobic and Cationic Subunits. *J. Am. Chem. Soc.* **2014,** *136* (41), 14530-14535.

65. Lienkamp, K.; Madkour, A. E.; Musante, A.; Nelson, C. F.; Nüsslein, K.; Tew, G. N., Antimicrobial Polymers Prepared by ROMP with Unprecedented Selectivity: A Molecular Construction Kit Approach. *J. Am. Chem. Soc.* **2008,** *130* (30), 9836-9843.

66. Kuroda, K.; DeGrado, W. F., Amphiphilic Polymethacrylate Derivatives as Antimicrobial Agents. *J. Am. Chem. Soc.* **2005,** *127* (12), 4128-4129.

67. Liu, S.; Ono, R. J.; Wu, H.; Teo, J. Y.; Liang, Z. C.; Xu, K.; Zhang, M.; Zhong, G.; Tan, J. P.; Ng, M.; Yang, C.; Chan, J.; Ji, Z.; Bao, C.; Kumar, K.; Gao, S.; Lee, A.; Favre, M.; Dong, H.; Ying, J. Y.; Li, L.; Fan, W.; Hedrick, J. L.; Yang, Y. Y., Highly potent antimicrobial polyionenes with rapid killing kinetics, skin biocompatibility and in vivo bactericidal activity. *Biomaterials* **2017,** *127*, 36-48.

68. Geng, Z.; Finn, M. G., Thiabicyclononane-Based Antimicrobial Polycations. *J. Am. Chem. Soc.* **2017,** *139* (43), 15401-15406.

69. Nederberg, F.; Zhang, Y.; Tan, J. P. K.; Xu, K.; Wang, H.; Yang, C.; Gao, S.; Guo, X. D.; Fukushima, K.; Li, L.; Hedrick, J. L.; Yang, Y.-Y., Biodegradable nanostructures with selective lysis of microbial membranes. *Nature Chemistry* **2011,** *3*, 409.

70. Pascual, A.; Tan, J. P. K.; Yuen, A.; Chan, J. M. W.; Coady, D. J.; Mecerreyes, D.; Hedrick, J. L.; Yang, Y. Y.; Sardon, H., Broad-Spectrum Antimicrobial Polycarbonate Hydrogels with Fast Degradability. *Biomacromolecules* **2015,** *16* (4), 1169-1178.

71. Bieser, A. M.; Thomann, Y.; Tiller, J. C., Contact-Active Antimicrobial and Potentially Self-Polishing Coatings Based on Cellulose. *Macromolecular Bioscience* **2011,** *11* (1), 111-121.

72. Abraham, R. J.; Warne, M. A.; Griffiths, L., Proton chemical shifts in NMR .10. Bromine and iodine substituent chemical shifts (SCS) and an analysis of the contributions to the SCS in halocyclohexanes. *J. Chem. Soc. Perkin Trans. 2* **1997,** (11), 2151-2160.

73. Converso, A.; Burow, K.; Marzinzik, A.; Sharpless, K. B.; Finn, M. G., 2,6-Dichloro-9-thiabicyclo[3.3.1]nonane: A Privileged, Bivalent Scaffold for the Display of Nucleophilic Components. *J. Org. Chem.* **2001,** *66* (12), 4386-4392.

74. Layman, J. M.; Borgerding, E. M.; Williams, S. R.; Heath, W. H.; Long, T. E., Synthesis and Characterization of Aliphatic Ammonium Ionenes: Aqueous Size Exclusion Chromatography for Absolute Molecular Weight Characterization. *Macromolecules* **2008,** *41* (13), 4635-4641.

75. Cao, Z.; Mi, L.; Mendiola, J.; Ella-Menye, J.-R.; Zhang, L.; Xue, H.; Jiang, S., Reversibly Switching the Function of a Surface between Attacking and Defending against Bacteria. *Angew. Chem. Int. Ed.* **2012,** *51* (11), 2602-2605.

76. Zhao, J.; Song, L.; Shi, Q.; Luan, S.; Yin, J., Antibacterial and Hemocompatibility Switchable Polypropylene Nonwoven Fabric Membrane Surface. *ACS Appl. Mater. Interfac.* **2013,** *5* (11), 5260-5268.

77. Díaz, D.; Converso, A.; Sharpless, K.; Finn, M., 2,6-Dichloro-9-thiabicyclo[3.3.1]nonane: Multigram Display of Azide and Cyanide Components on a Versatile Scaffold. *Molecules* **2006,** *11* (4), 212.

78. Samal, S. K.; Dash, M.; Van Vlierberghe, S.; Kaplan, D. L.; Chiellini, E.; van Blitterswijk, C.; Moroni, L.; Dubruel, P., Cationic polymers and their therapeutic potential. *Chem. Soc. Rev.* **2012,** *41* (21), 7147-7194.

79. Russ, V.; Elfberg, H.; Thoma, C.; Kloeckner, J.; Ogris, M.; Wagner, E., Novel degradable oligoethylenimine acrylate ester-based pseudodendrimers for in vitro and in vivo gene transfer. *Gene Ther.* **2007,** *15* (1), 18-29.

80. Luo, D.; Saltzman, W. M., Synthetic DNA delivery systems. *Nat Biotech* **2000,** *18* (1), 33-37.

81. Green, J. J.; Langer, R.; Anderson, D. G., A Combinatorial Polymer Library Approach Yields Insight into Nonviral Gene Delivery. *Acc. Chem. Res.* **2008,** *41* (6), 749-759.

82. Thanou, M.; Florea, B. I.; Geldof, M.; Junginger, H. E.; Borchard, G., Quaternized chitosan oligomers as novel gene delivery vectors in epithelial cell lines. *Biomaterials* **2002,** *23* (1), 153-159.

83. van der Aa, L. J.; Vader, P.; Storm, G.; Schiffelers, R. M.; Engbersen, J. F. J., Intercalating quaternary nicotinamide-based poly(amido amine)s for gene delivery. *J. Controlled Release* **2014,** *195*, 11-20.

84. Zhi, D.; Zhang, S.; Cui, S.; Zhao, Y.; Wang, Y.; Zhao, D., The Headgroup Evolution of Cationic Lipids for Gene Delivery. *Bioconjugate Chem.* **2013,** *24* (4), 487-519.

85. Abboud, J.-u. M.; Notario, R.; Bertrán, J.; Solà, M., One Century of Physical Organic Chemistry: The Menshutkin Reaction. In *Prog. Phys. Org. Chem.*, John Wiley & Sons, Inc.: 2007; pp 1-182.

86. Williams, S. R.; Borgerding, E. M.; Layman, J. M.; Wang, W.; Winey, K. I.; Long, T. E., Synthesis and Characterization of Well-Defined 12,12-Ammonium Ionenes: Evaluating Mechanical Properties as a Function of Molecular Weight. *Macromolecules* **2008,** *41* (14), 5216-5222.

87. Williams, S. R.; Long, T. E., Recent advances in the synthesis and structure–property relationships of ammonium ionenes. *Prog. Polym. Sci.* **2009,** *34* (8), 762-782.

88. Zelikin, A. N.; Litmanovich, A. A.; Paraschuk, V. V.; Sybatchin, A. V.; Izumrudov, V. A., Conformational Changes of Aliphatic Ionenes in Water-Salt Solutions as a Factor Controlling Stability of Their Complexes with Calf Thymus DNA. *Macromolecules* **2003,** *36* (6), 2066-2071.

89. Kugel, A.; Stafslien, S.; Chisholm, B. J., Antimicrobial coatings produced by "tethering" biocides to the coating matrix: A comprehensive review. *Prog. Org. Coat.* **2011,** *72* (3), 222-252.

90. Fischer, W.; Calderón, M.; Haag, R., Hyperbranched Polyamines for Transfection. In *Nucleic Acid Transfection*, Bielke, W.; Erbacher, C., Eds. Springer Berlin Heidelberg: Berlin, Heidelberg, 2010; pp 95-129.

91. Luo, K.; He, B.; Wu, Y.; Shen, Y.; Gu, Z., Functional and biodegradable dendritic macromolecules with controlled architectures as nontoxic and efficient nanoscale gene vectors. *Biotechnology Advances* **2014,** *32* (4), 818-830.

92. Kadlecova, Z.; Rajendra, Y.; Matasci, M.; Baldi, L.; Hacker, D. L.; Wurm, F. M.; Klok, H.-A., DNA delivery with hyperbranched polylysine: A comparative study with linear and dendritic polylysine. *Journal of Controlled Release* **2013,** *169* (3), 276-288.

93. Synatschke, C. V.; Schallon, A.; Jérôme, V.; Freitag, R.; Müller, A. H. E., Influence of Polymer Architecture and Molecular Weight of Poly(2-(dimethylamino)ethyl methacrylate) Polycations on Transfection Efficiency and Cell Viability in Gene Delivery. *Biomacromolecules* **2011,** *12* (12), 4247-4255.

94. Namivandi-Zangeneh, R.; Kwan, R. J.; Nguyen, T.-K.; Yeow, J.; Byrne, F. L.; Oehlers, S. H.; Wong, E. H. H.; Boyer, C., The effects of polymer topology and chain length on the antimicrobial activity and hemocompatibility of amphiphilic ternary copolymers. *Polymer Chemistry* **2018,** *9* (13), 1735-1744.

95. Geng, Z.; Finn, M. G., Fragmentable Polycationic Materials Based on Anchimeric Assistance. *Chem. Mater.* **2016,** *28* (1), 146-152.

96. Wang, H.; Wang, Y.; Wang, Y.; Hu, J.; Li, T.; Liu, H.; Zhang, Q.; Cheng, Y., Self‐Assembled Fluorodendrimers Combine the Features of Lipid and Polymeric Vectors in Gene Delivery. *Angewandte Chemie International Edition* **2015,** *54* (40), 11647-11651.

97. Kozielski, K. L.; Tzeng, S. Y.; Hurtado De Mendoza, B. A.; Green, J. J., Bioreducible Cationic Polymer-Based Nanoparticles for Efficient and Environmentally Triggered Cytoplasmic siRNA Delivery to Primary Human Brain Cancer Cells. *ACS Nano* **2014,** *8* (4), 3232-3241.

98. Tavares, L. S.; Silva, C. S. F.; de Souza, V. C.; da Silva, V. L.; Diniz, C. G.; Santos, M. O., Strategies and molecular tools to fight antimicrobial resistance: resistome, transcriptome, and antimicrobial peptides. *Front. Microbiol.* **2013,** *4*.

99. Kumariya, R.; Sood, S. K.; Rajput, Y. S.; Saini, N.; Garsa, A. K., Increased membrane surface positive charge and altered membrane fluidity leads to cationic antimicrobial peptide resistance in Enterococcus faecalis. *Biochim. Biophys. Acta - Biomembranes* **2015,** *1848* (6), 1367-1375.

100. Nuri, R.; Shprung, T.; Shai, Y., Defensive remodeling: How bacterial surface properties and biofilm formation promote resistance to antimicrobial peptides. *Biochim. Biophys. Acta - Biomembranes* **2015,** *1848* (11), 3089-3100.

101. Campos, M. A.; Vargas, M. A.; Regueiro, V.; Llompart, C. M.; Alberti, S.; Bengoechea, J. A., Capsule polysaccharide mediates bacterial resistance to antimicrobial peptides. *Infect. Immun.* **2004,** *72* (12), 7107-7114.

102. Henderson, J. C.; Fage, C. D.; Cannon, J. R.; Brodbelt, J. S.; Keatinge-Clay, A. T.; Trent, M. S., Antimicrobial Peptide Resistance of Vibrio cholerae Results from an LPS Modification Pathway Related to Nonribosornal Peptide Synthetases. *ACS Chem. Biol.* **2014,** *9* (10), 2382-2392.

103. Guina, T.; Yi, E. C.; Wang, H. L.; Hackett, M.; Miller, S. I., A PhoP-regulated outer membrane protease of Salmonella enterica serovar typhimurium promotes resistance to alpha-helical antimicrobial peptides. *J. Bacteriol.* **2000,** *182* (14), 4077-4086.

104. McPhee, J. B.; Lewenza, S.; Hancock, R. E. W., Cationic antimicrobial peptides activate a two-component regulatory system, PmrA-PmrB, that regulates resistance to polymyxin B and cationic antimicrobial peptides in Pseudomonas aeruginosa. *Mol. Microbiol.* **2003,** *50* (1), 205-217.

105. Georg, M.; Maudsdotter, L.; Tavares, R.; Jonsson, A. B., Meningococcal resistance to antimicrobial peptides is mediated by bacterial adhesion and host cell RhoA and Cdc42 signalling. *Cellular Microbiol.* **2013,** *15* (11), 1938-1954.

106. Oguri, T.; Yeo, W. S.; Bae, T.; Lee, H., Identification of EnvC and Its Cognate Amidases as Novel Determinants of Intrinsic Resistance to Cationic Antimicrobial Peptides. *Antimicrob. Agents Chemother.* **2016,** *60* (4), 2222-2231.

107. Hong, J.; Hu, J. Y.; Ke, F., Experimental Induction of Bacterial Resistance to the Antimicrobial Peptide Tachyplesin I and Investigation of the Resistance Mechanisms. *Antimicrob. Agents Chemother.* **2016,** *60* (10), 6067-6075.

108. Wang, Z.; Bie, P. F.; Cheng, J.; Lu, L.; Cui, B. Y.; Wu, Q. M., The ABC transporter YejABEF is required for resistance to antimicrobial peptides and the virulence of Brucella melitensis. *Sci. Rep.* **2016,** *6*.

109. Ilker, M. F.; Nüsslein, K.; Tew, G. N.; Coughlin, E. B., Tuning the Hemolytic and Antibacterial Activities of Amphiphilic Polynorbornene Derivatives. *J. Am. Chem. Soc.* **2004,** *126* (48), 15870-15875.

110. Lee, S. B.; Koepsel, R. R.; Morley, S. W.; Matyjaszewski, K.; Sun, Y.; Russell, A. J., Permanent, Nonleaching Antibacterial Surfaces. 1. Synthesis by Atom Transfer Radical Polymerization. *Biomacromolecules* **2004,** *5* (3), 877-882.

111. Xue, Y.; Xiao, H.; Zhang, Y., Antimicrobial Polymeric Materials with Quaternary Ammonium and Phosphonium Salts. *Int. J. Mol. Sci.* **2015,** *16* (2), 3626.

112. Zhang, J.; Chen, Y. P.; Miller, K. P.; Ganewatta, M. S.; Bam, M.; Yan, Y.; Nagarkatti, M.; Decho, A. W.; Tang, C., Antimicrobial Metallopolymers and Their Bioconjugates with Conventional Antibiotics against Multidrug-Resistant Bacteria. *J. Am. Chem. Soc.* **2014,** *136* (13), 4873-4876.

113. Strassburg, A.; Kracke, F.; Wenners, J.; Jemeljanova, A.; Kuepper, J.; Petersen, H.; Tiller, J. C., Nontoxic, Hydrophilic Cationic Polymers-Identified as Class of Antimicrobial Polymers. *Macromol. Biosci.* **2015,** *15* (12), 1710-1723.

114. Porter, E. A.; Weisblum, B.; Gellman, S. H., Mimicry of Host-Defense Peptides by Unnatural Oligomers: Antimicrobial β-Peptides. *J. Am. Chem. Soc.* **2002,** *124* (25), 7324-7330.

115. Patch, J. A.; Barron, A. E., Helical Peptoid Mimics of Magainin-2 Amide. *J. Am. Chem. Soc.* **2003,** *125* (40), 12092-12093.

116. Hilpert, K.; Volkmer-Engert, R.; Walter, T.; Hancock, R. E. W., High-throughput generation of small antibacterial peptides with improved activity. *Nature Biotech.* **2005,** *23* (8), 1008-1012.

117. Blondelle, S. E.; Houghten, R. A., Design of model amphipathic peptides having potent antimicrobial activities. *Biochemistry* **1992,** *31* (50), 12688-12694.

118. Al-Khalifa, S. E.; Jennings, M. C.; Wuest, W. M.; Minbiole, K. P. C., The Development of Next-Generation Pyridinium-Based multiQAC Antiseptics. *ChemMedChem* **2017,** *12* (4), 280-283.

119. Ator, L. E.; Jennings, M. C.; McGettigan, A. R.; Paul, J. J.; Wuest, W. M.; Minbiole, K. P. C., Beyond paraquats: Dialkyl 3,3′ - and 3,4′ -bipyridinium amphiphiles as antibacterial agents. *Bioorg. Med. Chem. Lett.* **2014,** *24* (16), 3706-3709.

120. Paniak, T. J.; Jennings, M. C.; Shanahan, P. C.; Joyce, M. D.; Santiago, C. N.; Wuest, W. M.; Minbiole, K. P. C., The antimicrobial activity of mono-, bis-, tris-, and tetracationic amphiphiles derived from simple polyamine platforms. *Bioorg. Med. Chem. Lett.* **2014,** *24* (24), 5824-5828.

121. Forman, M. E.; Jennings, M. C.; Wuest, W. M.; Minbiole, K. P. C., Building a Better Quaternary Ammonium Compound (QAC): Branched Tetracationic Antiseptic Amphiphiles. *ChemMedChem* **2016,** *11* (13), 1401-1405.

122. Zhu, C.; Yang, Q.; Liu, L.; Lv, F.; Li, S.; Yang, G.; Wang, S., Multifunctional Cationic Poly(p-phenylene vinylene) Polyelectrolytes for Selective Recognition, Imaging, and Killing of Bacteria Over Mammalian Cells. *Adv. Mater.* **2011,** *23* (41), 4805-4810.

123. Jennings, M. C.; Buttaro, B. A.; Minbiole, K. P. C.; Wuest, W. M., Bioorganic Investigation of Multicationic Antimicrobials to Combat QAC-Resistant Staphylococcus aureus. *ACS Infect. Dis.* **2015,** *1* (7), 304-309.

124. Gallo, R. L.; Hooper, L. V., Epithelial antimicrobial defence of the skin and intestine. *Nature Rev. Immunol.* **2012,** *12* (7), 503-516.

125. Costa, F.; Carvalho, I. F.; Montelaro, R. C.; Gomes, P.; Martins, M. C. L., Covalent immobilization of antimicrobial peptides (AMPs) onto biomaterial surfaces. *Acta Biomater.* **2011,** *7* (4), 1431-1440.

126. Han, J. H.; Floros, J. D., Casting antimicrobial packaging films and measuring their physical properties and antimicrobial activity. *J. Plastic Film & Sheeting* **1997,** *13* (4), 287-298.

127. Cha, D. S.; Chinnan, M. S., Biopolymer-based antimicrobial packaging: A review. *Crit. Rev. Food Sci. Nutr.* **2004,** *44* (4), 223-237.

128. Page, K.; Wilson, M.; Parkin, I. P., Antimicrobial surfaces and their potential in reducing the role of the inanimate environment in the incidence of hospital-acquired infections. *J. Mat. Chem.* **2009,** *19* (23), 3819-3831.

129. Siedenbiedel, F.; Tiller, J. C., Antimicrobial Polymers in Solution and on Surfaces: Overview and Functional Principles. *Polymers* **2012,** *4* (1), 46-71.

130. Kugler, R.; Bouloussa, O.; Rondelez, F., Evidence of a charge-density threshold for optimum efficiency of biocidal cationic surfaces. *Microbiol.-Sgm* **2005,** *151*, 1341-1348.

131. Lichter, J. A.; Van Vliet, K. J.; Rubner, M. F., Design of Antibacterial Surfaces and Interfaces: Polyelectrolyte Multilayers as a Multifunctional Platform. *Macromolecules* **2009,** *42* (22), 8573-8586.

132. Lichter, J. A.; Rubner, M. F., Polyelectrolyte Multilayers with Intrinsic Antimicrobial Functionality: The Importance of Mobile Polycations. *Langmuir* **2009,** *25* (13), 7686-7694.

133. Murata, H.; Koepsel, R. R.; Matyjaszewski, K.; Russell, A. J., Permanent, non-leaching antibacterial surfaces—2: How high density cationic surfaces kill bacterial cells. *Biomaterials* **2007,** *28* (32), 4870-4879.

134. Silverman, J. A.; Oliver, N.; Andrew, T.; Li, T., Resistance studies with daptomycin. *Antimicrob. Ag. Chemother.* **2001,** *45* (6), 1799-1802.